

Quantum simulation of highly-oscillatory many-body Hamiltonians for near-term devices

Guannan Chen¹, Mohammadali Foroozandeh², Chris Budd¹, and Pranav Singh¹

¹Department of Mathematical Sciences, University of Bath, Bath BA2 7AY, United Kingdom

²Chemistry Research Laboratory, University of Oxford, Mansfield Road, OX1 3TA Oxford, United Kingdom

We develop a fourth-order Magnus expansion based quantum algorithm for the simulation of many-body problems involving two-level quantum systems with time-dependent Hamiltonians, $\mathcal{H}(t)$. A major hurdle in the utilization of the Magnus expansion is the appearance of a commutator term which leads to prohibitively long circuits. We present a technique for eliminating this commutator and find that a single time-step of the resulting algorithm is only marginally costlier than that required for time-stepping with a time-independent Hamiltonian, requiring only three additional single-qubit layers. For a large class of Hamiltonians appearing in liquid-state nuclear magnetic resonance (NMR) applications, we further exploit symmetries of the Hamiltonian and achieve a surprising reduction in the expansion, whereby a single time-step of our fourth-order method has a circuit structure and cost that is identical to that required for a fourth-order Trotterized time-stepping procedure for time-independent Hamiltonians. Moreover, our algorithms are able to take time-steps that are larger than the wavelength of oscillation of the time-dependent Hamiltonian, making them particularly suited for highly-oscillatory controls. The resulting quantum circuits have shorter depths for all levels of accuracy when compared to first and second-order Trotterized methods, as well as other fourth-order Trotterized methods, making the proposed algorithm a suitable candidate for simulation of time-dependent Hamiltonians on near-term quantum devices.

1 Introduction

In this paper we develop effective methods for the Hamiltonian simulation for many-body two-level systems with time-dependent Hamiltonians, $\mathcal{H}(t)$, *i.e.*, for solving the ordinary differential equation,

$$i\frac{\partial}{\partial t}|\psi(t)\rangle = \mathcal{H}(t)|\psi(t)\rangle, \quad |\psi(0)\rangle = |\psi_0\rangle \in \mathcal{H} = \mathbb{C}^{2^M}, \quad t \in \mathbb{R}, \quad (1)$$

where $|\psi(t)\rangle$ describes the state of a quantum system at time t .

The quantum state $|\psi(t)\rangle$ resides in the Hilbert space \mathcal{H} , whose dimension increases exponentially for a many-body quantum system [1]. This *curse of dimensionality* potentially renders the solution of eq. (1) using classical computers infeasible beyond a small number of particles. On the other hand, due to a similarly exponential increase in the

Pranav Singh: ps2106@bath.ac.uk

Hilbert space of a quantum computer with the number of qubits, the Hamiltonian simulation problem can be solved very effectively on a fault-tolerant quantum computer in the case of time-independent Hamiltonians, $\mathcal{H}(t) = \mathcal{H}_0$.

The significance of this problem to computational quantum chemistry and physics, the suspected exponential difficulty for classical computers, and the demonstrably linear growth in terms of number of qubits required, makes Hamiltonian simulation problems for many-body systems an important class of candidates for demonstrating ‘*quantum advantage*’ [2–4]. Hamiltonian simulation is also a fundamental subroutine of other sophisticated quantum algorithms such as quantum phase estimation (QPE) [5] and the Harrow-Hassidim-Lloyd (HHL) algorithm [6] for solving linear system of equations.

Along with rapid development of quantum hardware [7–9], this has fuelled a resurgence of interest in the development of quantum algorithms for Hamiltonian simulation [10–16]. These algorithms typically solve eq. (1) by utilizing techniques for approximating the matrix exponential. Arguably the oldest and the most widely utilized among these techniques are *Trotterization* techniques [17], also known as *splitting* methods [18, 19], which lead to simpler circuit designs that are easier to implement [20], and that can be optimized [21] for near-term applications. Trotterized circuits have been utilized in recent attempts at demonstrating the utility of existing *noisy intermediate scale quantum* (NISQ) devices for Hamiltonian simulation [4, 22]. Another notable approach is the qubitization procedure of [16], which provides a substantially improved *additive complexity* for simulation of time-independent Hamiltonians, and is expected to prove superior in the context of large-scale fault-tolerant quantum computers.

Hamiltonian simulation for time-dependent Hamiltonians, which is required for describing the interaction of quantum systems with external time-dependent fields such as lasers, magnetic fields and light, involves solving a non-autonomous differential equation eq. (1) whose solution is no longer given by a direct exponential of the Hamiltonian. Thus, new techniques are required for the simulation of time-dependent Hamiltonians, and this has become an area of intense investigation with recent approaches including the interaction picture approach [23], approximation of the Dyson series [24], L1 norm scaling [25], the treatment of slowly varying time-dependent for lattice Hamiltonians [26], permutation expansion [27], approaches based on time-ordered operators [28], a Floquet based approach for periodic time-dependent Hamiltonians [29], and the autonomization approach of [30].

Time-dependent Hamiltonians in many-body two-level systems. Two-level quantum systems are ubiquitous in quantum technologies, and among other applications, they form the physical realization of qubits in a quantum computer [31, 32] and describe the phenomenon of nuclear magnetic resonance (NMR) [33]. They appear either naturally in systems that have only two energy levels (and eigenstates), *e.g.*, spin-1/2 systems, or as anharmonic quantum systems such as superconducting qubits, where the lowest two energy levels stay sufficiently separated from the rest during operation to effectively behave like a two-level system.

The Hamiltonians of interest in this paper are time-dependent Hamiltonians involving multiple interacting two-level systems. Such Hamiltonians appear prominently in the control of quantum technologies, including gate design and control of superconducting qubits [34–36], trapped ion control [37], NV-centers in diamond [38, 39], quantum error-correction and quantum information registers [40–42], pulse design in magnetic resonance spectroscopy (NMR) and imaging (MRI) [43–45], electron paramagnetic resonance (EPR) [46–48], cold atom interferometry [49–51], and terahertz technologies [52, 53], among others. A wide range of general purpose algorithms for the optimal control of such two-level systems have been developed, including GRAPE [54], CRAB [55], GOAT [56], and QOALA

[57], and have been employed widely in systems of practical interest.

An additional difficulty is posed by the highly-oscillatory *chirped* pulses that are often encountered in the control of quantum systems [58–60]. A highly-oscillatory Hamiltonian conventionally forces the use of small time-steps. For classical computers, this is undesirable due to longer computational times, but is otherwise achievable. On a quantum computer, where small time-steps correspond to larger circuit depths, the accumulation of errors in the quantum circuit can significantly restrict the feasibility of simulating such Hamiltonians on near-term quantum devices. This makes the Hamiltonian simulation problem for time-dependent Hamiltonians with highly-oscillatory pulses significantly harder than for time-independent Hamiltonians of the same structure.

Main contributions. In this manuscript we develop a fourth-order method for Hamiltonian simulation of many-body two-level system under time-dependent Hamiltonians, which can take long time-steps and achieve high accuracy. Our approach is independent of the frequency of the Hamiltonian oscillation and can handle a continuum of frequencies. A unique feature is that our method can take time-steps that are larger than the wavelength of oscillation of the Hamiltonian, allowing us to handle chirped pulses very effectively. The ability of our method to be used with long time-steps corresponds to shorter circuit depths. Moreover, all of this can be achieved using minor modifications of a Trotterized circuit for time-independent Hamiltonians, or a qubitized circuit for piecewise-constant Hamiltonians, and involves only a marginal increase in circuit depth.

Our approach is based on the use of the Magnus expansion [61, 62], which amounts to finding an effective Hamiltonian as an infinite series of nested integrals of nested commutators. Magnus based methods are utilised widely in classical algorithms for quantum dynamics [63–67].

Mean Hamiltonian. The first term of the effective Hamiltonian is simply the mean Hamiltonian, which has the same structure as a time-independent Hamiltonian, and techniques for exponentiating time-independent Hamiltonians such as Trotterization [17] and qubitization [16] can be applied without altering the circuit structure. However, as we demonstrate with numerical evidence, the second-order accuracy of this method is inadequate for simulating time-dependent Hamiltonians, requiring very small time-steps or long circuit depths for reasonable accuracy. This necessitates the development of higher-order schemes. In the context of chirped pulses, this is more immediately evident since they involve a continuous range of frequencies and the Hamiltonian averaging techniques is particularly poorly suited here.

Issues with commutators. The immediate problem in the use of higher-order Magnus expansions for quantum algorithms is the appearance of a commutator term. The time-independent and mean Hamiltonians have a common structure and can be expressed as a linear combination of $3M + \frac{1}{2}|C_{\text{in}}|$ unitaries, where M is the number of two-level systems and $|C_{\text{in}}| \leq 9M(M - 1)$ is the number of pairwise couplings. On the other hand, the commutator term appearing in the fourth-order Magnus expansion involves a linear combination of $\mathcal{O}(M^3)$ unitaries. This makes direct application of Trotterization or qubitization for exponentiating the fourth-order Magnus expansion infeasible due to a prohibitive increase in the circuit depth, and is arguably the biggest restriction in the application of Magnus-based methods for Hamiltonian simulation on a quantum computer.

Eliminating commutators. We present an approach that eliminates the commutator term in the fourth-order Magnus expansion for a general spin Hamiltonian, leaving us with an effective Hamiltonian that has the same structure as the time-independent and mean Hamiltonians. Consequently, it can be expressed as a linear combination of $3M + \frac{1}{2}|C_{\text{in}}|$ unitaries and efficiently exponentiated via qubitization, or combined with a Trotterized

approach with very minor modification of the circuit structure. Specifically the minor overhead is the appearance of two additional terms that can be computed with $\mathcal{O}(M)$ single-qubit gates. In the special case of *isotropic* coupling with identical controls, which appears frequently in liquid-state NMR applications, we find a surprising result that the commutator term vanishes due to certain symmetries of the Hamiltonian, leaving the circuit structure and depth identical to the case of mean Hamiltonians.

Numerical results. Numerical simulations of NMR spectra offer insights into molecular structures, interactions, and dynamics. Their significance is highlighted by the considerable attention they have received in the scientific community, as evidenced by the proliferation of dedicated software packages tailored for this purpose. Notable examples include SPINACH [68], EasySpin [69], SpinEvolution [70], and SIMPSON [71]. Motivated by the importance of NMR simulations, we present concrete Trotterized circuits for our fourth-order Magnus-based approach and demonstrate its efficacy in simulating spin dynamics in NMR.

In particular, the numerical evidence shows a significant advantage over the second-order approximation and an ability to take time-steps larger than the wavelength of the external pulse. The latter ability stems from our approach to decouple the resolution of the external pulses from the time-step of the numerical scheme, along the lines of [67, 72, 73]: Unlike traditional applications of the Magnus expansion, which discretize the integrals using a fixed number of Gauss–Legendre quadrature nodes, and therefore tie the resolution of the external pulse to the time-step, in these approaches the one and two-dimensional integrals in the fourth-order Magnus expansion are computed to high precision on a classical computer. In the context of many-body spin systems, the investigations by [74, Section 4.2], provided initial evidence of this phenomenon under weak fields.

The proposed approach is compared to first-order methods, second-order methods, and other fourth-order methods that are free of commutators, including a commutator-free quasi-Magnus approach and an autonomization approach described in Section 3.5. The proposed approach is found superior in all cases – producing shorter circuits for any given accuracy, with the circuit compression ratios higher for more oscillatory pulses.

Notable differences are found from the simulation of time-independent versions of the Hamiltonians, where the second-order method produces the shortest circuits for accuracies of practical interest ($\sim 10^{-2} - 10^{-5}$), with the fourth-order method only becoming more efficient for higher accuracies, which are not expected to be achievable in the near term. In contrast, for highly-oscillatory pulses that appear in control applications, we find that our fourth-order method produces the shortest circuits even when very low levels of accuracies ($\sim 10^{-1}$) are required. Nevertheless, the circuit depths required for the time-dependent case are found to be two orders of magnitude (~ 110) higher, which suggests that quantum simulation of time-dependent Hamiltonians that appear in the context of practical applications is a significantly harder task, and may remain a challenge even when ‘*quantum advantage*’ has been demonstrated on carefully chosen time-independent Hamiltonians, especially when taking into account the sparse couplings typically considered in recent attempts [4, 22].

Outline. In Section 2, we establish a theoretical framework for describing the dynamics of many-body two-level quantum systems using spin-1/2 systems as a primary example. This section introduces the Magnus expansion technique and highlights challenges in simulating time-dependent Hamiltonians. In Section 3, we discuss methods for approximating matrix exponentials using quantum computers, with a focus on a novel approach for eliminating commutators in the fourth-order Magnus expansion. Section 4 details the construction of Trotterized quantum circuits for the fourth-order Magnus expansion, and

provides gate and circuit complexities. In Section 5, we present numerical results comparing our Hamiltonian simulation method against other approaches. This section emphasizes the effectiveness of the proposed approach across different Hamiltonian types and pulse influences, and benchmarks the behaviour under a range of oscillatory pulses and coupling strengths. Finally, Section 6 concludes the paper with a brief discussion.

2 Theory

2.1 The Hamiltonian structure

We consider the evolution of an M -body quantum system, where each subsystem is a two-level system. In particular, we consider spin-1/2 systems, which serve as prominent examples of a two-level system. However, we emphasize that our technique extends to any two-level system, of which spin-1/2 systems are just one illustrative instance.

The state of an M -body spin system at time t is described by a density matrix $\varrho(t) \in \mathbb{C}^{2^M \times 2^M}$. In the absence of dissipative terms (*i.e.*, decoherence), the dynamics of the density matrix are governed by the Liouville-von Neumann equation,

$$\frac{\partial \varrho(t)}{\partial t} = -i[\mathcal{H}(t), \varrho(t)], \quad \varrho(0) = \varrho_0, \quad t \in \mathbb{R}, \quad (2)$$

where $\mathcal{H}(t)$ is a time-dependent Hamiltonian. Since the density matrix $\varrho(t)$ is an ensemble of pure states $\psi_j(t)$,

$$\varrho(t) = \sum_j p_j |\psi_j(t)\rangle \langle \psi_j(t)|, \quad \sum_j p_j = 1, \quad (3)$$

its evolution in the non-dissipative case can also be understood by studying the evolution of $|\psi_j(t)\rangle$, whose dynamics are described by the Schrödinger equation

$$i \frac{\partial}{\partial t} |\psi(t)\rangle = \mathcal{H}(t) |\psi(t)\rangle, \quad |\psi(0)\rangle = |\psi_0\rangle \in \mathbb{C}^{2^M}, \quad t \in \mathbb{R}. \quad (1)$$

We consider the Hamiltonian $\mathcal{H}(t)$ to consist of a single-spin (*i.e.*, non-interacting) sub-Hamiltonian $\mathcal{H}_{\text{ss}}(t)$ and a coupling or interaction sub-Hamiltonian \mathcal{H}_{in} ,

$$\mathcal{H}(t) = \mathcal{H}_{\text{ss}}(t) + \mathcal{H}_{\text{in}}. \quad (4)$$

For an M -body spin system, the Hamiltonian for non-interacting spins can be written as

$$\mathcal{H}_{\text{ss}}(t) = \mathbf{e}(t)^\top \mathbb{S} = \sum_{k=1}^M \sum_{\alpha \in \{X, Y, Z\}} \mathbf{e}_k^\alpha(t) \alpha_k, \quad (5)$$

where

$$\mathbf{e}(t) = \begin{pmatrix} \mathbf{e}^X(t) \\ \mathbf{e}^Y(t) \\ \mathbf{e}^Z(t) \end{pmatrix} \in C^\infty(\mathbb{R}; \mathbb{R}^{3M}),$$

are the *pulses* or *controls* and

$$\mathbb{S} = \begin{pmatrix} \mathbb{S}^X \\ \mathbb{S}^Y \\ \mathbb{S}^Z \end{pmatrix} \in \mathbb{C}^{3M \times (2^M \times 2^M)}, \quad \mathbb{S}^\alpha = \begin{pmatrix} \alpha_1 \\ \alpha_2 \\ \vdots \\ \alpha_M \end{pmatrix} \in \mathbb{C}^{M \times (2^M \times 2^M)}, \quad \alpha \in \{X, Y, Z\},$$

are vectors of tensorized Pauli matrices. Specifically, the matrices $\alpha \in \{X, Y, Z\}$ are the Pauli spin- $\frac{1}{2}$ matrices,

$$X = \begin{pmatrix} 0 & 1 \\ 1 & 0 \end{pmatrix}, \quad Y = \begin{pmatrix} 0 & -i \\ i & 0 \end{pmatrix}, \quad Z = \begin{pmatrix} 1 & 0 \\ 0 & -1 \end{pmatrix}, \quad (6)$$

and for a matrix $\alpha \in \mathbb{C}^{2 \times 2}$ we use α_k to denote the tensor

$$\alpha_k = \underbrace{\mathbb{1} \otimes \cdots \otimes \mathbb{1}}_{M-k \text{ times}} \otimes \underbrace{\alpha}_{k^{\text{th}}} \otimes \underbrace{\mathbb{1} \otimes \cdots \otimes \mathbb{1}}_{k-1 \text{ times}} \in \mathbb{C}^{2^M \times 2^M}, \quad (7)$$

whose action is to apply α to the k th spin and leave other spins unaffected – *i.e.*, the subscript k denotes the spin on which the matrix α acts. Here $\mathbb{1}$ is the 2×2 identity matrix.

Remark 1. In this paper, bold letters such as \mathbf{e} , $\mathbf{\Omega}$, and $\mathbf{1}$ denote column vectors. X , Y , Z , A and I denote matrices. Matrices with a single subscript such as X_k and A_k denote a tensor product of the matrix and identity matrices, as defined in eq. (7). \mathbb{S} , \mathbb{A} , and \mathbb{B} denote vectors of tensor products.

Remark 2. For $\mathbf{a} \in \mathbb{C}^{3M}$, we often write $\mathbf{a} = (\mathbf{a}^{X^\top}, \mathbf{a}^{Y^\top}, \mathbf{a}^{Z^\top})^\top$ with the subcomponents $\mathbf{a}^\alpha \in \mathbb{C}^M$, $\alpha \in \{X, Y, Z\}$.

Remark 3. Note that in NMR literature it is common to use I_k^x , I_k^y , and I_k^z in place of X_k , Y_k and Z_k , respectively, and to normalize them by a factor of $\frac{1}{2}$.

Remark 4. Throughout this work, we assume that the controls $\mathbf{e} \in C^\infty(\mathbb{R}; \mathbb{R}^{3M})$ are smooth functions of time. However, by splitting the temporal window of integration appropriately, our approach can be extended in a straightforward way to piecewise smooth controls.

Given an interaction tensor,

$$C_{\text{in}} = \begin{pmatrix} C^{X,X} & C^{X,Y} & C^{X,Z} \\ C^{Y,X} & C^{Y,Y} & C^{Y,Z} \\ C^{Z,X} & C^{Z,Y} & C^{Z,Z} \end{pmatrix}, \quad C^{\alpha,\beta} \in \mathbb{R}^{M \times M}, \quad \alpha, \beta \in \{X, Y, Z\}, \quad (8)$$

the interaction sub-Hamiltonian,

$$\mathcal{H}_{\text{in}} = \frac{1}{2} \mathbb{S}^\top C_{\text{in}} \mathbb{S} = \frac{1}{2} \sum_{j=1}^M \sum_{k=1}^M \sum_{\alpha \in \{X,Y,Z\}} \sum_{\beta \in \{X,Y,Z\}} C_{j,k}^{\alpha,\beta} \alpha_j \beta_k, \quad (9)$$

encodes all possible pairwise interactions between the M spins. We assume throughout that $C_{j,j}^{\alpha,\beta} = 0$ for all $\alpha, \beta \in \{X, Y, Z\}$ and $j = 1, \dots, M$, *i.e.*, the interaction terms are strictly pairwise. The $C_{j,j}^{\alpha,\beta} \neq 0$ case leads to scaled copies of the identity tensor in the Hamiltonian, which results in a global phase factor that is trivial to handle.

Remark 5. The typical practice in NMR is to express the interaction tensor as an $M \times M$ matrix of 3×3 submatrices. Instead, in eq. (8), we organize the interaction tensor as a 3×3 matrix C_{in} of $M \times M$ submatrices $C^{\alpha,\beta}$.

The overall Hamiltonian considered in this work is

$$\mathcal{H}(t) = \underbrace{\mathbf{e}(t)^\top \mathbb{S}}_{\mathcal{H}_{\text{ss}}} + \underbrace{\frac{1}{2} \mathbb{S}^\top C_{\text{in}} \mathbb{S}}_{\mathcal{H}_{\text{in}}}. \quad (10)$$

Hamiltonians of this form appear in many areas including nuclear magnetic resonance (NMR) [75–77], spin chains [78, 79], Ising models [80–82], and honeycomb Kitaev model [83, 84]. The complexity of the Hamiltonian may be substantially reduced in specific applications. For instance, couplings are typically symmetric, *i.e.*, $C^{\alpha,\alpha} = C^{\alpha,\alpha\top}$ and interactions can often be very sparse – *e.g.*, $C_{j,k}^{\alpha,\beta} = 0$ in spin chains unless $|j - k| = 1$.

Remark 6. *Our most general algorithm, developed in Section 3.3, involves no assumptions on C_{in} . The Trotterization procedure described in Sections 3 and 4 requires the absence of mixed coupling, *i.e.*, $C^{\alpha,\beta} = 0$ for $\alpha \neq \beta$. In principle, mixed couplings can be eliminated by performing a local change of basis [85, 86], and this is not a severely restrictive assumption. In Section 3.4 we consider the special case of isotropic couplings, where $C^{X,X} = C^{Y,Y} = C^{Z,Z} = C = C^\top$, and mixed couplings are absent. This case often appears in the context of liquid-state NMR.*

A crucial quantity in the accuracy (and difficulty) of the Hamiltonian simulation problem is the maximum spectral radius of the Hamiltonian over the interval of simulation $[0, T]$,

$$\rho = \max_{t \in [0, T]} \|\mathcal{H}(t)\|, \quad (11)$$

where $\|\cdot\|$ is the ℓ^2 norm. The norm ρ can be bounded from above as

$$\rho \leq 3M \max_{t \in [0, T]} \|\mathbf{e}(t)\|_\infty + \frac{1}{2} |C_{\text{in}}| \|C_{\text{in}}\|_{\max}, \quad (12)$$

i.e., $\rho = \mathcal{O}(\|\mathbf{e}\|_\infty M + |C_{\text{in}}| \|C_{\text{in}}\|_{\max})$, where $|C_{\text{in}}| \leq (9/2)M(M-1)$ is the number of non-zero entries in the interaction or coupling tensor, and the matrix max norm, $\|A\|_{\max} := \|\text{vec}(A)\|_\infty$, is the maximum over the absolute values of all entries in the matrix A .

2.2 The Magnus expansion

The Schrödinger equation, eq. (1), can be written in the form

$$\partial_t |\psi(t)\rangle = \mathcal{A}(t) |\psi(t)\rangle, \quad |\psi(0)\rangle = |\psi_0\rangle, \quad (13)$$

where $\mathcal{A}(t) = -i\mathcal{H}(t)$. Since $\mathcal{A}(t) \in \mathfrak{su}(2^M)$ is a skew-Hermitian matrix for all $t \in \mathbb{R}$, the solution of eq. (13) is given by

$$|\psi(T)\rangle = U(T, 0) |\psi(0)\rangle,$$

where $U(T, 0) \in \text{U}(2^M)$ is a unitary matrix for all $T \in \mathbb{R}$.

The problem of Hamiltonian simulation of eq. (13) effectively reduces to the approximation of $U(T, 0)$, and the development of quantum algorithms for its approximation is currently an area of intense activity. Among the various algorithms for solving the Schrödinger equation on classical computers, some of the most effective methods utilize the Magnus expansion [61].

The Magnus expansion is a Lie group method [62], which seeks an approximation of $U(T, 0) \in \text{U}(2^M)$ in the Lie algebra $\mathfrak{su}(2^M)$. In practice we seek a matrix $\Theta(T, 0)$ such that

$$U(T, 0) = \exp(\Theta(T, 0)), \quad \Theta(T, 0) \in \mathfrak{su}(2^M). \quad (14)$$

Since the exponential map ‘exp’ maps the Lie algebra to its Lie group, $\exp(\Theta(T, 0))$ is in $\text{U}(2^M)$. Moreover, any approximation of $\Theta(T, 0)$ in the Lie algebra $\mathfrak{su}(2^M)$ retains this unitarity property.

However, a matrix with the above properties is not always guaranteed to exist. The existence (or convergence) of the Magnus expansion for ordinary differential equations (ODEs) such as eq. (1) has been widely studied [87, 88], and very tight bounds for the convergence are known. Namely, if

$$\int_0^T \|\mathcal{A}(t)\| dt \leq \pi, \quad (15)$$

where $\|\cdot\|$ is the ℓ^2 norm, then there is always a $\Theta(T, 0)$ which satisfies the property (14), *i.e.*, the solution operator $U(T, 0)$ can be expressed as the exponential of a matrix in $\mathfrak{su}(2^M)$. Moreover, this is a tight bound, *i.e.*, there are examples of $\mathcal{A}(t)$ that violate the bound in eq. (15) and for which there is no $\Theta(T, 0)$ that satisfies eq. (14).

As a consequence, the Magnus expansion cannot provide global solutions in general (*i.e.*, over a long interval $[0, T]$ with a large T) and has to be used as a time-stepping scheme with a small time-step h over a time grid $t_n = nh$, $n \in \mathbb{N}_0$,

$$|\psi(t_{n+1})\rangle = U_n |\psi(t_n)\rangle, \quad n \in \mathbb{N}_0, \quad |\psi(t_0)\rangle = |\psi_0\rangle, \quad U_n := U(t_{n+1}, t_n) = e^{\Theta(t_{n+1}, t_n)} \quad (16)$$

Equivalently, the propagator $U(T, 0)$ is computed as

$$U(T, 0) = \prod_{n=0}^{N-1} U_n = \prod_{n=0}^{N-1} e^{\Theta(t_{n+1}, t_n)}, \quad t_N = T, \quad (17)$$

where the product $\prod_{n=0}^{N-1} U_n := U_{N-1} U_{N-2} \dots U_1 U_0$ needs to be considered as ordered.

For practical purposes we consider the Magnus expansion written as an infinite sum in the Lie algebra $\mathfrak{su}(2^M)$,

$$\Theta(t_{n+1}, t_n) = \lim_{k \rightarrow \infty} \Theta_k(t_{n+1}, t_n), \quad \Theta_k(t_{n+1}, t_n) = \sum_{j=1}^k \Theta^{[j]}(t_{n+1}, t_n), \quad (18)$$

where the terms $\Theta^{[j]}(t_{n+1}, t_n) \in \mathfrak{su}(2^M)$ are progressively smaller in size (in terms of their spectral radii) and the finite truncations Θ_k provide progressively accurate approximations to Θ . A practical algorithm for approximating $U(T, 0)$ in eq. (17) involves computing the exponential of a finite truncation of the Magnus expansion,

$$\exp(\Theta_k(t_{n+1}, t_n)) \approx U(t_{n+1}, t_n) = U_n.$$

Since $\Theta_k(t_{n+1}, t_n) \in \mathfrak{su}(2^M)$, its exponential also provides a unitary approximation to U_n .

The first two terms of the Magnus expansion which we will utilize in this work are

$$\Theta^{[1]}(t_{n+1}, t_n) = \int_0^h \mathcal{A}(t_n + \zeta) d\zeta = \mathcal{O}(h), \quad (19)$$

$$\Theta^{[2]}(t_{n+1}, t_n) = -\frac{1}{2} \int_0^h \int_0^\zeta [\mathcal{A}(t_n + \xi), \mathcal{A}(t_n + \zeta)] d\xi d\zeta = \mathcal{O}(h^3). \quad (20)$$

Here the notation $[\cdot, \cdot]$ represents the commutator of two matrices, defined as

$$[P, Q] = PQ - QP. \quad (21)$$

Note that the occurrence of two integrals in $\Theta^{[2]}(t_{n+1}, t_n)$ suggests that this term should scale as $\mathcal{O}(h^2)$ in the time-step h . However, due to time-symmetry and due to the cancellation of certain terms in the Taylor series, terms in the Magnus expansion tend to be

smaller than expected when \mathcal{A} is smooth in time [89]. In particular, it has been shown [62] that

$$\begin{aligned}\Theta(t_{n+1}, t_n) &= \Theta_1(t_{n+1}, t_n) + \mathcal{O}(h^3), \\ \Theta(t_{n+1}, t_n) &= \Theta_2(t_{n+1}, t_n) + \mathcal{O}(h^5).\end{aligned}$$

Remark 7. For ease of notation, we will often write $\Theta_k(t_n)$ or simply Θ_k for $\Theta_k(t_{n+1}, t_n)$ in the rest of the manuscript, taking either the time-step h or both h and t_n as implicitly implied. The same holds in general for any function $\mathbf{a}(t_n)$ which should be understood to be a function of both t_n and h .

Time-stepping with the truncated Magnus expansions $\Theta_k, k = 1, 2$,

$$|\tilde{\psi}_{n+1}^k\rangle = e^{\Theta_k(t_n)} |\tilde{\psi}_n^k\rangle, \quad n \in \mathbb{N}_0, \quad |\tilde{\psi}_0^k\rangle = |\psi_0\rangle, \quad (22)$$

results in a second-order method for $k = 1$ and a fourth-order method for $k = 2$. Specifically, for $k = 1, 2$, there exist constants c_k independent of h and n such that

$$\left\| |\tilde{\psi}_n^k\rangle - |\psi(t_n)\rangle \right\|_2 \leq c_k T \gamma \rho^{k+1} h^{2k}, \quad h \rightarrow 0, \quad nh \leq T, \quad (23)$$

where ρ , as defined in eqs. (11) and (12), is the maximum spectral radius of the Hamiltonian on the time interval of simulation $[0, T]$, and

$$\gamma = \max_{t \in [0, T]} \|\mathbf{e}'(t)\|_\infty \quad (24)$$

depends on the maximum frequency of the controls in this interval. Equivalently, the second and fourth-order approximations to $U(T, 0)$ have the *propagator errors*

$$\left\| U(T, 0) - \prod_{n=0}^{N-1} e^{\Theta_k(t_n)} \right\| \leq c_k T \gamma \rho^{k+1} h^{2k}, \quad h \rightarrow 0, \quad Nh = T. \quad (25)$$

For the derivation of these estimates, we refer the reader to [62].

In the following subsections, we present the concrete forms of the second and fourth-order Magnus expansions, Θ_1 and Θ_2 , for the Schrödinger equation (1) with the Hamiltonian (10). These are developed for an arbitrary interaction tensor C_{in} , eq. (8), and under the assumption of smooth controls, $\mathbf{e} \in C^\infty(\mathbb{R}; \mathbb{R}^{3M})$ (see remark 4).

2.3 Second-order Magnus expansion

The second-order Magnus expansion is

$$\Theta_1(t_n) = \Theta^{[1]}(t_n) = \int_0^h \mathcal{A}(t_n + \zeta) d\zeta. \quad (26)$$

We obtain the expansion for the Schrödinger equation (1) with the Hamiltonian (10) by substituting $\mathcal{A}(t_n + \zeta) = -i\mathcal{H}(t_n + \zeta) = -i\mathbf{e}(t)^\top \mathbb{S} - i\frac{1}{2}\mathbb{S}^\top C_{\text{in}} \mathbb{S}$,

$$\Theta_1(t_n) = \int_0^h \mathcal{A}(t_n + \zeta) d\zeta = -i\boldsymbol{\mu}(t_n)^\top \mathbb{S} - i\frac{h}{2}\mathbb{S}^\top C_{\text{in}} \mathbb{S}, \quad (27)$$

where

$$\boldsymbol{\mu}(t_n) = \int_0^h \mathbf{e}(t_n + \zeta) d\zeta. \quad (28)$$

Since $\mathbf{e} \in C^\infty(\mathbb{R}; \mathbb{R}^{3M})$, $\mathcal{A}(t)$ is smooth in time and using Θ_1 in the time-stepping scheme (22) or the propagator approximation in eq. (25) leads to a second-order method.

2.4 Fourth-order Magnus expansion

Since $\mathbf{e} \in C^\infty(\mathbb{R}; \mathbb{R}^{3M})$ and $\mathcal{A}(t)$ is smooth in time, the fourth-order Magnus expansion results from truncating the Magnus series (18) to two terms, $\Theta^{[1]}$ and $\Theta^{[2]}$,

$$\Theta_2(t_n) = \int_0^h \mathcal{A}(t_n + \zeta) d\zeta - \frac{1}{2} \int_0^h \int_0^\zeta [\mathcal{A}(t_n + \xi), \mathcal{A}(t_n + \zeta)] d\xi d\zeta. \quad (29)$$

The additional term $-\frac{1}{2} \int_0^h \int_0^\zeta [\mathcal{A}(t_n + \xi), \mathcal{A}(t_n + \zeta)] d\xi d\zeta$ in the fourth-order Magnus expansion is a source of numerous difficulties, arising primarily from the presence of the commutator term. When it comes to the M -body Hamiltonian (10), $\mathcal{A}(t) = i\mathcal{H}(t)$ has $3M$ single spin terms and $|C_{\text{in}}|$ pairwise coupling terms, which is reducible to $\frac{1}{2}|C_{\text{in}}|$ in case of symmetry, $C^{\alpha,\beta\top} = C^{\alpha,\beta}$ for $\alpha, \beta \in \{X, Y, Z\}$. For dense interactions, $|C_{\text{in}}| = \mathcal{O}(M^2)$, so that in general $\mathcal{A}(t)$ has $\mathcal{O}(M^2)$ pairwise coupling terms.

To estimate the complexity of the additional commutator $[\mathcal{A}(t_n + \xi), \mathcal{A}(t_n + \zeta)]$, a very naïve estimate can be obtained by considering the commutator definition of $[P, Q]$, eq. (21), and individually analysing the subcomponents PQ or QP . The term $\mathcal{A}(t_n + \xi)\mathcal{A}(t_n + \zeta)$, for instance, involves $\mathcal{O}(M^4)$ terms with four-way couplings of the form $\alpha_j \beta_k \gamma_\ell \delta_m$, where $\alpha, \beta, \gamma, \delta \in \{X, Y, Z\}$, in contrast to the pairwise couplings seen in the Hamiltonian (10). This would make any application of the fourth-order Magnus expansion infeasible in the near term. In Theorem 1, we see that this estimate is highly pessimistic and all four-way coupling terms in the commutator cancel due to the interactions in the Hamiltonian (10) being time-independent.

Definition 1. We define the wedge product between $\mathbf{a}(t) = (\mathbf{a}^X(t)^\top, \mathbf{a}^Y(t)^\top, \mathbf{a}^Z(t)^\top)^\top$ and $\mathbf{b}(t) = (\mathbf{b}^X(t)^\top, \mathbf{b}^Y(t)^\top, \mathbf{b}^Z(t)^\top)^\top$ as

$$\mathbf{c}(t, s) = (\mathbf{a} \wedge \mathbf{b})(t, s) = (\mathbf{c}^X(t, s)^\top, \mathbf{c}^Y(t, s)^\top, \mathbf{c}^Z(t, s)^\top)^\top, \quad (30)$$

where

$$\begin{aligned} \mathbf{c}^X(t, s) &= \mathbf{a}^Y(t) \odot \mathbf{b}^Z(s) - \mathbf{b}^Z(t) \odot \mathbf{a}^Y(s), \\ \mathbf{c}^Y(t, s) &= \mathbf{a}^Z(t) \odot \mathbf{b}^X(s) - \mathbf{b}^X(t) \odot \mathbf{a}^Z(s), \\ \mathbf{c}^Z(t, s) &= \mathbf{a}^X(t) \odot \mathbf{b}^Y(s) - \mathbf{b}^Y(t) \odot \mathbf{a}^X(s), \end{aligned}$$

where \odot is the Hadamard product.

Theorem 1. The fourth-order Magnus expansion for the Schrödinger equation (1) with the Hamiltonian (10) can be expressed as

$$\Theta_2(t_n) = -i\mathbf{r}(t_n)^\top \mathbb{S} - i\frac{h}{2} \mathbb{S}^\top C_{\text{in}} \mathbb{S} + [\mathbf{u}(t_n)^\top \mathbb{S}, \mathbb{S}^\top C_{\text{in}} \mathbb{S}], \quad (31)$$

where

$$\mathbf{u}(t_n) = -\frac{1}{2} \int_0^h \left(\zeta - \frac{h}{2} \right) \mathbf{e}(t_n + \zeta) d\zeta, \quad (32)$$

$$\mathbf{r}(t_n) = \boldsymbol{\mu}(t_n) - \int_0^h \int_0^\zeta (\mathbf{e} \wedge \mathbf{e})(t_n + \xi, t_n + \zeta) d\xi d\zeta. \quad (33)$$

Overall, the fourth-order Magnus expansion involves $3M$ single-spin terms of the form α_j , $|C_{\text{in}}|$ pairwise coupling terms of the form $\alpha_j \beta_k$, and $3M|C_{\text{in}}|$ three-way coupling terms of the form $\alpha_j \beta_k \gamma_\ell$.

Proof of Theorem 1. See Appendix A. \square

Theorem 1 is a minor extension of [74, Theorem 3.5], differing only in terms of the more compact form of the integrals derived here and the treatment of $\mathbf{e}^Z(t)$ as time-dependent, which requires the \wedge product notation.

The reduced complexity of the fourth-order Magnus expansion is due to the most expensive part of the commutator $[\mathcal{A}(t_n + \xi), \mathcal{A}(t_n + \zeta)]$ vanishing in Theorem 2. The remaining part of the commutator,

$$\left[\mathbf{u}(t_n)^\top \mathbb{S}, \mathbb{S}^\top C_{\text{in}} \mathbb{S} \right], \quad (34)$$

is somewhat simpler but nevertheless involves an additional $\mathcal{O}(|C_{\text{in}}|M)$ three-way coupling terms, which keeps the fourth-order Magnus expansion prohibitively more complex than the second-order Magnus expansion (27) and the time-independent Hamiltonian. In Section 3.3 we will develop techniques to eliminate this remaining commutator term. In Section 3.4 we consider a special but important case where this commutator vanishes on its own.

2.5 Approximating the integrals

It is a well-established convention in the application of Magnus expansions [62] that the integrals appearing in the Magnus expansion should be approximated with a quadrature method of a matching order of accuracy. Quadrature methods approximate an integral as a weighted sum of function values at specifically chosen points. For integrating over the interval $[0, h]$ as in eq. (19), the rule takes the form

$$\int_0^h \mathcal{A}(\xi) d\xi \approx \sum_{i=1}^k w_i \mathcal{A}(x_i), \quad (35)$$

where k is the number of sample points used, w_i are the quadrature weights, and x_i are the quadrature *knots*. The quadrature weights can be computed by integrating the Lagrange interpolation functions $\ell_i(\xi)$,

$$w_i = \int_0^h \ell_i(\xi) d\xi, \quad \text{where } \ell_i(x) = \prod_{\substack{j=1 \\ j \neq i}}^n \frac{x - x_j}{x_i - x_j}. \quad (36)$$

The choice of quadrature knots x_i as the roots of Legendre polynomials leads to the Gauss–Legendre quadrature, which has the highest asymptotic accuracy among all quadrature methods with a given number of nodes. In the context of the Magnus expansion, Gauss–Legendre quadrature methods achieve $\mathcal{O}(h^{2n+1})$ accuracy for n knots, which is one order higher than usually expected out of them in general [62]. The fourth-order Magnus expansion also features a term (20) with a double integral, a corresponding two-dimensional quadrature rule for which is given by

$$\int_0^h \int_0^\zeta [\mathcal{A}(\xi), \mathcal{A}(\zeta)] d\xi d\zeta = \sum_{i=1}^k \sum_{j=1}^k w_{i,j} [\mathcal{A}(x_i), \mathcal{A}(x_j)], \quad (37)$$

where the weights $w_{i,j}$ are computed via double integrals of the Lagrange interpolation functions,

$$\int_0^h \int_0^\zeta (\ell_i(\xi) \ell_j(\zeta) - \ell_j(\xi) \ell_i(\zeta)) d\xi d\zeta. \quad (38)$$

In the context of the second-order Magnus expansion, $\Theta_1(t_n)$, eq. (26), the prescribed quadrature is the Gauss–Legendre quadrature with a single knot, specifically the midpoint, $\frac{t_n+t_{n+1}}{2}$. For the fourth-order Magnus expansion, $\Theta_2(t_n)$, eq. (29), the prescribed quadrature is the Gauss–Legendre quadrature with two knots in each interval, $[t_n, t_{n+1}]$. However, in the presence of highly-oscillatory driving pulses, [66, 67, 72, 73] demonstrate the advantage of approximating the integrals in the Magnus expansion with quadratures with much higher accuracies than conventionally prescribed. In this manuscript, to facilitate the use of more quadrature knots, we use GLk to denote the use of a Gauss–Legendre quadrature with k knots for computing the integrals appearing in the Magnus expansion.

3 Approximating the matrix exponential

Time-stepping with the Magnus expansion (22), or equivalently, approximating the propagator $U(T, 0)$ in eq. (25), requires efficient procedures for approximating the matrix exponentials of the second and fourth-order Magnus expansions, Θ_1 and Θ_2 , respectively.

3.1 Trotterization

We start by considering the Trotterization technique for approximating the exponential of matrices of the form,

$$\Omega = -i\mathbf{a}^\top \mathbb{S} - i\frac{h}{2}\mathbb{S}^\top C_{\text{in}}\mathbb{S}. \quad (39)$$

In the context of Trotterization techniques, we assume that mixed couplings are not present in the interaction tensor, $C^{\alpha,\beta} = 0$ for $\alpha \neq \beta$, and matrices of the form (39) can be separated into X , Y and Z components,

$$\Omega = \Omega^X + \Omega^Y + \Omega^Z,$$

where

$$\Omega^\alpha = -i\mathbf{a}^{\alpha\top} \mathbb{S}^\alpha - \frac{h}{2}\mathbb{S}^{\alpha\top} C^{\alpha,\alpha} \mathbb{S}^\alpha, \quad \alpha \in \{X, Y, Z\}. \quad (40)$$

As a consequence of the following lemma, any two terms in a given component Ω^α commute with each other.

Lemma 1.

$$[A_j, A_k] = 0, \quad [A_i, A_j A_k] = 0, \quad [A_i A_\ell, A_j A_k] = 0, \quad i, j, k, \ell \in \{1, \dots, M\}. \quad (41)$$

Proof. These follow immediately from the definition of A_k , eq. (7), and the fact that a matrix commutes with itself and with the identity matrix. \square

As a consequence, the exponential of each component Ω^α scaled by an arbitrary real scalar s can be computed exactly as

$$e^{s\Omega^\alpha} = \prod_{\ell=1}^M e^{-is\mathbf{a}_\ell^\alpha \alpha_\ell} \prod_{j=1}^M \prod_{\substack{k=1 \\ k \neq j}}^M e^{-is\frac{h}{2}C_{j,k}^{\alpha,\alpha} \alpha_j \alpha_k}, \quad s \in \mathbb{R}, \quad (42)$$

which can be implemented using M rotation gates (fig. 1) and $|C^{\alpha,\alpha}|$ *Ising* coupling gates (fig. 2) with different gate parameters. Here $|C^{\alpha,\alpha}| \leq M(M-1)$ is the number of non-zero entries of $C^{\alpha,\alpha}$. When $C^{\alpha,\alpha^\top} = C^{\alpha,\alpha}$, we can combine half the exponents and compute

$$e^{s\Omega^\alpha} = \prod_{\ell=1}^M e^{-is\mathbf{a}_\ell^\alpha \alpha_\ell} \prod_{j=1}^M \prod_{k=j+1}^M e^{-ishC_{j,k}^{\alpha,\alpha} \alpha_j \alpha_k}, \quad s \in \mathbb{R}, \quad (43)$$

so that the number of Ising coupling gates required are $\frac{1}{2}|C^{\alpha,\alpha}| \leq \frac{1}{2}M(M-1)$.

As noted in remark 6, the absence of mixed couplings is not a serious restriction. In Section 4, each component e^{Ω^α} is implemented as described in eq. (43) and depicted by a block of gates in the circuit presented in fig. 3 (c).

However, this assumption is crucial in the context of Trotterization since it allows us to split Ω in components Ω^X, Ω^Y and Ω^Z , each of whose exponential can be computed exactly, as outlined above. A first-order time-stepping method can be obtained by approximating the exponential of Ω using the *Trotter splitting*,

$$e^{h(A+B+C)} = e^{hA}e^{hB}e^{hC} + \mathcal{O}(h^2). \quad (44)$$

Higher-order time-stepping methods can be derived by using higher-order *splittings* [18, 19], which are collectively also called *Trotterizations*. A second-order method is given by the *Strang* splitting [90],

$$e^{h(A+B+C)} = e^{\frac{h}{2}A}e^{\frac{h}{2}B}e^{hC}e^{\frac{h}{2}B}e^{\frac{h}{2}A} + \mathcal{O}(h^3), \quad (45)$$

and a fourth-order method by the *Yoshida* splitting [91],

$$e^{h(A+B+C)} = e^{\frac{xh}{2}A}e^{\frac{xh}{2}B}e^{xhC}e^{\frac{xh}{2}B}e^{\frac{(x+y)h}{2}A}e^{\frac{yh}{2}B}e^{yhC}e^{\frac{yh}{2}B}e^{\frac{(x+y)h}{2}A}e^{\frac{xh}{2}B}e^{xhC}e^{\frac{xh}{2}B}e^{\frac{xh}{2}A} + \mathcal{O}(h^5), \quad (46)$$

where

$$x = \frac{1}{2 - 2^{1/3}}, \quad y = 1 - 2x. \quad (47)$$

The error in a single time-step of a k th order splitting \mathcal{S}_k (e.g., the product of the exponentials in the right hand sides of eqs. (44), (45) or (46)) is bounded from above by

$$\|e^{h(A+B+C)} - \mathcal{S}_k\| \leq \tilde{c}_k (\max\{\|A\|, \|B\|, \|C\|\})^k h^{k+1}, \quad (48)$$

for some constant \tilde{c}_k .

When repeated for multiple steps, the first and last occurrences of e^{cA} can be combined together in the case of the Strang splitting and the fourth-order Yoshida splitting. On average, Strang splitting requires 4 exponentials per time-step and the fourth-order Yoshida splitting required 12 exponentials. In principle, for the exponentiation of Ω , we may assign $\Omega^X, \Omega^Y, \Omega^Z$ to A, B, C in any order. However, different choices can lead to different circuit depths and gate counts. In the fourth-order Yoshida splitting, on average 3 exponentials each of A and C are required per time-step and 6 of B . Ideally the component assigned to B should be the one involving the simplest circuit – this is expected to vary with the architecture as well as the coupling tensor C_{in} .

Trotterization techniques can be used for computing the matrix exponential of a time-independent Hamiltonian,

$$\mathcal{H}_0 = \mathbf{e}_0 + \frac{1}{2}\mathbb{S}^\top C_{\text{in}} \mathbb{S},$$

by time-stepping,

$$U(T, 0) = \exp(-iT\mathcal{H}_0) \approx \prod_{n=0}^{N-1} \exp(-ih\mathcal{H}_0), \quad Nh = T, \quad (49)$$

where each $\exp(-ih\mathcal{H}_0)$ is approximated by an appropriate splitting, eqs. (44) to (46). In the case of a time-dependent Hamiltonian, eq. (10), time-stepping with a piecewise-constant approximation of the Hamiltonian $\mathcal{H}(t_n)$,

$$U(T, 0) \approx \prod_{n=0}^{N-1} \exp(-ih\mathcal{H}(t_n)), \quad Nh = T, \quad (50)$$

where each $\exp(-ih\mathcal{H}(t_n))$ is approximated by the Trotter splitting (44), leads to a first-order method for eq. (1). We note that in both cases in eqs (49) and (50), the matrices to be exponentiated have the form (39), with $\mathbf{a} = h\mathbf{e}_0$ and $\mathbf{a} = h\mathbf{e}(t_n)$, respectively.

The second-order Magnus expansion, $\Theta_1(t_n)$ in eq. (27), also has the same structure (39), with $\mathbf{a} = \boldsymbol{\mu}(t_n)$, and we can approximate its exponential by utilizing the appropriate splitting – in this case the Strang splitting (45), which is a second-order method. Due to the common structure (39), each step of the second-order Magnus-based time-stepping method (25) is exactly as expensive as a time-step of Strang splitting method with a time-independent Hamiltonian (49), and only 33% more expensive than the first-order method (50) for time-dependent Hamiltonians.

Moreover, the circuit used for the Strang splitting of $\exp(-ih\mathcal{H}_0)$ can be re-used, with only the values of the coefficients ‘ \mathbf{a} ’ requiring a change – this involves changing some tuneable parameters of the quantum gates. Note that the integrals in $\boldsymbol{\mu}(t_n)$, eq. (28), are one-dimensional and can be easily computed a priori to a high accuracy on a classical computer.

The integrals, eqs. (32) and (33), appearing in the fourth-order Magnus expansion $\Theta_2(t_n)$ in eq. (31) look more complicated, but are only two-dimensional and can also be computed easily to high accuracy on a classical computer. A much more significant problem for the utilization of the fourth-order Magnus expansion is posed by the presence of the commutator term

$$\left[\mathbf{u}(t_n)^\top \mathbb{S}, \mathbb{S}^\top C_{\text{in}} \mathbb{S} \right] \quad (34)$$

in eq. (31), which means that $\Theta_2(t_n)$ does not have the structure (39). Thus, unlike the case of the second-order Magnus expansion, we cannot utilize the splittings in eqs. (44) to (46) directly, and in particular, we cannot re-use the circuit for the time-independent Hamiltonian by only changing the tunable gate parameters.

Moreover, by Theorem 1, the commutator term (34) has $\mathcal{O}(|C_{\text{in}}|M) \leq \mathcal{O}(M^3)$ three-way coupling terms of the form $\alpha_j \beta_k \gamma_\ell$. A Trotterized approach for the Magnus expansion in this form is highly problematic for multiple reasons: (i) the circuit depth and gate count must increase by a factor of $\mathcal{O}(M)$, (ii) the additional terms require three-qubit gates, and (iii) involve mixed three-way couplings. Due to the mixed couplings, there is no straightforward way of splitting Θ_2 into a sum of a small number of subcomponents where any two subterms commute.

In Section 3.3, we present a technique for eliminating this commutator, and in Section 3.4 we consider a special case where the commutator simplifies. This overcomes all the aforementioned challenges and allows the application of a Trotterized approach to the fourth-order Magnus expansion. A detailed Trotterized quantum circuit for the fourth-order Magnus expansion is presented in Section 4.

The Trotterization approach presented in this section for exponentiating (39) involves time-stepping. Higher accuracy requires smaller time-steps, which corresponds to larger circuit depths. In practice, Trotterization aims to achieve a reasonable balance – producing simple and relatively shallow circuits for reasonable accuracy in short-to-medium time simulation problems. This balance makes Trotterized algorithms among the few feasible candidates for Hamiltonian simulation on near-term quantum devices, and first-order Trotterized methods have been utilized in early attempts to explore utility of quantum computing in presence of noise [4]. Since the main emphasis in this work is shorter circuit depths for reasonable accuracy, Trotterisation is our method of choice. Nevertheless, we note that other alternatives do exist and comment upon some of them in Section 3.2 briefly.

3.2 Other approaches for matrix exponential

A significant contrast to the time-stepping approach in Trotterization is the recently developed qubitization procedure [16] which is a global approximation technique that does not require time-stepping. Qubitization achieves ‘*additive*’ query complexity for Hamiltonian simulation of time-independent Hamiltonians,

$$\mathcal{O}\left(\rho T + \frac{\log(1/\varepsilon)}{\log(e + \log(1/\varepsilon)/\rho T)}\right), \quad (51)$$

where $[0, T]$ is the time window of simulation, ε is the allowable error, ρ is the spectral radius (11) of the Hamiltonian, and the Hamiltonian to be exponentiated is given by a linear combination of unitaries as

$$\tilde{\mathcal{H}} = \sum_{j=1}^d u_j \mathcal{U}_j, \quad u_j \in \mathbb{R}, \quad \mathcal{U}_j^* \mathcal{U}_j = \mathcal{U}_j \mathcal{U}_j^* = I, \quad \text{and} \quad \rho = \|\tilde{\mathcal{H}}\| \leq \sum_{j=1}^d |u_j|. \quad (52)$$

While qubitization achieves the optimal complexity for Hamiltonian simulation and should be the method of choice when high accuracy is required over a long temporal window of simulation, it requires fully fault-tolerant quantum computers and involves larger overheads and circuit depths, potentially making it unsuitable for near term applications. The time-ordering approach of [28] and the Floquet-based approach of [29] extend the optimal (additive) complexity of qubitization to periodic-in-time Hamiltonians. However, no approach currently exists for combining qubitization with non-periodic time-dependent Hamiltonian and achieving additive complexity.

While qubitization can be combined with time-stepping methods (25) in a straightforward way at a less optimal query complexity,

$$\mathcal{O}\left(\frac{\rho T^2}{h} + \frac{T \log(1/\varepsilon)}{h \log(e + \log(1/\varepsilon)/\rho T)}\right), \quad (53)$$

where h is the time-step size, the simpler approach of BCKKS (Berry-Childs-Cleve-Kothari-Somma) [13] works equally well for small time-steps.

The overall gate complexity, with the exception of some overheads, can be estimated as a product of the query complexity and the gate complexity of the *oracle*. In this section, we briefly consider the gate complexity of the oracle required for time-stepping with eq. (39) and the fourth-order Magnus expansion (31).

Key to the applicability of qubitization and BCKKS to the exponentiation of eq. (39), is the fact that the *effective* Hamiltonian $\tilde{\mathcal{H}} := \frac{i}{h} \Omega$ can also be express as a linear combination

of unitaries,

$$\tilde{\mathcal{H}} = \sum_{j=1}^d u_j \mathcal{U}_j = \sum_{k=1}^M \sum_{\alpha \in \{X,Y,Z\}} \frac{\mathbf{a}_k^\alpha}{h} \alpha_k + \frac{1}{2} \sum_{j=1}^M \sum_{k=1}^M \sum_{\alpha \in \{X,Y,Z\}} \sum_{\beta \in \{X,Y,Z\}} C_{j,k}^{\alpha,\beta} \alpha_j \beta_k, \quad (54)$$

since α_k are unitary, and products of the unitaries $\alpha_j \beta_k$ is also unitary. In particular, $\tilde{\mathcal{H}}$ is a linear combination of $d = 3M + |C_{\text{in}}|$ unitaries, where $|C_{\text{in}}| \leq 9M(M-1)$ is the number of non-zero elements of the interaction tensor. If we assume symmetry of couplings, $C^{\alpha,\beta^\top} = C^{\alpha,\beta}$, we can express $\tilde{\mathcal{H}}$ as a linear combination of $d = 3M + \frac{1}{2}|C_{\text{in}}|$ unitaries. Further reductions are possible if mixed-couplings are eliminated by a suitable change of basis [85].

Let C_1 be the cost of implementing the unitary operator α_k in terms of the number of single-qubit gates (typically $C_1 = 1$), and let $C_{2,1}$ and $C_{2,2}$ be the cost of implementing the unitary operator $\alpha_j \beta_k$ in terms of the number of single-qubit and two-qubit gates, respectively, then a single query of the Hamiltonian oracle in the BCCKS or qubitization procedure requires $3MC_1 + |C_{\text{in}}|C_{2,1}$ single-qubit gates and $|C_{\text{in}}|C_{2,2}$ two-qubit gates (with $|C_{\text{in}}|$ being replaced by $\frac{1}{2}|C_{\text{in}}|$ if couplings are symmetric).

The exponential of the time-independent Hamiltonian \mathcal{H}_0 can be computed directly (*i.e.*, without time-stepping) using the qubitization procedure at the optimal query complexity (51). However, the second-order Magnus expansion $\Theta_1(t_n)$ and the piecewise-constant Hamiltonian $\mathcal{H}(t_n)$ both require time-stepping with a time-step h that is expected to be small. Both BCCKS and qubitization can be used in the time-stepping procedures (25) and (50), at the suboptimal query complexity (53). The gate complexity of the oracle in all three cases (time-independent, piecewise constant, and second-order Magnus expansion) is identical since they all conform to the structure (39). We note that the error in the Magnus expansions increases with the spectral radius, eq. (25), and as the number of spins, the connectivity, strength of controls, or coupling strengths increase, we need smaller time-steps due to an increase in spectral radius ρ , eq. (12). As mentioned previously, in the small time-step regime BCCKS is as effective as qubitization, and arguably simpler.

The direct application of BCCKS or qubitization to computing the exponential of the fourth-order Magnus expansion (31) in the context of the time-stepping procedure (25) becomes substantially more expensive due to the commutator term,

$$\left[\mathbf{u}(t_n)^\top \mathbb{S}, \mathbb{S}^\top C_{\text{in}} \mathbb{S} \right]. \quad (34)$$

By Theorem 1, the commutator term involves $\mathcal{O}(|C_{\text{in}}|M) \leq \mathcal{O}(M^3)$ three-way unitary terms of the form $\alpha_j \beta_k \gamma_\ell$. The direct implementation of the effective Hamiltonian, $\tilde{\mathcal{H}} = \frac{1}{h} \Theta_2(t_n)$, in this case requires an additional $\mathcal{O}(|C_{\text{in}}|M)$ three-qubit gates. This makes the gate complexity of the oracle extremely high and a direct application of BCCKS and qubitization to a fourth-Magnus expansion becomes prohibitively expensive in gate count and circuit depth. However, similar to the Trotterization case discussed in Section 3.1, this prohibitive cost is possible to avoid by eliminating the commutator (34) using the technique presented in Section 3.3, or when considering the special case described in Section 3.4.

3.3 Eliminating commutators

As we have seen in Sections 3.1 and 3.2, the commutator (34) is highly undesirable due to the prohibitive increase in circuit depths and gate counts, in both Trotterization and qubitization procedures. It seems reasonable to assume that once a commutator appears in a Magnus expansion, it must also appear in its splitting, and the additional cost due

to this commutator is unavoidable in fourth-order Magnus-based methods. However, by composition with carefully chosen exponentials it is possible to eliminate commutators even in sixth-order Magnus expansions [73]. We show that an asymmetric composition can eliminate the undesirable commutator term in our fourth-order Magnus expansion (31).

Theorem 2. The exponential of the fourth-order Magnus expansion $\Theta_2(t_n)$, eq. (31), can be approximated by the composition

$$e^{-E(t_n)}e^{W(t_n)}e^{E(t_n)} = e^{\Theta_2(t_n)} + \mathcal{O}(h^5), \quad (55)$$

where

$$E(t_n) = -i\frac{2}{h}\mathbf{u}(t_n)^\top \mathbb{S} \quad (56)$$

involves only single-spin terms, and

$$W(t_n) = -i\tilde{\mathbf{r}}(t_n)^\top \mathbb{S} - i\frac{h}{2}\mathbb{S}^\top C_{\text{in}}\mathbb{S} \quad (57)$$

is a term which conforms to the structure eq. (39), with

$$\tilde{\mathbf{r}}(t_n) = \mathbf{r}(t_n) + \frac{4}{h}(\mathbf{u}(t_n) \times \mathbf{r}(t_n)) \in \mathbb{C}^{3M}. \quad (58)$$

Here the cross product $\mathbf{c} = (\mathbf{a} \times \mathbf{b})$ is such that $\mathbf{c}_k = \mathbf{a}_k \times \mathbf{b}_k$ for $k = 1, \dots, 3M$, is the usual cross product on \mathbb{R}^3 , *i.e.* \times is the cross product with the Hadamard product \odot being underlying product.

Moreover, there exist constants \hat{c}_1 and \hat{c}_2 such that

$$\left\| e^{-E(t_n)}e^{W(t_n)}e^{E(t_n)} - e^{\Theta_2(t_n)} \right\| \leq \left(\hat{c}_1 M^2 \gamma_n^2 \rho_n + \hat{c}_2 M \gamma_n \rho_n^3 \right) h^5, \quad (59)$$

where $\gamma_n = \max_{t \in [t_n, t_{n+1}]} \|\mathbf{e}'(t)\|_\infty$ depends on the maximum frequency of the controls in the interval $[t_n, t_{n+1}]$, and $\rho_n = \max_{t \in [t_n, t_{n+1}]} \|\mathcal{H}(t)\|$ is the maximum spectral radius of the time-dependent Hamiltonian over this interval, which is the single time-step version of eq. (11).

Proof. The right hand side of eq. (55) can be expressed in terms of the *Baker–Campbell–Hausdorff* (BCH) expansion [92, 93],

$$e^{-E(t_n)}e^{W(t_n)}e^{E(t_n)} = e^{\tilde{\Theta}_2(t_n)}, \quad (60)$$

where

$$\tilde{\Theta}_2(t_n) := \text{BCH}(\text{BCH}(-E(t_n), W(t_n)), E(t_n)). \quad (61)$$

The asymmetric splitting in eqs. (60) and (61) is typically associated with a first-order approximation. However, for the specific choice of $E(t_n)$ and $W(t_n)$, we demonstrate that $\tilde{\Theta}_2(t_n)$ provides a fourth-order approximation of the fourth-order Magnus expansion $\Theta_2(t_n)$. We note in passing that the composition in eq. (60) is also a similarity transformation, although we do not explicitly exploit this fact here.

Since we seek a fourth-order approximation, we can ignore $\mathcal{O}(h^5)$ and smaller terms in the BCH expansions. In particular, commutators with four or more letters can be

ignored since these must feature at least one occurrence of $E(t_n) = \mathcal{O}(h^2)$, and since $W(t_n) = \mathcal{O}(h)$. Expanding both BCH series in eq. (61), we find

$$\begin{aligned}
\tilde{\Theta}_2(t_n) &= W + \underbrace{E - E}_{=0} + \frac{1}{2}[-E, W] + \frac{1}{2}[W, E] - \underbrace{\frac{1}{12}[W, [-E, W]] + \frac{1}{12}[W, [W, E]]}_{=0} \\
&\quad + \underbrace{\frac{1}{2}[-E, E] + \frac{1}{12}[-E, [-E, E]] + \frac{1}{12}[W, [-E, E]] - \frac{1}{12}[E, [-E, E]]}_{=0} \\
&\quad + \underbrace{\frac{1}{12}[-E, [-E, W]] + \frac{1}{4}[[-E, W], E] + \frac{1}{12}[-E, [W, E]] - \frac{1}{12}[E, [W, E]]}_{=\mathcal{O}(h^5)} + \mathcal{O}(h^5) \\
&= W(t_n) - [E(t_n), W(t_n)] + \mathcal{O}(h^5),
\end{aligned} \tag{62}$$

where we have written E and W as short form for $E(t_n)$ and $W(t_n)$, respectively. In the commutators involving three letters, instances with two occurrences of E are also $\mathcal{O}(h^5)$, and have been discarded.

Substituting eqs. (56) to (58) into eq. (62),

$$\begin{aligned}
\tilde{\Theta}_2(t_n) &= W(t_n) + \frac{2}{h}[\mathbf{u}(t_n)^\top \mathbb{S}, \mathbf{r}(t_n)^\top \mathbb{S}] + \frac{8}{h^2}[\mathbf{u}(t_n)^\top \mathbb{S}, (\mathbf{u}(t_n) \times \mathbf{r}(t_n))^\top \mathbb{S}] \\
&\quad + [\mathbf{u}(t_n)^\top \mathbb{S}, \mathbb{S}^\top C_{\text{in}} \mathbb{S}] + \mathcal{O}(h^5) \\
&= W(t_n) + \frac{2}{h}[\mathbf{u}(t_n)^\top \mathbb{S}, \mathbf{r}(t_n)^\top \mathbb{S}] + [\mathbf{u}(t_n)^\top \mathbb{S}, \mathbb{S}^\top C_{\text{in}} \mathbb{S}] + \mathcal{O}(h^5) \\
&= \underbrace{-i\mathbf{r}(t_n)^\top \mathbb{S} - i\frac{h}{2}\mathbb{S}^\top C_{\text{in}} \mathbb{S} + [\mathbf{u}(t_n)^\top \mathbb{S}, \mathbb{S}^\top C_{\text{in}} \mathbb{S}]}_{\Theta_2(t_n)} \\
&\quad - i\frac{4}{h}(\mathbf{u}(t_n) \times \mathbf{r}(t_n))^\top \mathbb{S} + \frac{2}{h}[\mathbf{u}(t_n)^\top \mathbb{S}, \mathbf{r}(t_n)^\top \mathbb{S}] + \mathcal{O}(h^5)
\end{aligned}$$

where $\frac{8}{h^2}[\mathbf{u}(t_n)^\top \mathbb{S}, (\mathbf{u}(t_n) \times \mathbf{r}(t_n))^\top \mathbb{S}] = \mathcal{O}(h^5)$ is discarded since $\mathbf{u}(t_n) = \mathcal{O}(h^3)$ and $\mathbf{r}(t_n) = \mathcal{O}(h)$.

In Appendix B we show that

$$[\mathbf{u}(t_n)^\top \mathbb{S}, \mathbf{r}(t_n)^\top \mathbb{S}] = 2i(\mathbf{u}(t_n) \times \mathbf{r}(t_n))^\top \mathbb{S}. \tag{63}$$

Thus,

$$\tilde{\Theta}_2(t_n) = \Theta_2(t_n) + \mathcal{O}(h^5),$$

and

$$e^{-E(t_n)}e^{W(t_n)}e^{E(t_n)} = e^{\tilde{\Theta}_2(t_n)} = e^{\Theta_2(t_n)} + \mathcal{O}(h^5).$$

Overall, in the BCH formula, the leading terms that are discarded either have two occurrences of $E(t_n)$ and one of $W(t_n)$, or one occurrence of $E(t_n)$ and three of $W(t_n)$. The only other term discarded is $\frac{8}{h^2}[\mathbf{u}(t_n)^\top \mathbb{S}, (\mathbf{u}(t_n) \times \mathbf{r}(t_n))^\top \mathbb{S}]$ which is certainly smaller than $\|E(t_n)\|\|W(t_n)\|$. Thus the leading error term is proportional to $\|E(t_n)\|^2\|W(t_n)\|$ and $\|E(t_n)\|\|W(t_n)\|^3$.

By Taylor expanding $\mathbf{e}(t + \zeta)$ at t , $\mathbf{e}(t + \zeta) = \mathbf{e}(t) + \zeta\mathbf{e}'(t + \xi)$ for some $\xi \in [0, \zeta] \subseteq [0, h]$, and substituting in eq. (32), we can get the bound

$$\|E(t_n)\| \leq \frac{3M}{h}\gamma_n \int_0^h \left(\zeta - \frac{h}{2}\right) \zeta d\zeta = \frac{M\gamma_n}{4}h^2,$$

where $\gamma_n = \max_{t \in [t_n, t_{n+1}]} \|\mathbf{e}'(t)\|_\infty$. By a similar application of Taylor series to the approximation of the integral in $\tilde{\mathbf{r}}$ (58) and the definition of the wedge product (30) we can show that there exists \hat{c}_3 such that

$$\|W(t_n)\| \leq \|\boldsymbol{\mu}(t_n)^\top \mathbb{S} + \frac{h}{2} \mathbb{S}^\top C_{\text{in}} \mathbb{S}\| + \|(\tilde{\mathbf{r}}(t_n) - \boldsymbol{\mu}(t_n))^\top \mathbb{S}\| \leq \rho_n h + \hat{c}_3 M \nu_n \gamma_n h^3,$$

where $\nu_n = \max_{t \in [t_n, t_{n+1}]} \|\mathbf{e}(t)\|_\infty$ is the maximum intensity of the controls in this interval. *i.e.*, up to $\mathcal{O}(h^3)$, the norm of $W(t_n)$ is approximated by the norm of $h\mathcal{H}(t_n)$. Equation (59) follows from substituting these bounds in the leading error terms, $\|\mathbf{E}(t_n)\|^2 \|W(t_n)\|$ and $\|\mathbf{E}(t_n)\| \|W(t_n)\|^3$. \square

The crucial achievement in Theorem 2 is that $W(t_n)$ has the structure (39). In particular, unlike the fourth-order Magnus expansion Θ_2 , eq. (31), it does not have any commutators. When utilizing qubitization in a time-stepping procedure, the cost of exponentiating $W(t_n)$ is no more expensive than a single step when time-stepping with a piecewise-constant Hamiltonian or the second-order Magnus expansion Θ_1 . In a Trotterized approach, the exponential of $W(t_n)$ needs to be computed to fourth-order accuracy using the Yoshida splitting eq. (46), the cost of which is identical to a single step of a fourth-order Trotterized time-stepping procedure for a time-independent Hamiltonian.

By approximating the exponential of the fourth-order Magnus expansion using eq. (60), only a small structural modification (*i.e.*, up to changes in gate parameters) to a fourth-order Trotterized circuit for a time-independent Hamiltonian is required: Namely, the additional layers to account for the $e^{\mathbf{E}(t_n)}$ and $e^{-\mathbf{E}(t_n)}$ terms. Similarly, these additional layers either side of a qubitized time-stepping circuit for a piecewise constant Hamiltonians result in a qubitized approach for the fourth-order Magnus expansion (up to changes in gate parameters).

Theorem 3. The exponential of a term $-\mathbf{i}\mathbf{a}^T \mathbb{S}$, which only contains single-spin terms, can be implemented exactly using three layers with M single-spin gates each,

$$e^{-\mathbf{i}\mathbf{a}^T \mathbb{S}} = e^{-\mathbf{i}\boldsymbol{\lambda}^X T \mathbb{S}^X} e^{-\mathbf{i}\boldsymbol{\lambda}^Y T \mathbb{S}^Y} e^{-\mathbf{i}\boldsymbol{\lambda}^Z T \mathbb{S}^Z}, \quad e^{-\mathbf{i}\boldsymbol{\lambda}^\alpha T \mathbb{S}^\alpha} = \bigotimes_{m=1}^M e^{-\mathbf{i}\lambda_m^\alpha \alpha}, \quad (64)$$

where the coefficients λ_m^α satisfy the equations,

$$\begin{aligned} \mathbf{a}_m^X &= q(\boldsymbol{\lambda}_m) \left(\sin(\lambda_m^Z) \sin(\lambda_m^Y) \cos(\lambda_m^X) + \sin(\lambda_m^X) \cos(\lambda_m^Z) \cos(\lambda_m^Y) \right), \\ \mathbf{a}_m^Y &= q(\boldsymbol{\lambda}_m) \left(\sin(\lambda_m^Y) \cos(\lambda_m^Z) \cos(\lambda_m^X) - \sin(\lambda_m^Z) \cos(\lambda_m^Y) \sin(\lambda_m^X) \right), \\ \mathbf{a}_m^Z &= q(\boldsymbol{\lambda}_m) \left(\sin(\lambda_m^Z) \cos(\lambda_m^Y) \cos(\lambda_m^X) + \sin(\lambda_m^Y) \cos(\lambda_m^Z) \sin(\lambda_m^X) \right), \end{aligned} \quad (65)$$

and

$$q(\boldsymbol{\lambda}_m) = p \left(\prod_{\alpha \in \{X,Y,Z\}} \cos(\lambda_m^\alpha) - \prod_{\alpha \in \{X,Y,Z\}} \sin(\lambda_m^\alpha) \right), \quad p(x) = \frac{\arccos(x)}{\sin(\arccos(x))}.$$

Proof of Theorem 3. See Appendix C. \square

It follows from Theorem 3 that $e^{\mathbf{E}(t_n)}$ and $e^{-\mathbf{E}(t_n)}$ can be computed using $3M$ single-qubit gates each, which represents a very marginal increase in gate count and circuit depth for the fourth-order Magnus expansion. The non-linear system of equations, eq. (65), can

be solved on a classical computer a priori, once the integral $\mathbf{u}(t_n)$ has been computed. In the context of its application in the fourth-order Magnus-based method developed here, the solution of λ_m^α only needs to be computed to an accuracy of $\mathcal{O}(h^5)$, but it can be computed to much higher accuracies cheaply, if needed.

3.4 Isotropic Hamiltonians with identical controls

In this section, we demonstrate that for a large class of Hamiltonians appearing in NMR applications, the additional commutator (34) vanishes, and does not require the elimination procedure outlined in Section 3.3. Specifically, we consider Hamiltonians with *isotropic* couplings and identical controls. Hamiltonians of this form appear frequently in the context of liquid-state NMR when there is only one *specie* of NMR active nuclei. In such cases, the time-dependent control pulses that accompany X and Y are identical across all spins and the component accompanying Z is a spin-dependent but time-independent scalar quantity Ω_k which is called a *spin offset* or a *chemical shift*,

$$\mathbf{e}(t) = (p_x(t)\mathbf{1}^\top, p_y(t)\mathbf{1}^\top, \boldsymbol{\Omega}^\top)^\top, \quad \boldsymbol{\Omega} = (\Omega_1, \dots, \Omega_M)^\top \in \mathbb{R}^M,$$

where $\mathbf{1} = (1, \dots, 1)^\top \in \mathbb{R}^M$. The *isotropic* nature of the coupling strengths corresponds to $C^{X,X} = C^{Y,Y} = C^{Z,Z} = C = C^\top \in \mathbb{R}^{M \times M}$ and $C^{\alpha,\beta} = 0$ for $\alpha \neq \beta$, *i.e.* coupling strengths are symmetric and equal in all directions, while mixed couplings are absent. Overall, the interaction tensor C_{in} becomes

$$C_{\text{iso}} = \begin{pmatrix} C & 0 & 0 \\ 0 & C & 0 \\ 0 & 0 & C \end{pmatrix}, \quad C^\top = C, \quad C \in \mathbb{R}^{M \times M}.$$

This is in contrast to the strongly *anisotropic* case commonly encountered in solid-state NMR. In liquid-state NMR, anisotropic interactions are typically averaged out due to molecular motion, especially for isotropic solutions, which simplifies the treatment to isotropic couplings. The same phenomena is responsible for the absence of mixed couplings.

We start by stating an important observation in Lemma 2 that proves helpful in simplifying the fourth-order Magnus expansion in the isotropic case.

Lemma 2.

$$\left[\mathbf{1}^\top \mathbb{S}^\alpha, \sum_{\beta \in \{X,Y,Z\}} \mathbb{S}^\beta^\top C \mathbb{S}^\beta \right] = 0, \quad \alpha \in \{X,Y,Z\}. \quad (66)$$

Proof of Lemma 2. See Appendix D. □

Theorem 4. For isotropic Hamiltonians with identical controls, the fourth-order Magnus expansion in eq. (31) reduces to the form

$$\Theta_2(t_n) = -i\mathbf{r}(t_n)^\top \mathbb{S} - i\frac{h}{2}\mathbb{S}^\top C_{\text{iso}} \mathbb{S}, \quad (67)$$

where

$$\begin{aligned} \mathbf{r}^X(t_n) &= \left(\int_0^h p_x(t_n + \zeta) d\zeta \right) \mathbf{1} + \left(\int_0^h (2\zeta - h) p_y(t_n + \zeta) d\zeta \right) \boldsymbol{\Omega}, \\ \mathbf{r}^Y(t_n) &= \left(\int_0^h p_y(t_n + \zeta) d\zeta \right) \mathbf{1} - \left(\int_0^h (2\zeta - h) p_x(t_n + \zeta) d\zeta \right) \boldsymbol{\Omega}, \\ \mathbf{r}^Z(t_n) &= \left(- \int_0^h \int_0^\zeta (p_x(t_n + \xi) p_y(t_n + \zeta) - p_x(t_n + \zeta) p_y(t_n + \xi)) d\xi d\zeta \right) \mathbf{1} + h\boldsymbol{\Omega}. \end{aligned} \quad (68)$$

Proof of Theorem 4. The integral \mathbf{r} is as defined in eq. (33) but assume a simpler form due to the identical controls in the Hamiltonian – in particular, we only need four scalar integrals over an interval and one scalar integral over a triangular region. Similarly, $\mathbf{u}(t_n)$, eq. (32), simplifies to

$$\begin{aligned}\mathbf{u}^X(t_n) &= \left(\frac{1}{2} \int_0^h (2\zeta - h) p_x(t_n + \zeta) d\zeta \right) \mathbf{1}, \\ \mathbf{u}^Y(t_n) &= \left(\frac{1}{2} \int_0^h (2\zeta - h) p_y(t_n + \zeta) d\zeta \right) \mathbf{1}, \\ \mathbf{u}^Z(t_n) &= \frac{1}{2} \int_0^h (2\zeta - h) \Omega d\zeta = 0.\end{aligned}\tag{69}$$

Due to $\mathbf{u}^Z(t_n) = 0$, the commutator (34) becomes

$$\begin{aligned}\frac{1}{2} \left(\int_0^h (2\zeta - h) p_x(t_n + \zeta) d\zeta \right) [\mathbf{1}^\top \mathbb{S}^X, \mathbb{S}^\top C_{\text{iso}} \mathbb{S}] \\ + \frac{1}{2} \left(\int_0^h (2\zeta - h) p_y(t_n + \zeta) d\zeta \right) [\mathbf{1}^\top \mathbb{S}^Y, \mathbb{S}^\top C_{\text{iso}} \mathbb{S}].\end{aligned}\tag{70}$$

However, by Lemma 2 both commutators in eq. (70) vanish. \square

As a consequence of Theorem 4, the fourth-order Magnus expansion for isotropic Hamiltonians, eq. (67), has the structure (39). Consequently, time-stepping with the fourth-order Magnus expansion (67) combined with the fourth-order Yoshida splitting (46) is precisely as costly as time-stepping with a time-independent Hamiltonian using the fourth-order Yoshida splitting. When combined with a qubitization procedure, it is as expensive time-stepping with piecewise-constant Hamiltonian, while providing a fourth-order accuracy in contrast to the first-order accuracy of the latter. Moreover, we can utilize circuits with an identical structure.

Remark 8. While the structure of the fourth-order Magnus expansion $\Theta_2(t_n)$, eq. (67), is the same as the second-order Magnus expansion $\Theta_1(t_n)$, eq. (27), it should be noted that the values of the singles-spin parameters are different – while these are given by the integral $\boldsymbol{\mu}(t_n)$, eq. (28), for the second-order Magnus expansion, the integrals $\mathbf{r}(t_n)$, eq. (33) and eq. (68), for the fourth-order Magnus expansion involve additional terms. These additional terms are essential for the fourth-order accuracy.

3.5 Other methods without commutators

In Section 3.3, we developed a novel technique for eliminating commutators appearing in the fourth-order Magnus method, while in Section 3.4 we find that for Hamiltonians of certain types these commutators vanish by themselves. The appearance of commutators is a problem that occurs specifically in high-order Magnus-based methods for time-dependent Hamiltonians, which has been a hurdle in their adoption for Hamiltonian simulation using quantum circuits. However, these are not the only methods for time-dependent Hamiltonians that are able to avoid commutators. In this subsection we mention two notable alternatives that can handle arbitrary time-dependent (not just time-periodic) Hamiltonians without using commutators, and which lead to comparable circuits.

Commutator-free or quasi-Magnus methods. Commutator-free methods [94], also called quasi-Magnus methods [95], are specifically designed to sidestep the need for

computing commutators in the Magnus expansion. Specifically, they approximate the exponential of the Magnus expansion by a product of two or more exponentials, each of which is free of commutators but involves linear combinations of the Hamiltonian evaluated at different time knots or of its integrals. In particular, we will consider the CF42 integrator [94],

$$U(T, 0) \approx \prod_{n=0}^{N-1} U_n = \prod_{n=0}^{N-1} \exp\left(\frac{1}{2}\mathcal{A}_1(t_n) + \frac{1}{3}\mathcal{A}_2(t_n)\right) \exp\left(\frac{1}{2}\mathcal{A}_1(t_n) - \frac{1}{3}\mathcal{A}_2(t_n)\right), \quad (71)$$

where

$$\mathcal{A}_1(t_n) = \int_0^h \mathcal{A}(t_n + \zeta) d\zeta, \quad \mathcal{A}_2(t_n) = 3 \int_0^h \left(\frac{2\zeta}{h} - 1\right) \mathcal{A}(t_n + \zeta) d\zeta.$$

The prefix ‘CF4’ in CF42 indicates its status as a fourth-order integrator, whereas the suffix ‘2’ highlights an optimization in the integrator’s design. It is notable that in this approach, despite the vanishing of nested commutator, the number of exponential stages doubles, which is undesirable in terms of the depth of the quantum circuit.

Autonomization. A standard technique for converting a non-autonomous system of ordinary differential equations (ODEs),

$$x' = f(x, t), \quad x(0) = x_0 \in \mathbb{R}^d,$$

to an autonomous system is to consider a coupled system of ODEs,

$$\begin{aligned} x' &= f(x, \tau), & x(0) &= x_0 \in \mathbb{R}^d, \\ \tau' &= 1, & \tau(0) &= 0 \in \mathbb{R}, \end{aligned} \quad (72)$$

where the derivative in x' and τ' are with respect to t . The technique of introducing an ‘artificial’ time variable τ to transform nonautonomous problems into autonomous problems is a well-established concept [96, 97], which has been applied widely in classical algorithms for Hamiltonian simulation [98]. When considering

$$f(x, t) = f_1(x, t) + f_2(x) + f_3(x, t),$$

i.e., where one of the components (here f_2) is not explicitly time-dependent, we can approximate the solution of eq. (72) by creating an augmented state (x, τ) , and considering the Trotter splitting in terms of *flows* [18, 19, 99],

$$(x_{n+1}, \tau_{n+1}) \approx \Phi_h^{[3]} \circ \Phi_h^{[2]} \circ \Phi_h^{[1]}(x_n, \tau_n), \quad (73)$$

where $\Phi_h^{[j]}$ is the flow under f_j , for $j = 1, 2, 3$. In particular, the computation of

$$(x_{n+1}^{[1]}, \tau_{n+1}^{[1]}) := \Phi_h^{[1]}(x_n, \tau_n)$$

corresponds to freezing $\tau = t_n$ and solving

$$y' = f_1(y, \tau), \quad y(0) = x_n, \quad (74)$$

exactly for time h with initial condition x_n , *i.e.*, $x_{n+1}^{[1]} := y(h)$ and $\tau_{n+1}^{[1]} = t_n$. The second step of eq. (73) involves computing $(x_{n+1}^{[2]}, \tau_{n+1}^{[2]}) = \Phi_h^{[2]}(x_{n+1}^{[1]}, \tau_{n+1}^{[1]})$ by solving the system of equations,

$$\begin{aligned} y' &= f_2(y), & y(0) &= x_{n+1}^{[1]}, \\ s' &= 1, & s(0) &= \tau_{n+1}^{[1]} = t_n, \end{aligned} \quad (75)$$

for time h with initial conditions $(x_{n+1}^{[1]}, t_n)$, *i.e.*, $x_{n+1}^{[2]} := y(h)$ and $\tau_{n+1} := s(h) = t_{n+1}$. Lastly, we solve

$$y' = f_2(y, \tau), \quad y(0) = x_{n+1}^{[2]}, \quad (76)$$

for time h with initial condition $(x_{n+1}^{[2]}, t_{n+1})$ and with $\tau = t_{n+1}$ frozen, *i.e.*, $x_{n+1} := y(h)$, completing one step of eq. (73). Note that eqs. (74) to (76) are all autonomous.

When considering linear non-autonomous equations, with

$$f_1(|\psi\rangle, \tau) = -i\mathcal{H}^x(\tau)|\psi\rangle, \quad f_2(|\psi\rangle) = -i\mathcal{H}^z|\psi\rangle, \quad f_3(|\psi\rangle, \tau) = -i\mathcal{H}^y(\tau)|\psi\rangle,$$

the corresponding flows are

$$\begin{aligned} \Phi_{\alpha h}^{[1]}(|\psi\rangle, \tau) &= \left(e^{-i\alpha h \mathcal{H}^x(\tau)} |\psi\rangle, \tau \right), \\ \Phi_{\alpha h}^{[2]}(|\psi\rangle, \tau) &= \left(e^{-i\alpha h \mathcal{H}^z} |\psi\rangle, \tau + \alpha h \right), \\ \Phi_{\alpha h}^{[3]}(|\psi\rangle, \tau) &= \left(e^{-i\alpha h \mathcal{H}^y(\tau)} |\psi\rangle, \tau \right), \end{aligned}$$

i.e., the *internal* time variable τ only advances with the flow of \mathcal{H}^z , which is the autonomous component, and does so proportional to αh where $\alpha \in \mathbb{R}$ is a splitting coefficient.

Effectively, the autonomization approach involves applying a series of exponential operators in a time-sequential manner, each corresponding to the Hamiltonian sampled at specific times. For instance, the autonomization approach for the Yoshida 4th-order method in eq. (46) yields the splitting,

$$e^{-i\alpha_{13}\mathcal{H}^x(\tau_6)} e^{-i\alpha_{12}\mathcal{H}^z} e^{-i\alpha_{11}\mathcal{H}^y(\tau_5)} \dots e^{-i\alpha_3\mathcal{H}^y(\tau_1)} e^{-i\alpha_2\mathcal{H}^z} e^{-i\alpha_1\mathcal{H}^x(\tau_0)}, \quad (77)$$

where the internal time progression is defined by

$$\tau_k = \tau_{k-1} + h\alpha_{2k}, \quad \tau_0 = t_n, \quad k \in \{1, \dots, 6\},$$

where α_k are the coefficients of the splitting in eq. (46).

4 Trotterized quantum circuit construction

As we have seen in Section 3.4, in the case of isotropic Hamiltonians with identical controls, the fourth-order Magnus expansion does not have any commutators, and has the form (39). For general Hamiltonians, the commutator in the fourth-order Magnus expansion can be eliminated due to Theorem 2, and each time-step involves the computation of $e^{-E(t_n)} e^{W(t_n)} e^{E(t_n)}$, where $e^{-E(t_n)}$ and $e^{E(t_n)}$ are single-spin terms and $W(t_n)$ has the form (39). Thus, central exponential $e^{W(t_n)}$ in eq. (55) or the exponential of the fourth-order Magnus expansion for isotropic Hamiltonians with identical controls, eq. (67), can be implemented on the QPU by Trotterization, BCCKS [13] or qubitization [16], as outlined in Sections 3.1 and 3.2.

In this section, we discuss how to design a Trotterized quantum circuit to implement the time-stepping procedure in eq. (22) or eq. (25) for the fourth-order Magnus expansions, eqs. (55) and (67). Along the lines of Section 3.1, in this section we assume the absence of mixed couplings, $C^{\alpha, \beta} = 0$ for $\alpha \neq \beta$.

We start by presenting a fourth-order Trotterized circuit for computing the exponential of a matrix of the form eq. (39). In the absence of mixed couplings, $\Omega = \Omega^X + \Omega^Y + \Omega^Z$, scaled exponentials of each component, $e^{s\Omega^\alpha}$, can be computed to fourth-order accuracy using eqs. (43) and (46). In eq. (43) we have assumed symmetric couplings, $C^{\alpha, \alpha^\top} = C^{\alpha, \alpha}$,

which has allowed us to halve the exponents in the coupling term. A generalization of the circuit presented in this section to non-symmetric couplings (42) is straightforward.

The exponential of a single component, $e^{s\Omega^\alpha}$ in eq. (43), contains terms of the form $e^{-ic\alpha_k}$ and $e^{-ic\alpha_j\alpha_k}$, where c are some real-valued scalars. The circuit implementation of these terms is hardware dependent. The single-spin term $e^{-ic\alpha_k}$ can be implemented in a quantum circuit as a rotation or a Pauli- α gate, $\alpha \in \{X, Y, Z\}$, acting on the k -th qubit as shown in Figure 1. Rotation gates are available on many quantum computing architectures as elementary single-qubit gates, but can always be created with the composition of a few single-qubit gates on all architectures. A term $e^{-ic\alpha_k}$ with scalar parameter c is implemented by the rotation gate $R_\alpha(\theta)$ with $\theta = 2c$.

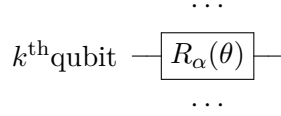


Figure 1: α rotation gates implement the single-spin terms $e^{-ic\alpha_k}$, with $\theta = 2c$.

The pairwise coupling term $e^{-ic\alpha_j\alpha_k}$ can be implemented in a quantum circuit as an Ising coupling gate acting on two qubits, the j -th qubit and the k -th qubit, as shown on the left of Figure 2. A term $e^{-ic\alpha_j\alpha_k}$ with parameter c can be implemented by the Ising coupling gate $R_{\alpha\alpha}(\theta)$ with $\theta = 2c$. Ising coupling gates are less commonly available natively, *i.e.*, as elementary gates. On such architectures, they can be implemented as a combination of elementary gates, for example as shown on the right of Figure 2. Here we have assumed an architecture with full connectivity. In practise, many swap gates are required to overcome the limited connectivity which is more typical of many current quantum architectures. In the case that coupling interactions are not dense, *i.e.*, each spin is coupled only to a few other spins, the optimal assignment of spins to physical qubits (in terms of swap gate counts) can depend heavily on the underlying connectivity as well as the sparsity pattern of the interaction tensor C_{in} .

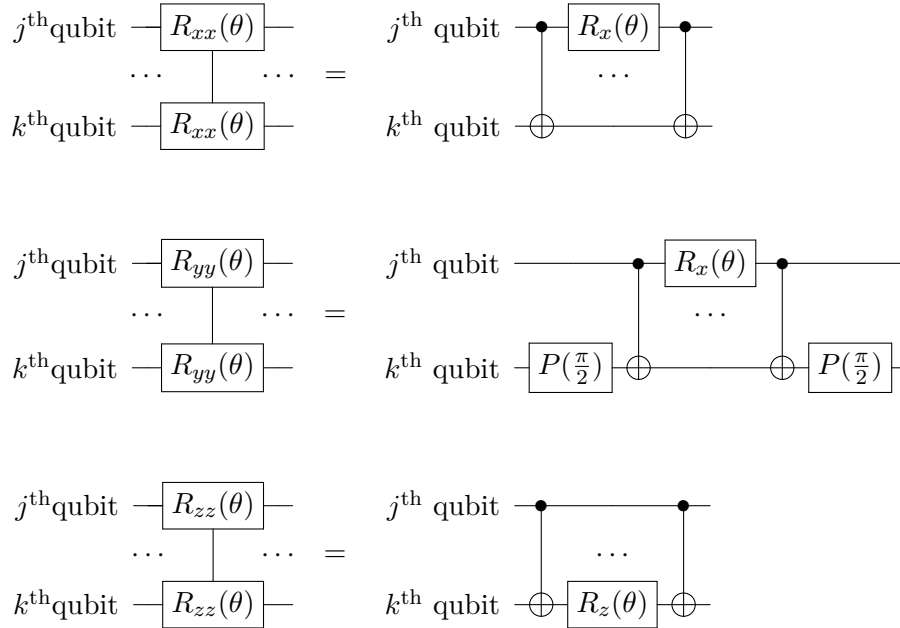


Figure 2: $\alpha\alpha$ Ising coupling gates implement the exponential of two-spin couplings, $e^{-ic\alpha_j\alpha_k}$, with $\theta = 2c$.

Overall, each component $e^{s\Omega^\alpha}$ in eq. (43) can be implemented by a block of single-qubit (fig. 1) and two-qubit (fig. 2) gates as depicted in the circuit in fig. 3 (c).

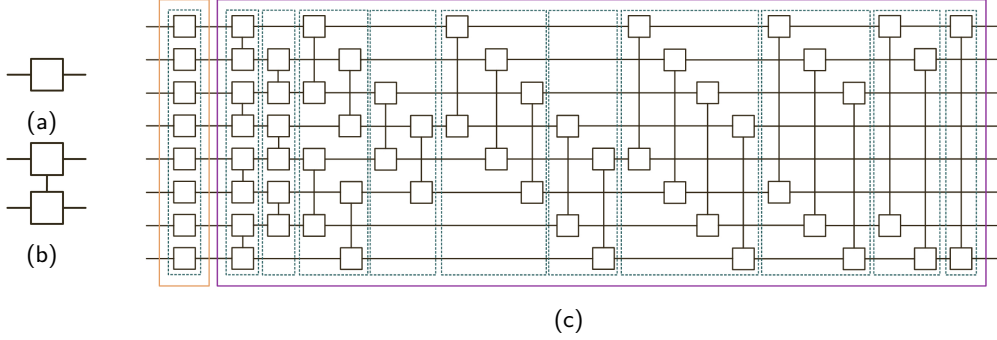


Figure 3: Block example for implementing eq. (43) for 8 qubits. (a) and (b) represent single rotation gates and coupling gates respectively. Gates circled in the orange box in (c) are the single-qubit rotation gates, and gates circled in the purple box in (c) are the two-qubit coupling gates. In each green box, the gates could be conducted parallelly, so each green box adds depth 1 to the circuit.

A fourth-order approximation of the exponential of eq. (39) requires the fourth-order Yoshida splitting, eq. (46). As noted in Section 3, time-stepping with eq. (46) involves (on average) half the number of e^{hC} and e^{hA} terms compared to e^{hB} (3 vs 6). Thus it is desirable to keep the splitting component B the simplest in terms of gate and circuit complexity. The optimal choices varies with the qubit connectivity and elementary gates available in the quantum architecture, as well as the sparsity of spin couplings in the interaction tensor C_{in} . Given fully dense interactions and a fully connected architecture where the coupling gates are not available and need to be implemented as the compositions shown on the right side of fig. 2, for instance, the YY Ising gate R_{yy} is the most expensive in terms of elementary gates, while R_{xx} and R_{zz} are less expensive. In such a case a reasonable choice of components in the splitting (46) is

$$hA = \Omega^X, \quad hB = \Omega^Z, \quad hC = \Omega^Y, \quad (78)$$

resulting in the following Trotterization,

$$\begin{aligned} \Upsilon &:= e^{\frac{x}{2}\Omega^X} \Gamma e^{\frac{x}{2}\Omega^X} \approx e^\Omega, \\ \Gamma &= e^{\frac{x}{2}\Omega^Z} e^{x\Omega^Y} e^{\frac{x}{2}\Omega^Z} e^{\frac{x+y}{2}\Omega^X} e^{\frac{y}{2}\Omega^Z} e^{y\Omega^Y} e^{\frac{y}{2}\Omega^Z} e^{\frac{x+y}{2}\Omega^X} e^{\frac{x}{2}\Omega^Z} e^{x\Omega^Y} e^{\frac{x}{2}\Omega^Z}. \end{aligned} \quad (79)$$

For the isotropic Hamiltonians considered in Section 3.4, the Trotterization (79) suffices for exponentiating the fourth-order Magnus expansion, eq. (67) by setting $\Omega := \Theta_2(t_n) = -i\mathbf{r}(t_n)^\top \mathbb{S} - i\frac{h}{2}\mathbb{S}^\top C_{\text{iso}}\mathbb{S}$. As mentioned previously, the circuit structure and gate count is identical to a fourth-order Trotterized circuit for a time-independent Hamiltonian.

For general Hamiltonians, where a single time-step involves computing $e^{-E(t_n)}e^{W(t_n)}e^{E(t_n)}$, we set $\Omega := W(t_n) = -i\tilde{\mathbf{r}}(t_n)^\top \mathbb{S} - i\frac{h}{2}\mathbb{S}^\top C_{\text{in}}\mathbb{S}$, eq. (57), for the central exponent. Due to Theorem 3, the single-spin term $e^{E(t_n)}$ can be implemented as

$$e^{E(t_n)} = e^{\tilde{E}(t_n)^x} e^{\tilde{E}(t_n)^y} e^{\tilde{E}(t_n)^z},$$

using three layers of M single-qubit rotation gates each, where the parameters of the rotation gates in eq. (64) are computed by solving the non-linear system of equations eq. (65). $e^{-E(t_n)}$ is obtained from the expression for $e^{E(t_n)}$ by negating the sign and

reversing the order of the exponentials. Overall, each time-step of the fourth-order Magnus expansion for general Hamiltonians has the form

$$\tilde{\Upsilon} := e^{-\tilde{E}^Z} e^{-\tilde{E}^Y} e^{-\tilde{E}^X + \frac{x}{2}\Omega^X} \Gamma e^{\frac{x}{2}\Omega^X + \tilde{E}^X} e^{\tilde{E}^Y} e^{\tilde{E}^Z} \approx e^{\Theta_2}. \quad (80)$$

where Γ is as defined in eq. (79), and the $-\tilde{E}^X$ and \tilde{E}^X terms are subsumed along with $\frac{x}{2}\Omega^X$, with which they commute due to Lemma 1.

4.1 Error estimates

Theorem 5. *Let $\tilde{\Upsilon}(t_n)$ be the Magnus-based method described in eq. (80) for time-stepping over the interval $[t_n, t_{n+1}]$. There exists a constant c such that*

$$\left\| U(T, 0) - \prod_{n=1}^{N-1} \tilde{\Upsilon}(t_n) \right\| \leq cT \left[\rho^4 + M\gamma\rho (M\gamma + \rho^2) + \gamma\rho^3 \right] h^4, \quad h \rightarrow 0, \quad Nh = T, \quad (81)$$

where $\gamma = \max_{t \in [0, T]} \|\mathbf{e}'(t)\|_\infty$ is related to the maximum frequency of the controls in the interval $[0, T]$, and ρ is the maximum spectral radius of the Hamiltonian over $[0, T]$, eq. (11).

Proof. The proof follows in a straightforward way from the local error estimates of the splitting error (48), the local error estimates of the commutator elimination error (59), and the global error estimates of the Magnus expansion (25).

In particular, for the splitting error, eq. (48), we use the fact that $\|\mathcal{H}^\alpha(t)\| \leq \|\mathcal{H}(t)\|$ for $\alpha \in \{X, Y, Z\}$ so that $\max\{\|A\|, \|B\|, \|C\|\} \leq \rho$, and its contribution to the global error is $CT\rho^4 h^4$. Note that since the equation eq. (1) is a linear equation, and the time-evolution operators and their approximations are unitary, the methods described in this paper are unconditionally stable. In fact, due to unitarity, the local errors accumulate linearly [63]. \square

From eq. (81) we note that unless γ is very large (i.e., the frequency of the controls increases excessively), we can assume that the largest term is the $\rho^4 h^4$ error due to Yoshida splitting, giving an upper bound $cT(\rho h)^4$. Thus for accuracy $cT(\rho h)^4 \leq \varepsilon$, we need a time-step size

$$h = \mathcal{O} \left(\frac{1}{\rho} \left(\frac{\varepsilon}{T} \right)^{1/4} \right)$$

and a total of

$$N = \mathcal{O} \left(\rho \left(\frac{T}{\varepsilon} \right)^{1/4} \right) \quad (82)$$

time-steps of eq. (80). The complexity of the number of time steps obtained here is multiplicative in terms of the accuracy and spectral radius, unlike the additive complexity of the qubitization procedure, eq. (53).

Remark 9. *As before, in a time-stepping procedure, the first and last exponents can be combined. It should be noted that in eq. (80), E^α stands for $E^\alpha(t_n)$, i.e., its value changes across time-steps. Thus, while $e^{-\frac{1}{2}E^Z(t_n)}$ can be combined with $e^{-\frac{1}{2}E^Z(t_{n+1})}$ from the next time-step, they do not cancel out.*

Remark 10. *Compared to the circuit for fourth-order Trotterized time-stepping with a time-independent Hamiltonian, the additional cost of each time-step for time-stepping with eq. (80), on average, is $3M$ single-qubit gates due to the 3 terms of the form e^{sE^α} , and M single-qubit gates and $\frac{1}{2}|C^{X,X}|$ two-qubit gates due to the Ω^X that can no longer be combined across consecutive time-steps.*

4.2 Circuit complexity per time-step

The overall time-stepping procedure (25) involves N steps of the fourth-order Trotterization – eq. (80) for general Hamiltonians and eq. (79) for isotropic Hamiltonians. We pre-compute the vectors of integrals – $\mathbf{r}(t_n), \mathbf{u}(t_n) \in \mathbb{C}^{3M}$, eqs. (32) and (33), for the general case and $\mathbf{r}(t_n) \in \mathbb{C}^{3M}$, eq. (68), for the isotropic case – for each time-step, $n = 1, \dots, N$, on a classical computer, and input these into the quantum computer as the parameters of the various rotation and coupling gates, as outlined earlier in this subsection.

Method	Order	1-qubit gates	2-qubit gates
--------	-------	---------------	---------------

(a) Time-stepping with Ω , eq. (39).

(i) Coupling gates available, Ω^α assigned to hA, hB, hC arbitrarily.

Trotter, eq. (44)	1	$3MN$	$3N C_{\text{in}} $
Strang, eq. (45)	2	$4MN + M$	$4N C_{\text{in}} + C_{\text{in}} $
Yoshida, eq. (46)	4	$12MN + M$	$12N C_{\text{in}} + C_{\text{in}} $

(ii) Coupling gates implemented as shown in fig. 2, $hA = \Omega^X, hB = \Omega^Z, hC = \Omega^Y$.

Trotter, eq. (44)	1	$(3M + 5 C_{\text{in}})N$	$6 C_{\text{in}} N$
Strang, eq. (45)	2	$(4M + 6 C_{\text{in}})N + M + C_{\text{in}} $	$8 C_{\text{in}} N + 2 C_{\text{in}} $
Yoshida, eq. (46)	4	$(12M + 18 C_{\text{in}})N + M + C_{\text{in}} $	$24 C_{\text{in}} N + 2 C_{\text{in}} $

(b) Time-stepping with $e^{\mathbf{E}}e^{\mathbf{W}}e^{-\mathbf{E}}$, eq. (55).

(i) Coupling gates available, Ω^α assigned to hA, hB, hC arbitrarily.

Modified Yoshida, eq. (80)	4	$16MN + M$	$13 C_{\text{in}} N$
----------------------------	---	------------	----------------------

(ii) Coupling gates implemented as shown in fig. 2, $hA = \Omega^X, hB = \Omega^Z, hC = \Omega^Y$.

Modified Yoshida, eq. (80)	4	$(16M + 19 C_{\text{in}})N + M$	$26 C_{\text{in}} N$
----------------------------	---	----------------------------------	----------------------

Table 1: Gate counts for N time-steps of Trotterized time-stepping for M spins for: Ω , eq. (39) (top two sub-tables, (a) (i) & (a) (ii)) and $e^{\mathbf{E}}e^{\mathbf{W}}e^{-\mathbf{E}}$, eq. (55) (bottom two sub-tables, (b) (i) & (b) (ii)).

The overall gate count and circuit depth required for N time steps of different Trotterized time-stepping methods are enumerated in Tables 1 and 2, respectively. For a time-independent Hamiltonian, \mathcal{H}_0 , a Trotterized time-stepping procedure can involve a first, second, or fourth-order method, depending on the accuracy required. For time-dependent Hamiltonians, a piecewise-constant Hamiltonian, $\mathcal{H}(t_n)$, constitutes a first-order approximation, and should be combined with the first-order method – the Trotter splitting, eq. (44). Similarly, the second-order Magnus expansion, $\Theta_2(t_n)$ in eq. (27), constitutes a second-order approximation, and should be combined with the second-order method – the Strang splitting, eq. (45). Since the exponent in all of these cases has the common form Ω , eq. (39), the relevant subtables for these cases are (a)(i) and (a)(ii), depending on whether coupling gates are natively available or not, respectively.

For fourth-order Magnus expansion $\Theta_2(t_n)$, as we have seen in Sections 3.3 and 3.4, the situation differs depending on whether the Hamiltonian is isotropic or not. For isotropic

Method	Order	Circuit Depth, M odd	Circuit Depth, M even
--------	-------	------------------------	-------------------------

(a) Time-stepping with Ω , eq. (39).

(i) Coupling gates available, Ω^α assigned to hA, hB, hC arbitrarily.

Trotter, eq. (44)	1	$(\frac{9M}{2} - \frac{3}{2}) N$	$(\frac{9M}{2} - 3) N$
Strang, eq. (45)	2	$(6M - 2) N + \frac{3M}{2} - \frac{1}{2}$	$(6M - 4) N + \frac{3M}{2} - 1$
Yoshida, eq. (46)	4	$(18M - 6) N + \frac{3M}{2} - \frac{1}{2}$	$(18M - 12) N + \frac{3M}{2} - 1$

(ii) Coupling gates implemented as shown in fig. 2, $hA = \Omega^X, hB = \Omega^Z, hC = \Omega^Y$.

Trotter, eq. (44)	1	$(\frac{33M}{2} - \frac{27}{2}) N$	$(\frac{33M}{2} - 19) N$
Strang, eq. (45)	2	$(21M - 17) N + \frac{9M}{2} - \frac{7}{2}$	$(21M - 24) N + \frac{9M}{2} - 5$
Yoshida, eq. (46)	4	$(63M - 51) N + \frac{9M}{2} - \frac{7}{2}$	$(63M - 72) N + \frac{9M}{2} - 5$

(b) Time-stepping with $e^E e^W e^{-E}$, eq. (55).

(i) Coupling gates available, Ω^α assigned to hA, hB, hC arbitrarily.

Modified Yoshida, eq. (80)	4	$(\frac{39M}{2} - \frac{7}{2}) N + 1$	$(\frac{39M}{2} - 10) N + 1$
----------------------------	---	---------------------------------------	------------------------------

(ii) Coupling gates implemented as shown in fig. 2, $hA = \Omega^X, hB = \Omega^Z, hC = \Omega^Y$.

Modified Yoshida, eq. (80)	4	$(\frac{135M}{2} - \frac{103}{2}) N + 1$	$(\frac{135M}{2} - 74) N + 1$
----------------------------	---	--	-------------------------------

Table 2: Circuit depths for N time-steps of Trotterized time-stepping for M spins for: Ω , eq. (39) (top two sub-tables, (a) (i) & (a) (ii)) and $e^E e^W e^{-E}$, eq. (55) (bottom two sub-tables, (b) (i) & (b) (ii)). Here we have assumed that $|C_{\text{in}}| = 9M(M - 1)$, i.e., the spins are fully connected, $C^{\alpha, \beta} = 0, \alpha \neq \beta$, and $C^{\alpha, \alpha^\top} = C^{\alpha, \alpha}$. For sparse couplings, e.g., $|C_{\text{in}}| = \mathcal{O}(M)$, the circuit depth can depend strongly on the connectivity. For spin chains, for example, circuit depth is independent of M , while for a star topology, where one *central* spin is connected to all other spins, circuit depth remains $\mathcal{O}(M)$.

Hamiltonians, $\Theta_2(t_n)$ in eq. (67) has the common form Ω , eq. (39), and the relevant subtables are again (a)(i) and (a)(ii). For more general cases, to eliminate the extra commutator, we need the asymmetric splitting $e^{E(t_n)} e^{W(t_n)} e^{-E(t_n)}$, eq. (55), which is implemented as the modified Yoshida splitting eq. (80), with $\Omega = W(t_n)$. The relevant subtables in this case are (b)(i) and (b)(ii).

4.3 Overall circuit complexity.

For simulating Hamiltonians (10) with fully-dense interactions, i.e. where each spin interacts with every other spin, we can see from eq. (12) that the Hamiltonian spectral radius grows quadratically with M , i.e., $\rho = \mathcal{O}(M^2)$. Consequently, using the time-step complexity estimate in eq. (82), the number of time-steps required for achieving a prescribed accuracy also grow quadratically as $N = \mathcal{O}(M^2)$. Referring to the circuit depth analysis given in Table 2, the Yoshida method yields a circuit depth of $\mathcal{O}(MN)$. Overall, for achieving a prescribed accuracy for fully-dense interactions in an M body two-level system, the circuit depth needs to increase as $\mathcal{O}(M^3)$ and quantum volume as $\mathcal{O}(M^4)$.

For sparse Hamiltonians where each spin interacts with a fixed number of spins (e.g.,

spin chains, Ising models, and Kitaev models), the Hamiltonian spectral radius only grows linearly, $\rho = \mathcal{O}(M)$, so that the circuit depth grows as $\mathcal{O}(M)$ and quantum volume as $\mathcal{O}(M^2)$. This makes simulation of sparse Hamiltonians a significantly easier problem, especially for large M , where any quantum advantage is expected to be demonstrated.

5 Numerical results

5.1 Chirped pulse

Chirped pulses belong to a broader group of swept-frequency pulses and are parametric pulses in which the frequency of irradiation varies over time, typically in a linear fashion. They are frequently used in the control of spin systems, superconducting qubits [100], NMR [60, 101], and atomic as well as molecular processes [58]. The broadband motion of the pulse allows efficient control of spins with a wide range of frequencies. However, the highly oscillatory nature of these pulses makes them especially challenging to handle numerically.

A general expression for a chirped pulse is

$$p(t) = p_x(t) + ip_y(t) = A(t) \exp(i\phi(t)), \quad (83)$$

where the amplitude envelope $A(t)$ and the phase $\phi(t)$ are arbitrary real-valued functions of time. For a chirped pulse with peak amplitude A_{\max} , bandwidth ΔF , duration τ_p , and overall phase ϕ_0 , the amplitude envelope is given by

$$A(t) = A_{\max} \exp \left[-4 \left(\frac{2t}{\tau_p} - 1 \right)^\eta \right], \quad \eta \in 2\mathbb{N}_0, \quad t \in [0, \tau_p], \quad (84)$$

which is a *super-Gaussian* envelope. If the frequency of the pulse is swept linearly

$$\omega(t) = \pi \Delta F \left(\frac{2t}{\tau_p} - 1 \right), \quad (85)$$

the phase is

$$\phi(t) = \int \omega(t) dt = \phi_0 + \pi \Delta F t \left(\frac{t}{\tau_p} - 1 \right). \quad (86)$$

The maximum amplitude of a chirped pulse can be calculated using the three parameters ΔF , τ_p , and \mathcal{Q}_0 as

$$A_{\max} = \sqrt{\frac{2\pi \Delta F \mathcal{Q}_0}{\tau_p}}, \quad (87)$$

where \mathcal{Q}_0 is the *adiabaticity* factor at time $\tau_p/2$, where $t \in [0, \tau_p]$,

$$\mathcal{Q}_0 = \frac{2}{\pi} \ln \left(\frac{2}{\cos(\theta) + 1} \right), \quad (88)$$

for a desired *pulse flip angle* θ . Since the effective flip angle of a chirped pulse approaches 180° asymptotically as A_{\max} increases, for most practical purposes a value of \mathcal{Q}_0 is chosen (normally 5) to satisfy the adiabatic condition while avoiding excessive pulse amplitudes.

5.2 Spin systems

Example 1 (isotropic coupling with identical pulses). We consider a three-spin-1/2 isotropic system appearing in liquid-state NMR applications, where the pulse is identical for each spin,

$$\begin{aligned} \mathcal{H}(t) = & \frac{1}{2}p_x(t)(X_1 + X_2 + X_3) + \frac{1}{2}p_y(t)(Y_1 + Y_2 + Y_3) + \pi\Omega_1 Z_1 + \pi\Omega_2 Z_2 + \pi\Omega_3 Z_3 \\ & + \frac{\pi}{2} \sum_{\alpha \in \{X,Y,Z\}} J_{1,2} \alpha_1 \alpha_2 + \frac{\pi}{2} \sum_{\alpha \in \{X,Y,Z\}} J_{2,3} \alpha_2 \alpha_3 + \frac{\pi}{2} \sum_{\alpha \in \{X,Y,Z\}} J_{1,3} \alpha_1 \alpha_3, \end{aligned} \quad (89)$$

where Ω_1 , Ω_2 , and Ω_3 are the *spin offsets*. This Hamiltonian can be described in the form (10), with

$$\mathbf{e}(t) = \frac{1}{2} \left(p_x(t) \mathbf{1}^\top, p_y(t) \mathbf{1}^\top, 2\pi \mathbf{\Omega}^\top \right)^\top, \quad \mathbf{\Omega} = (\Omega_1, \Omega_2, \Omega_3)^\top,$$

and

$$C^{\alpha,\beta} = 0 \text{ for } \alpha \neq \beta, \quad C^{X,X} = C^{Y,Y} = C^{Z,Z} = C = \frac{\pi}{2} \begin{bmatrix} 0 & J_{1,2} & J_{1,3} \\ J_{1,2} & 0 & J_{2,3} \\ J_{1,3} & J_{2,3} & 0 \end{bmatrix}.$$

The three-spin system we consider in this example has the offsets $\Omega_1 = 2$ kHz, $\Omega_2 = 1.5$ kHz, and $\Omega_3 = 1.6$ kHz, and the coupling constants are defined by $J_{1,2} = 7$ Hz, $J_{1,3} = 12$ Hz, and $J_{2,3} = 20$ Hz. We consider three different choices for the set of parameters defining the pulses $p_x(t)$ and $p_y(t)$:

- (i) **Time-independent Hamiltonian.** $p_x(t) = p_y(t) = 0$, which corresponds to $A_{\max} = 0$.
- (ii) **Gaussian pulse.** A general expression of the Gaussian pulse is given by

$$p(t) = p_x(t) + ip_y(t) = \theta \frac{\exp \left[-4 \left(\frac{2t}{\tau_p} - 1 \right)^\eta \right]}{\int_0^{\tau_p} \exp \left[-4 \left(\frac{2t}{\tau_p} - 1 \right)^\eta \right] dt} \exp [i(\phi_0 + 2\omega t)]. \quad (90)$$

Gaussian pulses can be selective in nature – by tuning $\omega = \Omega$, the pulse in eq. (90) can control spins with offset Ω , without affecting other spins. This can also be a limitation when we seek to control multiple spins with varying offsets, where the pulse may only influence one specific spin. In this section we consider a Gaussian pulse with $\theta = \pi$, $\eta = 2$, $\omega = \Omega_1 = 2000$ Hz, $\phi_0 = 0$ rad, and $\tau_p = 10$ ms. The real and imaginary components of the pulse, $p_x(t)$ and $p_y(t)$ are shown in fig. 4.

- (iii) **Chirped pulse.** $A_{\max} = 2\pi \times 1545$ rad/s, $\Delta F = 30$ kHz, $\tau_p = 10$ ms, and $\eta = 40$. The real and imaginary components of the pulse, $p_x(t)$ and $p_y(t)$, are shown in fig. 5.

In fig. 6, we observe three interacting spins under the three different pulses defined in Example 1. All three spins start from the Z-up position. The figure shows that the behaviour of the spins under a time-independent pulse is trivial. The Gaussian pulse can only flip one spin, specifically the one it is tuned for. However, it fails to completely drive the spin to the Z-down position – this failure is due to a non-trivial interaction between the spins. The other two spins are minimally impacted and return to their original position eventually. In contrast, a chirped pulse is capable of flipping all three spins simultaneously – doing so despite the interactions that are not explicitly taken into account in its design.

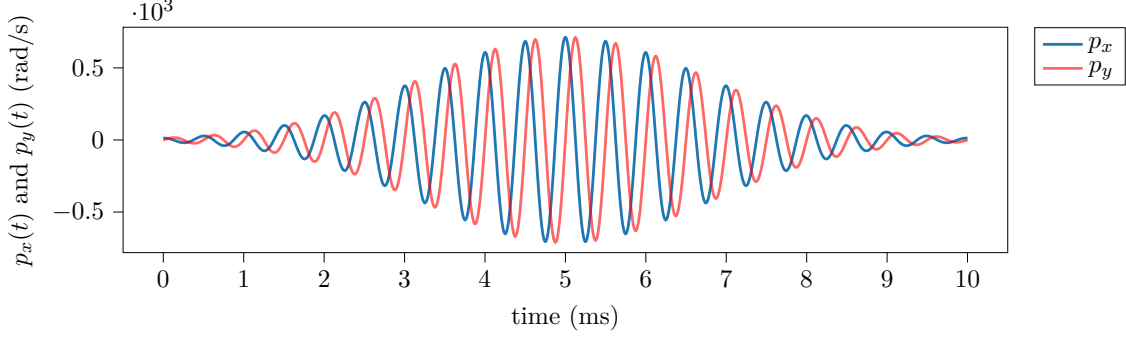


Figure 4: An exemplar Gaussian pulse, eq. (90), with $\tau_p = 10$ ms, $\phi_0 = 0$ rad, and $\eta = 2$, $\omega = \Omega_1$.

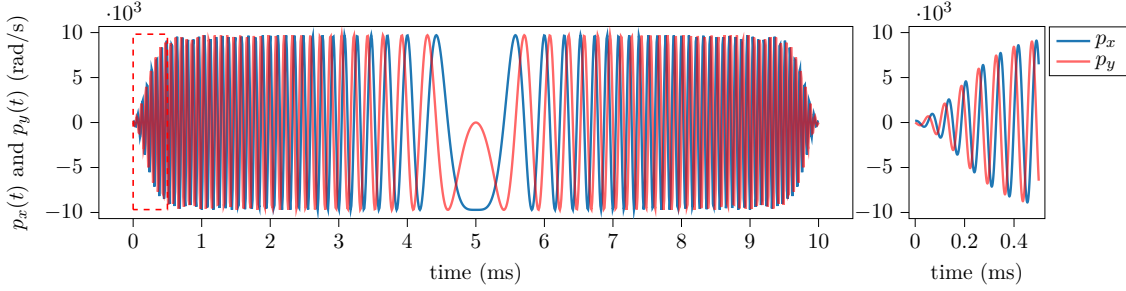


Figure 5: An exemplar chirp pulse, eqs. (83) to (88), with $\Delta F = 30$ kHz, $\tau_p = 10$ ms, $\phi_0 = 0$ rad, and $\eta = 40$. On the right, we show a zoomed view of the highly oscillatory part of the pulse, from 0 ms to 0.5 ms.

While a sequence of three Gaussian pulses could theoretically achieve a similar result, it would require a specifically tuned pulse for each spin, significantly increasing the required time as the number of spins with different offsets grows. Moreover, the efficacy is expected to be limited in the presence of coupling terms.

On the other hand, compared to the Gaussian pulse shown in fig. 4, which has a longer wavelength, the chirped pulse shown in fig. 5 is much more oscillatory, making it more challenging to resolve numerically. A similar phenomenon is observed in the dynamics of spins, which is much more oscillatory under a chirped pulse compared to the case of a Gaussian pulse. This is evident, for instance, in fig. 6, where the X and Y observables are particularly oscillatory under the chirped pulse.

Example 2 (General Hamiltonian). We consider a more general three-spin system with individual control pulses for each spin and non-isotropic couplings. The parameters of the Hamiltonian in (10) are given by

$$\mathbf{e}(t) = \frac{1}{2} \left((p_{x,1}(t), p_{x,2}(t), p_{x,3}(t))^{\top}, (p_{y,1}(t), p_{y,2}(t), p_{y,3}(t))^{\top}, 2\pi\mathbf{\Omega}^{\top} \right)^{\top},$$

where $p_{x,k}, p_{y,k}$ are p_x, p_y defined in eqs. (83) to (88) with parameters $\{\phi_0, \Delta F\}$ replaced by $\{\phi_{0,k}, \Delta F_k\}$, where $\phi_{0,1} = \pi$, $\Delta F_1 = 30$ kHz, $\phi_{0,2} = \pi/6$, $\Delta F_2 = 15$ kHz, and $\phi_{0,3} = -\pi/6$, $\Delta F_3 = 45$ kHz. $\mathbf{\Omega}$ remains the same as in Example 1. We consider two cases for the couplings:

(i) **Without mixed couplings.**

$$C^{\alpha,\beta} = 0 \text{ for } \alpha \neq \beta, \quad C^{\alpha,\alpha} = \frac{\pi}{2} \begin{bmatrix} 0 & J_{1,2}^{\alpha,\alpha} & J_{1,3}^{\alpha,\alpha} \\ J_{1,2}^{\alpha,\alpha} & 0 & J_{2,3}^{\alpha,\alpha} \\ J_{1,3}^{\alpha,\alpha} & J_{2,3}^{\alpha,\alpha} & 0 \end{bmatrix}, \quad \alpha \in \{X, Y, Z\},$$

X components – $\text{Tr}(\rho_k^\dagger X_k)$ for spin k Y components – $\text{Tr}(\rho_k^\dagger Y_k)$ for spin k Z components – $\text{Tr}(\rho_k^\dagger Z_k)$ for spin k

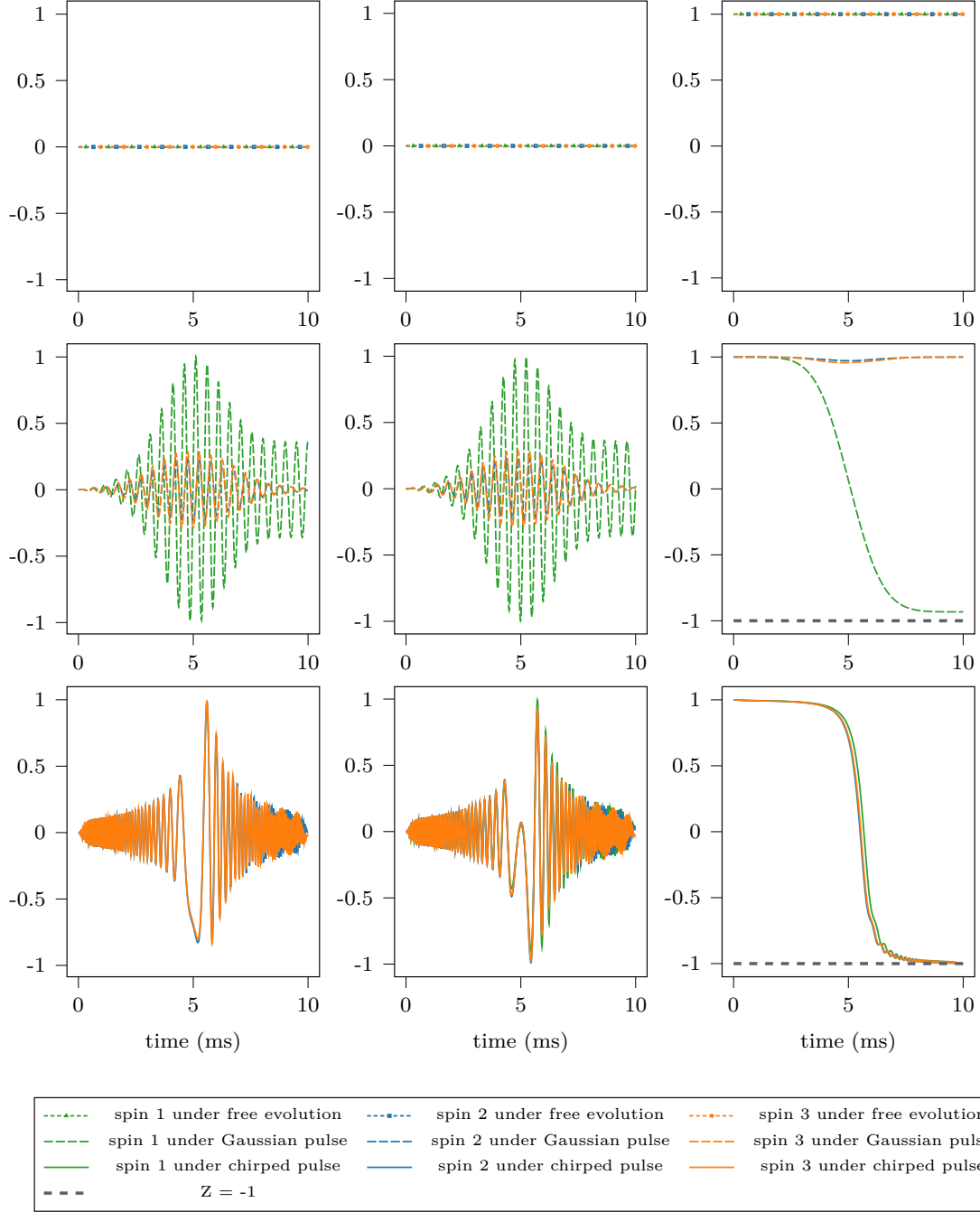


Figure 6: The time evolution of the X, Y and Z component observables, respectively, for a system of 3 interacting spins described in Example 1, each initially in the Z-up direction. Three choices of pulses are considered: Free evolution – *i.e.*, under Example 1, pulse (i); a Gaussian pulse – Example 1, pulse (ii); a chirped pulse – Example 1, pulse (iii).

where the values of $J_{j,k}^{\alpha,\beta}$ (in Hz) for $\alpha, \beta \in \{X, Y, Z\}$ and $j, k \in \{1, 2, 3\}$ can be found in Table 3 in row labeled j, k and column labeled α, β .

Table 3: Coupling constants in Hz, Example 2, case (i)

$\alpha, \beta \backslash j, k$	X, X	Y, Y	Z, Z
1, 2	10	5	12
1, 3	2	8	4
2, 3	4	9	11

(ii) **With mixed coupling.**

$$C^{\alpha,\beta} = \frac{\pi}{2} \begin{bmatrix} 0 & J_{1,2}^{\alpha,\beta} & J_{1,3}^{\alpha,\beta} \\ J_{1,2}^{\alpha,\beta} & 0 & J_{2,3}^{\alpha,\beta} \\ J_{1,3}^{\alpha,\beta} & J_{2,3}^{\alpha,\beta} & 0 \end{bmatrix}, \quad \alpha, \beta \in \{X, Y, Z\},$$

where the values of $J_{j,k}^{\alpha,\beta}$ (in Hz) for $\alpha, \beta \in \{X, Y, Z\}$ and $j, k \in \{1, 2, 3\}$ can be found in Table 4 in row labeled j, k and column labeled α, β .

Table 4: Coupling constants in Hz, Example 2, case (ii)

$\alpha, \beta \backslash j, k$	X, X	Y, Y	Z, Z	X, Y	X, Z	Y, Z	Y, X	Z, X	Z, Y
1, 2	10	5	12	13	18	4	15	15	6
1, 3	2	8	4	19	10	14	9	13	9
2, 3	4	9	11	2	11	10	6	4	5

Remark 11. In all cases we restrict our attention to

$$\left(J^{\alpha,\beta}\right)^\top = J^{\alpha,\beta}, \quad \text{i.e.,} \quad \left(C^{\alpha,\beta}\right)^\top = C^{\alpha,\beta},$$

since this is typically the case in practical applications. We note, however, that our derivations do not require these assumptions, and our algorithm also works for cases with $\left(C^{\alpha,\beta}\right)^\top \neq C^{\alpha,\beta}$.

5.3 Results

Naming and other conventions

Splittings. In this section, for the case of time-dependent Hamiltonians, we will be pairing Magnus expansions with various quadrature approximations for the integrals and appropriate Trotterization methods. For clarity, unless otherwise specified, first-order methods will be paired with Trotter splitting, eq. (44), second-order methods with Strang splitting, eq. (45), and fourth-order methods with Yoshida splitting, eq. (79).

Integrals. Our standard approach involves using `scipy` to approximate integrals in eqs. (32) and (33) in the Magnus expansion as well as the commutator-free method CF42, eq. (71), to machine precision. However, for Θ_1 , eq. (27), which is normally a second-order Magnus expansion, we will also explore using the starting point, i.e., $\Theta_1 \approx -i\hbar\mathcal{H}(t_n)$, which leads to a first-order method, as well as the midpoint $\Theta_1 \approx -i\hbar\mathcal{H}(t_n + h/2)$, which

leads to a second-order method. For Θ_2 , eq. (67), we will also examine the effects of using Gauss–Legendre (GL) quadratures, which are described in Section 2.5. In particular, GLk will refer to the Gauss–Legendre quadrature with k knots.

Naming conventions. All Magnus expansion-based methods are named in the format

$$\Theta_k(t_n), \text{ eq. (n), quadrature-method}$$

for $k \in \{1, 2\}$, where ‘eq. (n)’ is the equation number for the Magnus expansion (and occasionally for the concrete form, when combined with an appropriate splitting), and ‘quadrature-method’ refers to the approach for approximating the integrals in the Magnus expansion. As described earlier in this subsection, the splitting to be used is governed by the order. The commutator-free method CF42 (71) follows a similar convention, with $\Theta_k(t_n)$ replaced by CF42, while the autonomized Yoshida splitting (77) is written without denoting a quadrature method since it does not feature integrals.

Error. Throughout this manuscript, the numerical simulations of the quantum circuits are carried out on a classical computer and the error depicted is the ℓ^2 error in the propagator, as defined, for example in eq. (25).

Time-independent pulse, isotropic Hamiltonian (Example 1, pulse (i))

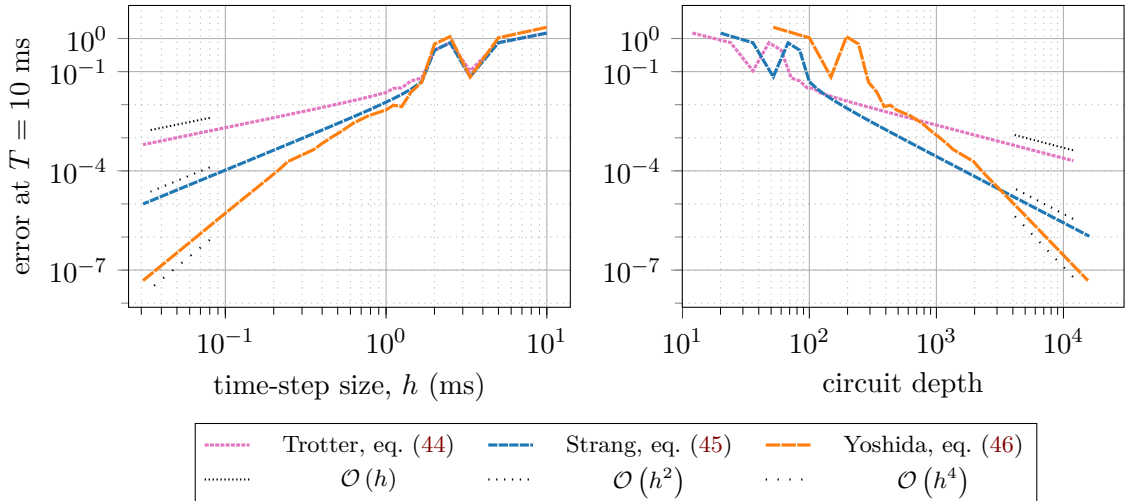


Figure 7: (*Time-independent isotropic Hamiltonian; splitting methods*) The accuracy of Hamiltonian simulation for isotropic Hamiltonian (89) under free evolution, *i.e.*, Example 1 with pulse (i).

Figure 7 shows the time-step size and circuit depth required for achieving a prescribed accuracy for the case of the time-independent Hamiltonian described in Example 1, *i.e.*, for pulse (i): $p_x(t) = p_y(t) = 0$. Higher accuracies require either smaller time-steps, which correspond to longer circuits, or the use of higher-order splittings.

Even for a low accuracy of 10^{-2} , the second-order Strang splitting, eq. (45), requires a shallower circuit, with circuit depth 180 and quantum volume 540, than the first-order Trotter splitting, whose circuit depth is around 252 (*i.e.*, a 40% longer circuit) and quantum volume around 756. Strang splitting stays competitive till an accuracy of 10^{-5} , at which point Yoshida splitting, eq. (46), becomes a more efficient approach. For five digits of accuracy, Yoshida splitting requires a circuit depth of 4,036 and quantum volume of 12,108, as compared to the circuit depth of 5,188 required for the Strang splitting. These are roughly 7 and 28 times longer than those required for an accuracy of 10^{-2} using Yoshida (with circuit depth requirement of 532) and Strang, respectively.

Relevance to practical circuits. These observations suggest that for simulation of time-independent Hamiltonians, second-order methods may lead to shorter circuits compared to first-order methods, even when relatively low accuracies are sought, for example on near-term quantum devices. Higher-order methods are not expected to be useful for the time-independent Hamiltonians considered in this paper until accuracies at the level of 10^{-5} are desired and feasible in terms of circuit depths as well as circuit noise levels, which may require fault-tolerant quantum computing. For $M \gg 3$ spin systems, where any quantum advantage is expected to be demonstrated, the error (82) is expected to grow linearly with the number of spins for sparse Hamiltonians and quadratically for Hamiltonians with dense couplings eq. (12). However, since these error bounds are not tight, precise error levels for large M are hard to estimate.

Chirped pulse, isotropic Hamiltonian (Example 1, pulse (iii))

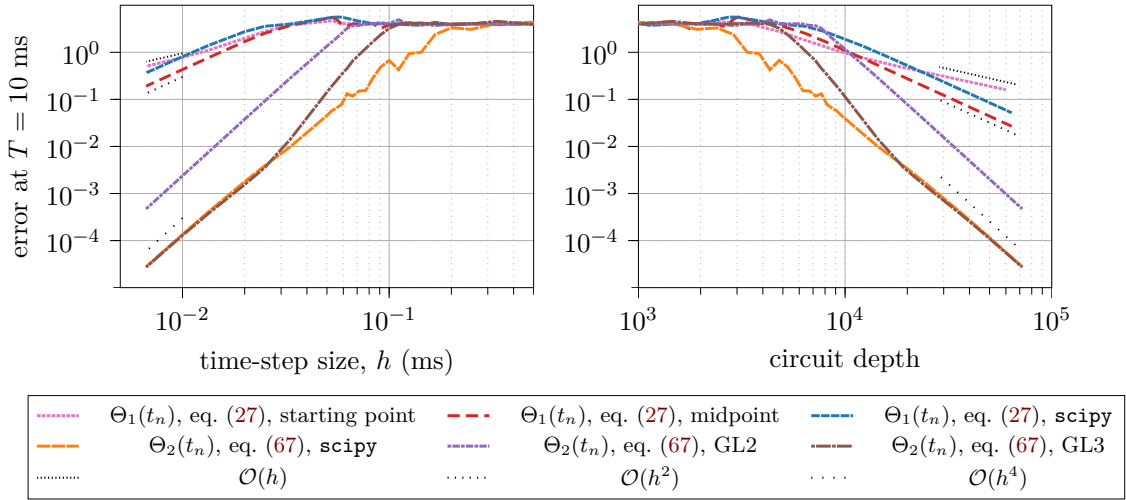


Figure 8: (*Isotropic Hamiltonian under chirped pulse; Magnus-based methods*) The accuracy of Hamiltonian simulation for isotropic Hamiltonian (89) under a chirped pulse, *i.e.*, Example 1 with pulse (iii), which is highly oscillatory as shown in fig. 5. The methods compared are the first-order method using piecewise constant Hamiltonian $\mathcal{H}(t_n)$, *i.e.*, at the start pointing, combined with Trotter splitting (44), the second-order method using piecewise constant Hamiltonian $\mathcal{H}(t_n + h/2)$, *i.e.*, at the mid-point, combined with Strang splitting (45), the second-order Magnus expansion (27) with integrals computed using `scipy` and combined with the Strang splitting (45), and the fourth-order Magnus expansion (67) combined with Yoshida splitting (46). The integrals in the fourth-order Magnus expansions are either computed to machine precision using the Python package `scipy` or approximated with two or three *Gauss–Legendre* quadrature nodes. The corresponding plots are labeled `scipy`, GL2, and GL3 respectively.

Figure 8 shows the time-step size and circuit depth required for achieving a prescribed accuracy for the case of the highly-oscillatory chirped pulse, *i.e.*, pulse (iii) in Example 1. As evident from this figure, even achieving a 10^{-1} accuracy, where the numerical results are barely reliable, becomes extremely challenging in the case of the chirped pulse. In case of the time-independent Hamiltonian – Example 1, pulse (i) – the accuracy of which is depicted in Figure 7, the first-order method requires a circuit depth of 72 for an accuracy of 10^{-1} , while the second-order method requires a circuit depth of 52. In contrast, in Figure 8 which shows the accuracy under the chirped pulse, the first-order method ($\Theta_1(t_n)$ at starting point combined with Trotter splitting) requires a circuit depth of 98,028 and quantum volume of 294,084, while the second-order method ($\Theta_1(t_n)$ at midpoint combined with Strang splitting) requires a circuit depth of 33,108 and quantum volume of 99,324

for the same accuracy – *i.e.*, circuit depths that are 1,361 and 636 times longer, respectively. This highlights the significantly increased difficulty of Hamiltonian simulation under time-dependent pulses compared to time-independent Hamiltonians, particularly when the pulses are as oscillatory as chirped pulses.

The fourth-order method $\Theta_2(t_n)$ with integrals computed using `scipy` and combined with Yoshida splitting achieves an accuracy of 10^{-1} with a circuit depth of roughly 7,876, which is 76.2% shorter than that required by the best second-order method and 92% shorter than that required by the first-order method. Nevertheless, this is roughly 3.48 times the circuit depth required for 10^{-4} accuracy in the time-independent case shown in Figure 7. An advantage of a higher-order method is that achieving 10^{-2} accuracy requires a relatively smaller increase in circuit depth – in particular, the method “ $\Theta_2(t_n)$, eq. (67), `scipy`” requires a circuit depth of 14,596 and quantum volume of 43,788 for 10^{-2} accuracy, compared to a circuit depth of 104,820 expected for “ $\Theta_1(t_n)$, eq. (27), midpoint”, *i.e.*, 86.1% shorter than the best second-order method.

Relevance to practical circuits. In contrast to the case of time-independent Hamiltonians, Hamiltonian simulation for time-dependent pulses such as chirped pulses seems to benefit from higher-order methods even when extremely low accuracies are sought, for example when using near-term quantum devices, which are characterised by high circuit noise. On the other hand, the circuit depths required for Hamiltonian simulation applications with time-dependent Hamiltonians are very large even for the 3 spin systems considered here. Moreover, the circuit depths are expected to grow linearly in M for sparse Hamiltonians and cubically for densely connected Hamiltonians (cf. section 4.3), making the Hamiltonian simulation problem for time-dependent Hamiltonians significantly more challenging for large M .

Large time-steps. Consistent with the observations of [67, 72, 73] for the cases of electronic and nuclear Schrödinger equations under highly-oscillatory external pulses, and the preliminary confirmation of the same phenomenon in the context of many-body spin systems under weak fields [74, Section 4.2], we find that the Magnus expansion combined with a highly-accurate approximation of the integrals allows time-steps that can easily span a whole wavelength of the driving pulse. In Figure 8, time-stepping with a time-step of 0.061 ms leads to an accuracy of 10^{-1} , when using $\Theta_2(t_n)$ with `scipy` integrals. In Figure 5 (b), which covers an interval of 0.5 ms, there are roughly 7.5 wavelengths. A time-step of 0.061 ms corresponds to nearly one whole wavelength. At twice the bandwidth, $\Delta F = 60$ kHz, while the number of wavelengths double, the time-step required for an accuracy of 10^{-1} decreases only marginally to 0.051, highlighting the resilience of the proposed method to highly oscillatory pulses.

The effect of approximating integrals. By computing the integrals in eqs. (32) and (33) to machine precision using integration routines in the Python package `scipy`, we find that we achieve higher accuracy when compared to GL2, or, equivalently, can take a substantially larger time-step for a prescribed accuracy. For instance, in fig. 8 we see that when utilizing GL2, we require a time-step of 0.0255 ms for accuracy of 10^{-1} , which is roughly 58.1% smaller than 0.0609 ms that is required with `scipy` integrals, resulting in a 138% longer circuit (circuit depth of 7,876 with `scipy` and 18,772 with GL2). For low accuracies, the GL3 method has a similar behavior, requiring longer circuit than `scipy`. However, for accuracies higher than 10^{-2} , it starts to become as effective as the `scipy` approach for computing integrals. The specifics of this transition are expected to be heavily dependent on the oscillatory nature of the pulse, with more oscillatory pulses requiring higher accuracy quadrature, as seen in fig. 12. However, since the quadratures can be computed cheaply on a classical computer to a very high precision, increasing accuracy

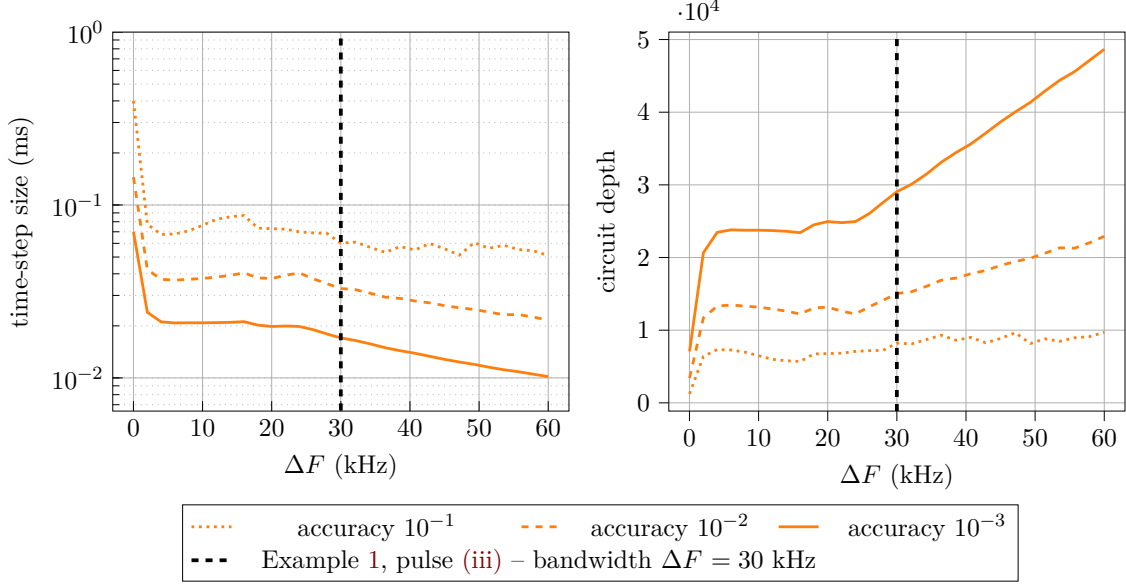


Figure 9: Plots comparing time-step sizes and circuit depths required to reach accuracies of 10^{-1} , 10^{-2} , and 10^{-3} against various bandwidths, using $\Theta_2(t_n)$, eq. (67), `scipy`.

of Hamiltonian simulation without affecting the circuit complexity, there seems to be no good reason for preferring low accuracy quadratures.

Other methods without commutators. In fig. 10, we compare the propagator accuracies for three fourth-order methods that are free of commutators: the fourth-order Magnus-based method, eq. (67), proposed in this paper, the commutator-free approach CF42, eq. (71), and the fourth-order autonomized Yoshida splitting, eq. (77). We find that our fourth-order Magnus based method consistently requires a shallower circuit than the CF42 and the autonomized Yoshida splitting. Even for an extremely low accuracy 10^{-1} , where the circuit depth of our method, eq. (67), is 7,876, CF42 eq. (71) and the autonomized Yoshida splitting (77) require circuit depths of 46,804 and 38,932, respectively – *i.e.*, circuit depths that are roughly 4.85 and 3.94 times longer, respectively. These observations remain similar when we require higher accuracies.

Benchmarking the effect of oscillatory pulses

One of the advantages of our fourth-order Magnus-based method, eq. (67), is its efficacy for highly oscillatory pulses. The oscillatory nature of a chirped pulse, eqs. (83) to (88), increases with the bandwidth, ΔF . In fig. 11 we compare the circuit depths required for achieving a prescribed propagator accuracy for a wide range of bandwidths, with other parameters of the pulse and the specification of the Hamiltonian remaining the same as in Example 1, pulse (iii). For reference, the bandwidth used in Example 1, pulse (iii), is marked by a black dashed vertical line (the behaviour under these parameters has been studied earlier in this subsection, in figs. 8 and 10.)

In addition to the proposed method “ $\Theta_2(t_n)$, eq. (67), `scipy`” we benchmark the methods “ $\Theta_1(t_n)$, eq. (27), midpoint”, “ $\Theta_1(t_n)$, eq. (27), `scipy`” and “CF42, eq. (71) `scipy`” – these methods are chosen for benchmarking since they were found to be the most efficient first-order, second-order and fourth-order alternatives to our approach in fig. 8. In fig. 11, the x-axis represents different bandwidths, while the y-axis shows the *circuit compression ratio*. This ratio indicates how many times deeper circuit is required for the three comparative methods compared to the proposed method, which is treated as a baseline method

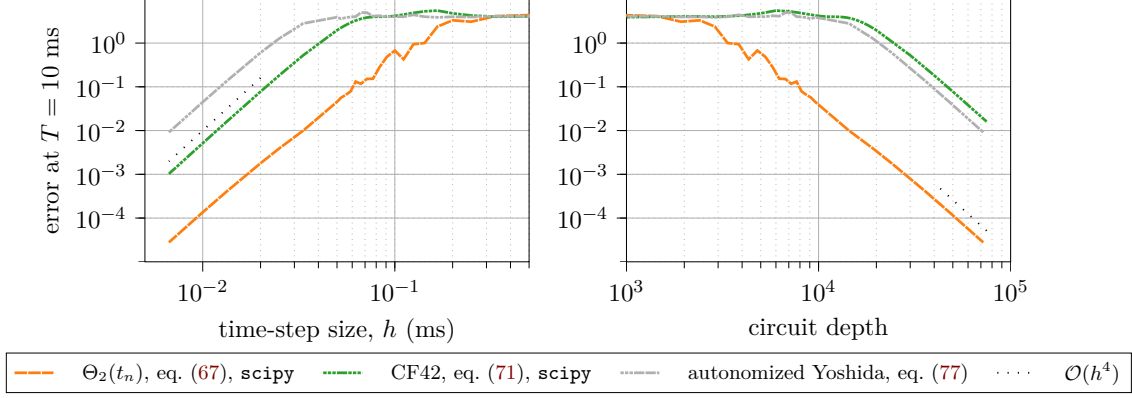


Figure 10: (*Isotropic Hamiltonian under chirped pulse; fourth-order methods without commutators*) The accuracy of Hamiltonian simulation for isotropic Hamiltonian (89) under a chirped pulse, *i.e.*, Example 1 with pulse (iii). The methods compared are the fourth-order methods based on Magnus expansion (67) with Yoshida splitting (46), the CF42 commutator-free method with two exponents (71), and the autonomized Yoshida splitting (77). The integrals in the Magnus expansion and the CF42 method are computed using `scipy`, while the autonomized Yoshida splitting involves sampling the Hamiltonian at discrete points by design, and does not feature any integrals.

and is depicted for reference with a circuit compression ratio of 1. A higher value on the y-axis signifies a less efficient method. In particular, values higher than 1 signify a method less efficient than the proposed method, while values lower than 1 signify a method more efficient than the proposed method.

Each subplot in fig. 8 corresponds to a specific accuracy target, 10^{-1} , 10^{-2} and 10^{-3} , with lower accuracies being of more immediate relevance to near-term quantum devices. The benchmarking demonstrates that our fourth-order Magnus-based method consistently outperforms the others across all accuracy levels and almost all bandwidths, with a minor exception being a combination of extremely slowly varying pulses (small bandwidth, ΔF) and low accuracies. As bandwidth increases, the relative advantage conferred by our method compared to the other methods increases as well, indicating its increased benefits under the typically hard to simulate case of highly-oscillatory pulses.

As evident in fig. 9, this is largely due to a resilience of our method to highly oscillatory pulses, which requires a very mild increase in circuit depths for increasingly oscillatory pulses. We note that the maximum amplitude of the pulses defined in eqs. (83) to (88) grows as $\max_{t \in [0, T]} \|\mathbf{e}(t)\|_\infty = \mathcal{O}(\sqrt{\Delta F})$, which increases the Hamiltonian spectral radius ρ in eq. (12) as a consequence. We suspect that, along with the increase in γ (24) due to increased oscillations, this could be the reason for the increase in circuit-depth for higher bandwidths in fig. 9 seen for the higher-accuracy of 10^{-3} .

Figure 12 compares circuit depths required when applying our fourth-order method, eq. (67), in combination with different methods for approximating the integrals, namely, `scipy`, GL2 and GL3. Across all levels of accuracy investigated here, `scipy` method maintains a clear advantage over the GL2 method. However, the advantage of `scipy` over GL3 diminishes for accuracy levels of 10^{-3} . As noted earlier, since integrals can be computed cheaply on a classical computer, there is no compelling reason to prefer GL2 or GL3 over `scipy`.

Benchmarking the effect of coupling strengths

We benchmark the effect of coupling strengths on the four different methods considered above, namely “ $\Theta_2(t_n)$, eq. (67), `scipy`”, “ $\Theta_1(t_n)$, eq. (27), midpoint”, “ $\Theta_1(t_n)$, eq. (27),

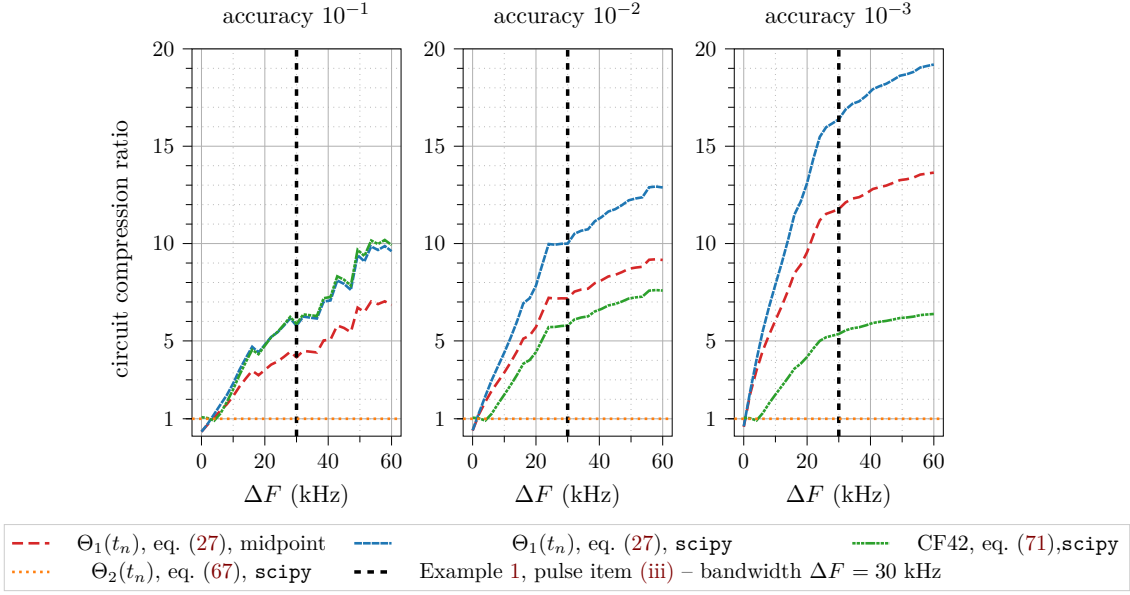


Figure 11: (*Circuit compression ratios for oscillatory pulses; methods of different orders*) Comparison of circuit depth across four computational methods at varying bandwidths, ΔF , for different accuracy levels, 10^{-1} , 10^{-2} , and 10^{-3} . The y-axis shows the circuit compression ratio, indicating each method's efficiency relative to the proposed method, " $\Theta_2(t_n)$, eq. (67), `scipy`", with integrals computed using `scipy`. Black dashed vertical lines indicate the reference values used in Example 1, pulse (iii), where the bandwidth is $\Delta F = 30$ kHz. The horizontal line at $y = 1$ marks the point where the efficiency of the methods being compared is equivalent to that of the proposed method. Higher values signify a less efficient method.

`scipy`" and "CF42, eq. (71) `scipy`", using random coupling strengths in Example 1, case (iii), with other parameters kept constant. To quantify the coupling strength, we compute the ℓ^2 norm of the interaction Hamiltonian, $\|\mathcal{H}_{\text{in}}\|$, which is depicted on the x-axis of fig. 13, while the y-axis shows the circuit compression ratio. The mean circuit compression ratio is shown as a function of $\|\mathcal{H}_{\text{in}}\|$ with thick lines, while the shadowed areas around it represent a single standard deviation. As before, the black dashed vertical line indicates the reference setup, *i.e.*, Example 1, case (iii), where $\|\mathcal{H}_{\text{in}}\| \approx 187.4$.

It is evident in fig. 13 that, while our fourth-order Magnus-based method has the highest comparative advantage under a smaller norm of the interaction Hamiltonian (indicating weaker coupling strengths) and for higher accuracies, it consistently outperforms the other three methods across all levels of accuracy considered here, 10^{-1} , 10^{-2} and 10^{-3} , and an extremely wide range of interaction strengths. However, as the strength of the interaction, measured by $\|\mathcal{H}_{\text{in}}\|$ increases, the circuit compression ratio indicating our method's superiority does decrease. In particular, CF42 becomes as efficient as the proposed approach for $\|\mathcal{H}_{\text{in}}\| = 10^5$, while the first and second-order methods remain less efficient across the entire range of interaction strengths considered.

Figure 14 illustrates a comparison of the circuit depths required when applying our fourth-order method, eq. (67), in combination with different integral approximation techniques, *i.e.*, `scipy`, GL2 and GL3. Across all three levels of accuracy considered here, the use of `scipy` for approximating the integrals maintains a clear comparative advantage over the GL2 method, except for extremely strong interaction strengths, where GL2 becomes as efficient. However, `scipy` only outperforms GL3 for relatively smaller values of $\|\mathcal{H}_{\text{in}}\|$, and only for accuracy levels of 10^{-1} . For higher accuracies and interaction strengths, it loses

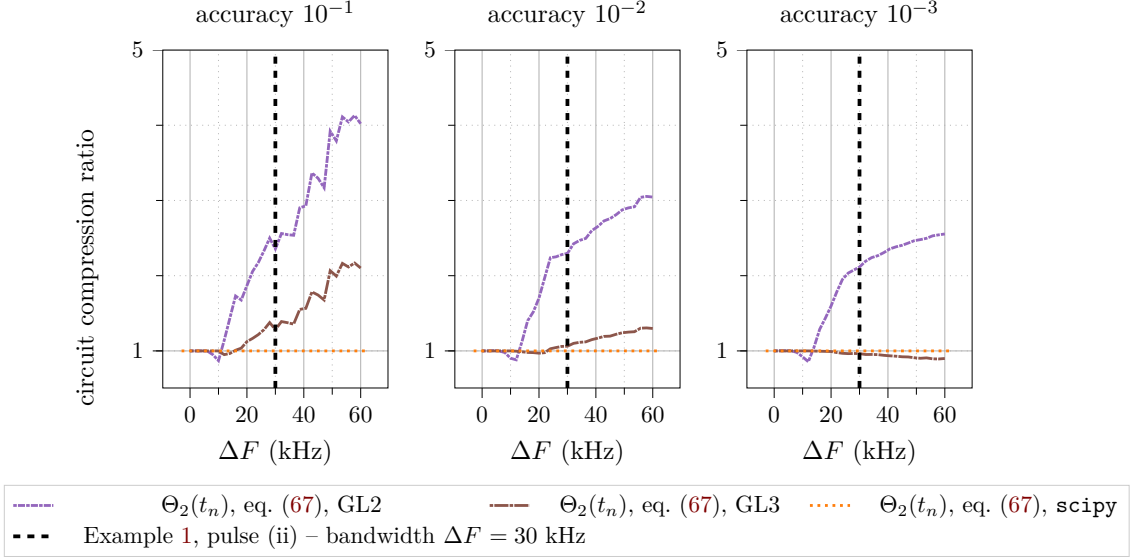


Figure 12: (Circuit compression ratios for oscillatory pulses; effect of quadrature on fourth-order Magnus) Comparison of the fourth-order Magnus expansion Θ_2 , eq. (67), when combined with GL2 and GL3 integration methods for approximating the integrals in eqs. (32) and (33), against the baseline provided by `scipy`, which allows us to compute the integrals to machine precision. The y-axis represents the circuit compression ratio, highlighting the relative efficiency of the GL2 and GL3 integrations in comparison to the standard `scipy` implementation. Black dashed vertical lines represent Example 1, pulse (iii), where the bandwidth is $\Delta F = 30$ kHz. The horizontal line at $y = 1$ marks the point where the efficiency of the methods being compared is equivalent to that of the proposed method. Higher values signify a less efficient method.

its comparative advantage. However, as noted earlier, since integrals can be computed cheaply on a classical computer, there is no compelling reason to prefer GL2 or GL3 over `scipy`.

As described by the time-step complexity in eq. (82), the circuit depth required for achieving a prescribed accuracy grows linearly with the Hamiltonian spectral radius ρ (11),

$$\rho = \max_{t \in [0, T]} \|\mathcal{H}(t)\| \leq \max_{t \in [0, T]} \|\mathcal{H}_{ss}(t)\| + \|\mathcal{H}_{in}\|.$$

Conversely, the time-step size needs to decrease inversely as ρ .

In our baseline case, Example 1, pulse (iii), $\|\mathcal{H}_{in}\| \approx 187.4$, while $\max_{t \in [0, T]} \|\mathcal{H}_{ss}(t)\| = 35511.92$. In fig. 15, it takes a while until $\|\mathcal{H}_{in}\|$ dominates and essentially dictates the value of ρ , at which point the circuit depth of our fourth-order method, eq. (67), almost converges to a linear growth with $\|\mathcal{H}_{in}\|$. Conversely, the time-step size decreases inversely with $\|\mathcal{H}_{in}\|$ at this point, as expected.

Chirped pulse, general Hamiltonian without mixed coupling (Example 2, case (i))

For the case of the general Hamiltonian without mixed couplings described in Example 2, case (i), the fourth-order Magnus expansion requires the elimination of commutators before combination with the Yoshida splitting, and leads to the proposed method described in eq. (80). As we can see in fig. 16, even for an accuracy of 10^{-1} , “ $\Theta_1(t_n)$, eq. (27), `scipy`” requires a circuit depth of 53,924, while “ $\Theta_2(t_n)$, eq. (67), `scipy`” achieves the same accuracy with circuit depth of 8,932, which is 83.4% shorter. Figure 16 also shows that the choice of integration methods is critical for an accuracy level of 10^{-1} : for example, $\Theta_2(t_n)$

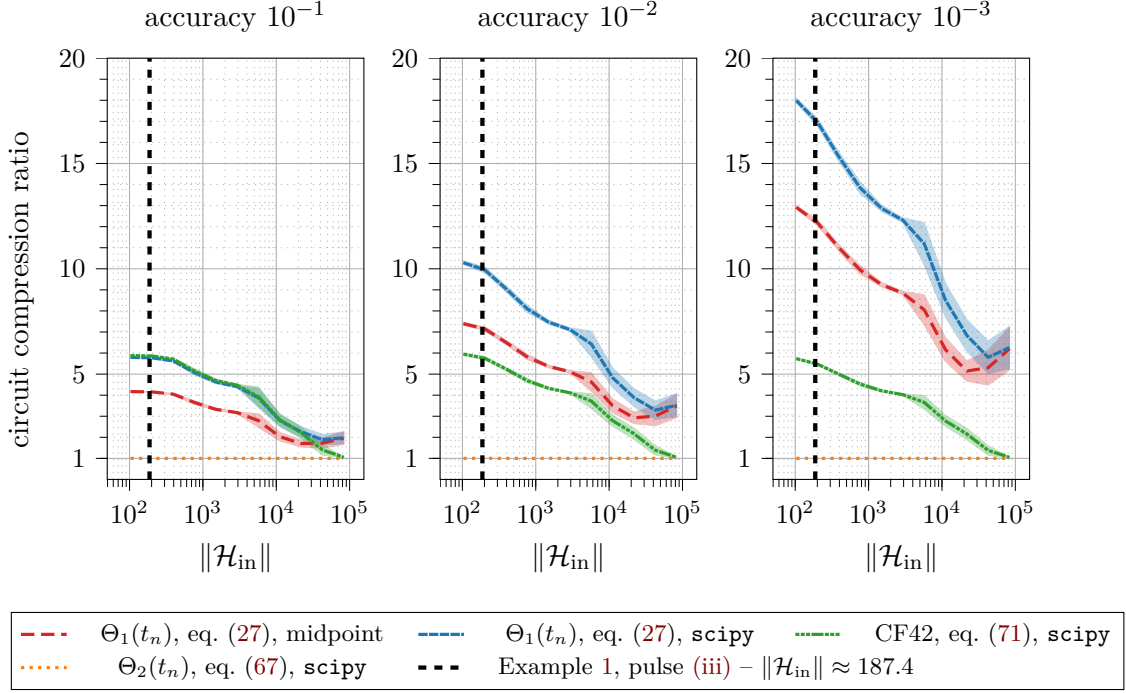


Figure 13: (Circuit compression ratios for oscillatory pulses with different coupling strength; methods of different orders) Comparison of circuit depth across four computational methods at varying $\|\mathcal{H}_{\text{in}}\|$ for different accuracy levels, 10^{-1} , 10^{-2} , and 10^{-3} . The y-axis shows the circuit compression ratio, indicating each method's efficiency relative to the proposed method, eq. (67), with integrals computed using `scipy`. Black dashed vertical lines indicate the reference values used in Example 1, pulse (iii), where $\|\mathcal{H}_{\text{in}}\| = 187.4$. The horizontal line at $y = 1$ marks the point where the efficiency of the methods being compared is equivalent to that of the proposed method. Higher values signify a less efficient method.

combining with GL3 requires a circuit depth of 12,820, which is 43.5% longer than when combined with `scipy`.

For 10^{-3} or higher accuracies, the three integral methods we are examining converge to the same behaviour, all of which require a circuit depth of 42,916. The circuit depth required here is 52.3% longer than in Example 1, pulse (iii), where the fourth-order Magnus method with `scipy` integrals required a circuit depth of 28,180.

Chirped pulse, general Hamiltonian with mixed coupling (Example 2, case (ii))

We do not have Trotterized circuits for general Hamiltonians with mixed couplings. Instead, we compute the exponentials in eq. (60) by brute force. As shown in fig. 17, we observe similar behaviours to previous examples, *i.e.*, the proposed fourth-order method, “ $\Theta_2(t_n)$, eq. (60), `scipy`”, allows larger time-step sizes than the second-order method, “ $\Theta_1(t_n)$, eq. (27), `scipy`”. Within the context of eq. (60), using `scipy` for computing integrals allows larger time-step sizes than GL3 and GL7.

6 Conclusions

In this paper we consider the efficacy of various Trotterized algorithms for Hamiltonian simulation of coupled many-body two-level systems, with a particular focus on producing shorter depth circuits for applications on near-term quantum devices.

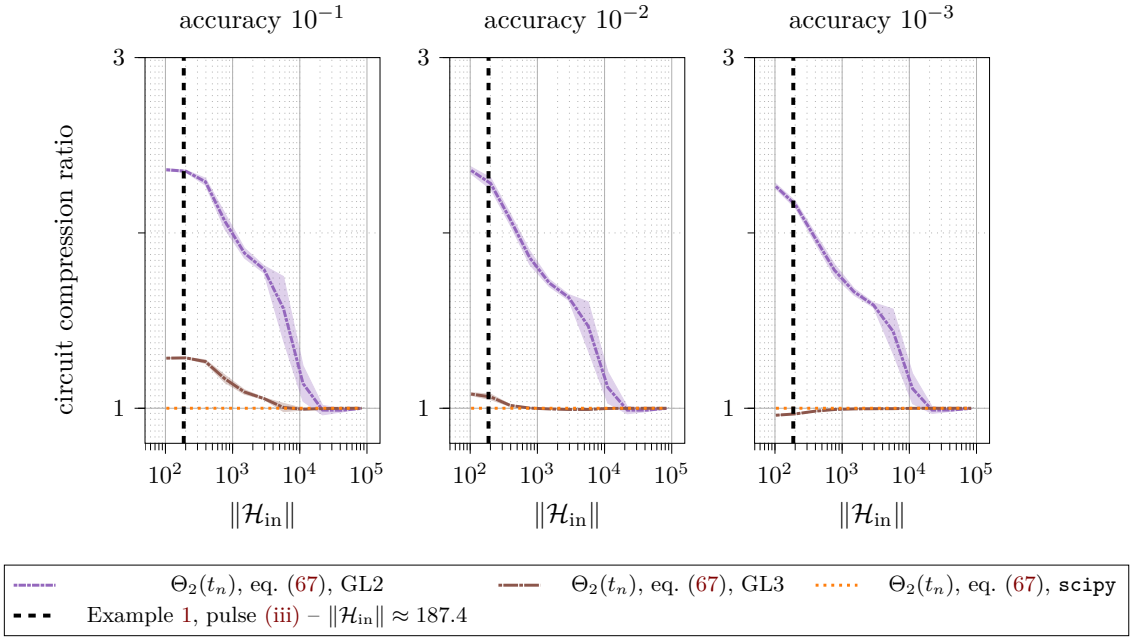


Figure 14: (Circuit compression ratios for oscillatory pulses with different coupling strength; effect of quadrature on fourth-order Magnus) Comparison of the fourth-order Magnus expansion Θ_2 eq. (67), when combined with GL2 and GL3 integration methods for approximating the integrals in eqs. (32) and (33), against the baseline provided by `scipy`, which allows us to compute the integrals to machine precision. The y-axis represents the circuit compression ratio, highlighting the relative efficiency of the GL2 and GL3 integrations in comparison to the standard `scipy` implementation. Black dashed vertical lines represent Example 1, pulse (iii), where $\|\mathcal{H}_{\text{in}}\| = 187.4$. The horizontal line at $y = 1$ marks the point where the efficiency of the methods being compared is equivalent to that of the proposed method. Higher values signify a less efficient method.

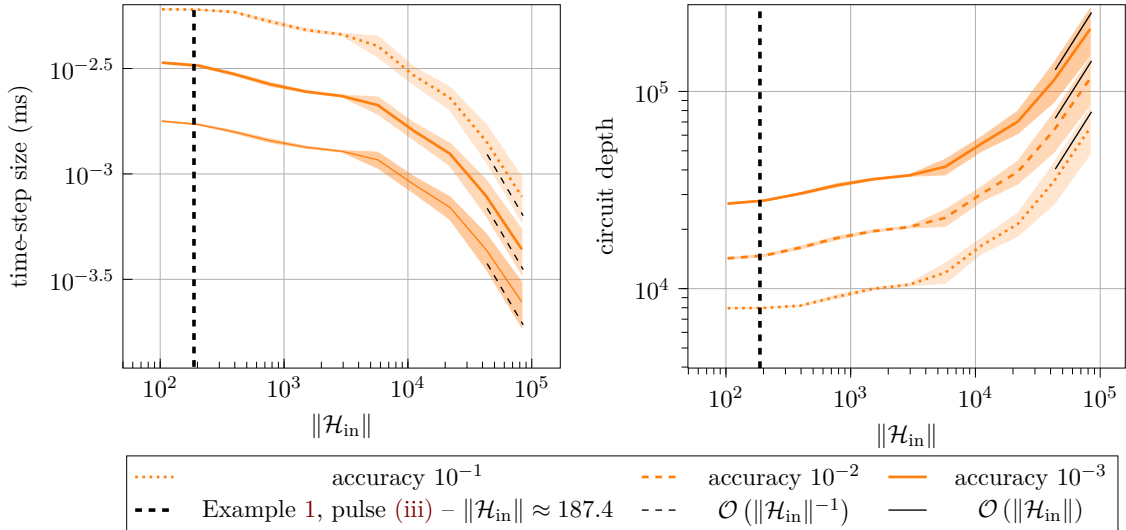


Figure 15: Plots comparing time-step sizes and circuit depths required to reach accuracies of 10^{-1} , 10^{-2} , and 10^{-3} against various coupling strengths, using $\Theta_2(t_n)$, eq. (67), `scipy`.

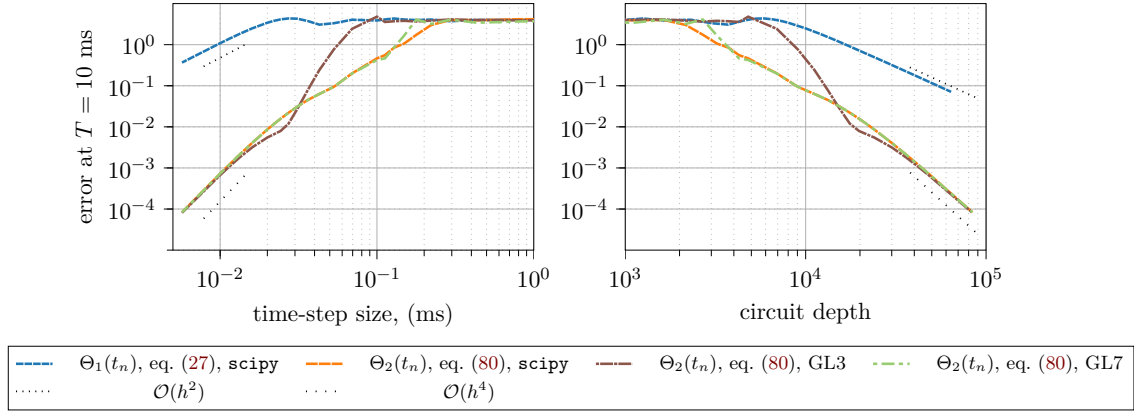


Figure 16: (*Non-isotropic Hamiltonian without mixed couplings under multiple chirped pulses; Magnus-based methods*) The accuracy of Hamiltonian simulation for non-isotropic Hamiltonian without mixed couplings under a chirped pulse, *i.e.*, Example 2, case (i). The methods compared are the second-order Magnus expansion (27) with integrals computed using `scipy` and combined with the Strang splitting (45), and the fourth-order Magnus expansion with commutator eliminated (80) and combined with Yoshida splitting (46). The integrals in the fourth-order Magnus expansions are either computed to machine precision using the Python package `scipy` or approximated with three or seven *Gauss–Legendre* quadrature nodes. The corresponding plots are labeled `scipy`, `GL3`, and `GL7` respectively.

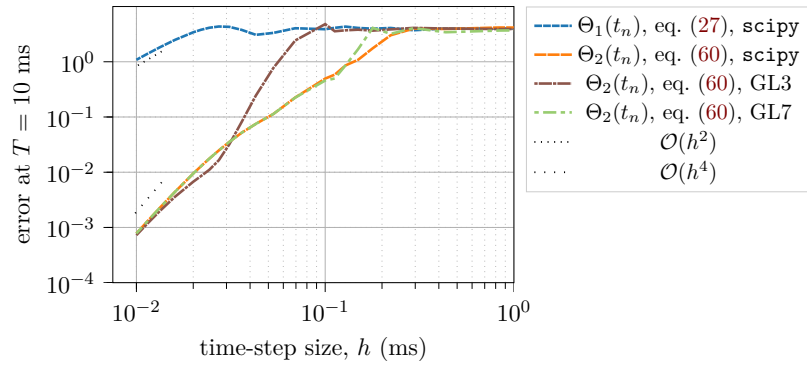


Figure 17: (*Non-isotropic Hamiltonian with mixed couplings under multiple chirped pulses; Magnus-based methods*) The accuracy of Hamiltonian simulation accuracy for non-isotropic Hamiltonian with mixed couplings under a chirped pulse, *i.e.*, Example 2, case (ii). The methods compared are the second-order Magnus expansion (27) with integrals computed using `scipy` and combined with the Strang splitting (45), and the fourth-order Magnus expansion with commutator eliminated (60) and exponentials computed by brute force. The integrals in the fourth-order Magnus expansions are either computed to machine precision using the Python package `scipy` or approximated with three or seven *Gauss–Legendre* quadrature nodes. The corresponding plots are labeled `scipy`, `GL3`, and `GL7` respectively.

Time-independent Hamiltonians. While high-order numerical methods are typically thought to have relevance only for high accuracies, and some recent attempts at Hamiltonian simulation on existing quantum devices have utilized the first-order Trotter splitting [4], our numerical experiments (cf. Figure 7) suggest that the second-order Strang splitting produces circuits that are shorter than those produced by the first-order Trotter splitting, even for relatively low accuracies ($\sim 10^{-2} - 10^{-5}$) for a three-body problem. Consequently, Strang splitting should be the method of choice for time-independent Hamiltonian simulation for demonstrating *quantum advantage* on near-term devices, where high accuracies are neither achievable nor essential.

Time-dependent Hamiltonians. For the simulation of time-dependent many-body two-level Hamiltonians, we compare a range of first-order, second-order and fourth-order algorithms that produce Trotterized circuits which are reasonable candidates for implementation on near-term devices. In contrast to the time-independent case, we find that fourth-order methods are required for the simulation of time-dependent Hamiltonians, even for extremely low levels of accuracy $\sim 10^{-1}$ (cf. Figures 8, 16 and 17) for a three-body problem. In fact, all the fourth-order methods considered here produce circuits that are shorter than the first and second-order methods for propagator errors of 1 or lower. We expect that for large spin systems, where any quantum advantage is likely to be demonstrable, the increased spectral radius will make the need for higher-order methods more pronounced.

Circuit compression ratio. The fourth-order Magnus expansion-based method developed in this paper produces circuits that are consistently found to be shorter in depth than the first-order, second-order and other fourth-order methods considered here, for a very wide range of driving pulse frequencies and interaction strengths, and across all levels of accuracy (cf. Figures 11 and 13). Moreover, the *circuit compression ratios* (which measure how much shorter the circuit produced by the proposed method is, as compared to the other methods) increases when we require higher accuracy and with the frequency of the controls. The latter stems from an ability to take time-steps that seem almost frequency-independent and can be larger than the wavelength (cf. Figures 8 and 9). This is achievable due to the decoupling of the time-step of the time-stepping procedure (25) from the resolution of the driving pulses via the computation of the integrals, (28), (32) and (33), appearing in the Magnus expansion.

Circuit structure. Moreover, the proposed approach results in circuits that are obtained as minor modifications (80) of fourth-order Trotterized circuits (cf. Figure 3 and eq. (79)) used for simulating time-independent Hamiltonians, making their implementation straightforward. Specifically, the modifications involve (i) three additional single-qubit gate layers (*i.e.*, $3M$ single-qubit gates) per time-step on average (an overhead that disappears entirely in the special case of isotropic coupling with identical spins, which appears frequently in liquid-state NMR applications), and (ii) tweaking the parameters of existing gates in the fourth-order Trotterized circuit for time-independent Hamiltonians. Computing the parameters for the gates requires the approximation of multiple one-dimensional and two-dimensional integrals appearing in the Magnus expansion, which can be computed efficiently to arbitrary accuracy on classical computers.

The straightforward circuit structure and consistent out-performance across various accuracy levels, control frequencies and coupling strengths highlights the robustness and broad applicability of our fourth-order Magnus-based method, and we recommend it as the method of choice for circuit design for simulation of time-dependent Hamiltonians on near-term devices, even when a very low level of accuracy is achievable or desired.

A fourth-order Magnus-based classical algorithm based on [74] is implemented in the open source Python package `magpy`, which is available on `github` [102] and can be installed from the Python Package Index (PyPI) as `pip install magpy`. Further extensions to this classical algorithm, based on some of the techniques presented in this manuscript, are currently under development and are also expected to be made available in `magpy`.

7 Acknowledgements

GC acknowledges support from EPSRC (EP/S022945/1). CB acknowledges support from EPSRC (EP/V026259/1).

References

- [1] R. P. Feynman, “*Simulating physics with computers*,” *International Journal of Theoretical Physics* **21**, 467 (1982).
- [2] A. M. Childs, D. Maslov, Y. Nam, N. J. Ross, and Y. Su, “*Toward the first quantum simulation with quantum speedup*,” *Proceedings of the National Academy of Sciences* **115**, 9456 (2018).
- [3] K. Seetharam, D. Biswas, C. Noel, A. Risinger, D. Zhu, O. Katz, S. Chattopadhyay, M. Cetina, C. Monroe, E. Demler, *et al.*, “*Digital quantum simulation of NMR experiments*,” *Science Advances* **9**, eadh2594 (2023).
- [4] Y. Kim, A. Eddins, S. Anand, K. X. Wei, E. van den Berg, S. Rosenblatt, H. Nayfeh, Y. Wu, M. Zaletel, K. Temme, and A. Kandala, “*Evidence for the utility of quantum computing before fault tolerance*,” *Nature* **618**, 500 (2023).
- [5] A. Y. Kitaev, “*Quantum measurements and the abelian stabilizer problem*,” *Electronic Colloquium on Computational Complexity* **TR96** (1995).
- [6] A. W. Harrow, A. Hassidim, and S. Lloyd, “*Quantum algorithm for linear systems of equations*,” *Physical Review Letters* **103**, 150502 (2009).
- [7] D. Castelvecchi, “*IBM releases first-ever 1,000-qubit quantum chip*,” *Nature*, (2023).
- [8] S. A. Moses, C. H. Baldwin, M. S. Allman, R. Ancona, L. Ascarrunz, C. Barnes, J. Bartolotta, B. Bjork, P. Blanchard, M. Bohn, *et al.*, “*A race track trapped-ion quantum processor*,” (2023), [arXiv:2305.03828](https://arxiv.org/abs/2305.03828).
- [9] D. Bluvstein, S. J. Evered, A. A. Geim, S. H. Li, H. Zhou, T. Manovitz, S. Ebadi, M. Cain, M. Kalinowski, D. Hangleiter, *et al.*, “*Logical quantum processor based on reconfigurable atom arrays*,” *Nature*, (2023).
- [10] A. M. Childs and N. Wiebe, “*Hamiltonian simulation using linear combinations of unitary operations*,” *Quantum Information and Computation* **12**, (2012).
- [11] D. W. Berry, A. M. Childs, R. Cleve, R. Kothari, and R. D. Somma, “*Exponential improvement in precision for simulating sparse Hamiltonians*,” *Proceedings of the forty-sixth annual ACM Symposium on Theory of Computing*, 283 (2014).
- [12] D. W. Berry, A. M. Childs, and R. Kothari, “*Hamiltonian simulation with nearly optimal dependence on all parameters*,” *2015 IEEE 56th Annual Symposium on Foundations of Computer Science*, 792 (2015).
- [13] D. W. Berry, A. M. Childs, R. Cleve, R. Kothari, and R. D. Somma, “*Simulating Hamiltonian dynamics with a truncated Taylor series*,” *Physical Review Letters* **114**, 090502 (2015).
- [14] G. H. Low and I. L. Chuang, “*Hamiltonian simulation by uniform spectral amplification*,” (2017), [arXiv:1707.05391](https://arxiv.org/abs/1707.05391).

- [15] G. H. Low and I. L. Chuang, “Optimal Hamiltonian simulation by quantum signal processing,” *Physical Review Letters* **118**, 010501 (2017).
- [16] G. H. Low and I. L. Chuang, “Hamiltonian simulation by qubitization,” *Quantum* **3**, 163 (2019).
- [17] H. F. Trotter, “On the product of semi-groups of operators,” *Proceedings of the American Mathematical Society* **10**, 545 (1959).
- [18] R. I. McLachlan and G. R. W. Quispel, “Splitting methods,” *Acta Numerica* **11**, 341 (2002).
- [19] S. Blanes, F. Casas, and A. Murua, “Splitting and composition methods in the numerical integration of differential equations,” *Boletín de la Sociedad Española de Matemática Aplicada* **45**, 89 (2008).
- [20] Y. Nam and D. Maslov, “Low-cost quantum circuits for classically intractable instances of the Hamiltonian dynamics simulation problem,” *npj Quantum Information* **5**, 44 (2019).
- [21] M. S. J. Tepaske, D. Hahn, and D. J. Luitz, “Optimal compression of quantum many-body time evolution operators into brickwall circuits,” *SciPost Physics* **14** (2023), 10.21468/scipostphys.14.4.073.
- [22] A. Smith, M. Kim, F. Pollmann, and J. Knolle, “Simulating quantum many-body dynamics on a current digital quantum computer,” *npj Quantum Information* **5**, 106 (2019).
- [23] G. H. Low and N. Wiebe, “Hamiltonian simulation in the interaction picture,” (2019), [arXiv:1805.00675](https://arxiv.org/abs/1805.00675).
- [24] M. Kieferová, A. Scherer, and D. W. Berry, “Simulating the dynamics of time-dependent Hamiltonians with a truncated Dyson series,” *Physical Review A* **99**, 042314 (2019).
- [25] D. W. Berry, A. M. Childs, Y. Su, X. Wang, and N. Wiebe, “Time-dependent Hamiltonian simulation with l^1 -norm scaling,” *Quantum* **4**, 254 (2020).
- [26] J. Haah, M. B. Hastings, R. Kothari, and G. H. Low, “Quantum algorithm for simulating real time evolution of lattice Hamiltonians,” *SIAM Journal on Computing*, FOCS18 (2021).
- [27] Y.-H. Chen, A. Kalev, and I. Hen, “Quantum algorithm for time-dependent Hamiltonian simulation by permutation expansion,” *PRX Quantum* **2**, 030342 (2021).
- [28] J. Watkins, N. Wiebe, A. Roggero, and D. Lee, “Time-dependent Hamiltonian simulation using discrete clock constructions,” (2022), [arXiv:2203.11353](https://arxiv.org/abs/2203.11353).
- [29] K. Mizuta and K. Fujii, “Optimal Hamiltonian simulation for time-periodic systems,” *Quantum* **7**, 962 (2023).
- [30] Y. Cao, S. Jin, and N. Liu, “Quantum simulation for time-dependent Hamiltonians – with applications to non-autonomous ordinary and partial differential equations,” (2023), [arXiv:2312.02817](https://arxiv.org/abs/2312.02817).
- [31] D. P. DiVincenzo, “The physical implementation of quantum computation,” *Fortschritte der Physik: Progress of Physics* **48**, 771 (2000).
- [32] M. H. Devoret, A. Wallraff, and J. M. Martinis, “Superconducting qubits: A short review,” (2004), [arXiv:cond-mat/0411174](https://arxiv.org/abs/cond-mat/0411174).
- [33] R. R. Ernst, G. Bodenhausen, and A. Wokaun, *Principles of Nuclear Magnetic Resonance in One and Two Dimensions* (Oxford University Press, 1990).
- [34] A. Blais, R.-S. Huang, A. Wallraff, S. M. Girvin, and R. J. Schoelkopf, “Cavity quantum electrodynamics for superconducting electrical circuits: An architecture for quantum computation,” *Physical Review A* **69**, 062320 (2004).

- [35] A. Spörl, T. Schulte-Herbrüggen, S. Glaser, V. Bergholm, M. Storz, J. Ferber, and F. Wilhelm, “Optimal control of coupled Josephson qubits,” *Physical Review A* **75**, 012302 (2007).
- [36] P. Krantz, M. Kjaergaard, F. Yan, T. P. Orlando, S. Gustavsson, and W. D. Oliver, “A quantum engineer’s guide to superconducting qubits,” *Applied Physics Reviews* **6**, (2019).
- [37] M. Zhao and D. Babikov, “Coherent and optimal control of adiabatic motion of ions in a trap,” *Physical Review A* **77**, 012338 (2008).
- [38] Y. Chou, S. Huang, and H. Goan, “Optimal control of fast and high-fidelity quantum gates with electron and nuclear spins of a Nitrogen-vacancy center in diamond,” *Physical Review A* **91**, 052315 (2015).
- [39] J. Tian, T. Du, Y. Liu, H. Liu, F. Jin, R. S. Said, and J. Cai, “Optimal quantum optical control of spin in diamond,” *Physical Review A* **100**, 012110 (2019).
- [40] J. Zhang, R. Laflamme, and D. Suter, “Experimental implementation of encoded logical qubit operations in a perfect quantum error correcting code,” *Physical Review Letters* **109**, 100503 (2012).
- [41] G. Waldherr, Y. Wang, S. Zaiser, M. Jamali, T. Schulte-Herbrüggen, H. Abe, T. Ohshima, J. Isoya, J. F. Du, P. Neumann, and J. Wrachtrup, “Quantum error correction in a solid-state hybrid spin register,” *Nature* **506**, 204 (2014).
- [42] F. Dolde, V. Bergholm, Y. Wang, I. Jakobi, B. Naydenov, S. Pezzagna, J. Meijer, F. Jelezko, P. Neumann, T. Schulte-Herbrüggen, J. Biamonte, and J. Wrachtrup, “High-fidelity spin entanglement using optimal control,” *Nature Communications* **5**, 1 (2014).
- [43] T. E. Skinner, T. O. Reiss, B. Luy, N. Khaneja, and S. J. Glaser, “Application of optimal control theory to the design of broadband excitation pulses for high-resolution NMR,” *Journal of Magnetic Resonance* **163**, 8 (2003).
- [44] Z. Töšner, S. J. Glaser, N. Khaneja, and N. C. Nielsen, “Effective Hamiltonians by optimal control: Solid-state NMR double-quantum planar and isotropic dipolar recoupling,” *Journal of Chemical Physics* **125**, 184502 (2006).
- [45] E. V. Reeth, H. Ratiney, K. Tse Ve Koon, M. Tesch, D. Grenier, O. Beuf, S. J. Glaser, and D. Sugny, “A simplified framework to optimize MRI contrast preparation,” *Magnetic Resonance in Medicine* **81**, 424 (2019).
- [46] P. E. Spindler, Y. Zhang, B. Endeward, N. Gershernzon, T. E. Skinner, S. J. Glaser, and T. F. Prisner, “Shaped optimal control pulses for increased excitation bandwidth in EPR,” *Journal of Magnetic Resonance* **218**, 49 (2012).
- [47] A. Doll, S. Pribitzer, R. Tschaggelar, and G. Jeschke, “Adiabatic and fast passage ultra-wideband inversion in pulsed EPR,” *Journal of Magnetic Resonance* **230**, 27 (2013).
- [48] T. Kaufmann, T. J. Keller, J. M. Franck, R. P. Barnes, S. J. Glaser, J. M. Martinis, and S. Han, “DAC-board based X-band EPR spectrometer with arbitrary waveform control,” *Journal of Magnetic Resonance* **235**, 95 (2013).
- [49] J. C. Saywell, I. Kuprov, D. Goodwin, M. Carey, and T. Freegarde, “Optimal control of mirror pulses for cold-atom interferometry,” *Physical Review A* **98**, 023625 (2018).
- [50] J. Saywell, M. Carey, I. Kuprov, and T. Freegarde, “Biselective pulses for large-area atom interferometry,” *Physical Review A* **101**, 063625 (2020).
- [51] J. C. Saywell, M. Carey, M. Belal, I. Kuprov, and T. Freegarde, “Optimal control of Raman pulse sequences for atom interferometry,” *Journal of Physics B* **53**, 085006 (2020).

- [52] L. H. Coudert, “Optimal control of the orientation and alignment of an asymmetric-top molecule with terahertz and laser pulses,” *Journal of Chemical Physics* **148**, 094306 (2018).
- [53] E. Räsänen, A. Castro, J. Werschnik, A. Rubio, and E. K. Gross, “Optimal control of quantum rings by terahertz laser pulses,” *Physical Review Letters* **98**, 157404 (2007).
- [54] N. Khaneja, T. Reiss, C. Kehlet, T. Schulte-Herbrüggen, and S. J. Glaser, “Optimal control of coupled spin dynamics: design of NMR pulse sequences by gradient ascent algorithms,” *Journal of Magnetic Resonance* **172**, 296 (2005).
- [55] T. Caneva, T. Calarco, and S. Montangero, “Chopped random-basis quantum optimization,” *Physical Review A* **84**, 022326 (2011).
- [56] S. Machnes, E. Assémat, D. Tannor, and F. K. Wilhelm, “Tunable, flexible, and efficient optimization of control pulses for practical qubits,” *Physical Review Letters* **120**, 150401 (2018).
- [57] D. L. Goodwin, P. Singh, and M. Foroozandeh, “Adaptive optimal control of entangled qubits,” *Science Advances* **8**, eabq4244 (2022).
- [58] B. Amstrup, J. D. Doll, R. A. Sauerbrey, G. Szabó, and A. Lorincz, “Optimal control of quantum systems by chirped pulses,” *Physical Review A* **48**, 3830 (1993).
- [59] M. Garwood and L. DelaBarre, “The return of the frequency sweep: designing adiabatic pulses for contemporary NMR,” *Journal of Magnetic Resonance* **153**, 155 (2001).
- [60] M. Foroozandeh, “Spin dynamics during chirped pulses: applications to homonuclear decoupling and broadband excitation,” *Journal of Magnetic Resonance* **318**, 106768 (2020).
- [61] W. Magnus, “On the exponential solution of differential equations for a linear operator,” *Communications on Pure and Applied Mathematics* **7**, 649 (1954).
- [62] A. Iserles, H. Z. Munthe-Kaas, S. P. Nørsett, and A. Zanna, “Lie-group methods,” *Acta Numerica* **9**, 215 (2000).
- [63] M. Hochbruck and C. Lubich, “On Magnus integrators for time-dependent Schrödinger equations,” *SIAM Journal on Numerical Analysis* **41**, 945 (2003).
- [64] K. Kormann, S. Holmgren, and H. O. Karlsson, “Accurate time propagation for the Schrödinger equation with an explicitly time-dependent Hamiltonian,” *The Journal of Chemical Physics* **128**, (2008).
- [65] S. Blanes, F. Casas, J.-A. Oteo, and J. Ros, “The Magnus expansion and some of its applications,” *Physics Reports* **470**, 151 (2009).
- [66] A. Iserles, K. Kropielnicka, and P. Singh, “Magnus–Lanczos methods with simplified commutators for the Schrödinger equation with a time-dependent potential,” *SIAM Journal on Numerical Analysis* **56**, 1547 (2018).
- [67] A. Iserles, K. Kropielnicka, and P. Singh, “Solving Schrödinger equation in semiclassical regime with highly oscillatory time-dependent potentials,” *Journal of Computational Physics* **376**, 564 (2019).
- [68] H. Hogben, M. Krzystyniak, G. Charnock, P. Hore, and I. Kuprov, “Spinach - a software library for simulation of spin dynamics in large spin systems,” *Journal of Magnetic Resonance* **208**, 179 (2011).
- [69] S. Stoll and A. Schweiger, “EasySpin, a comprehensive software package for spectral simulation and analysis in EPR,” *Journal of Magnetic Resonance* **178**, 42 (2006).
- [70] M. Veshtort and R. G. Griffin, “SPINEVOLUTION: A powerful tool for the simulation of solid and liquid state NMR experiments,” *Journal of Magnetic Resonance* **178**, 248 (2006).
- [71] M. Bak, J. T. Rasmussen, and N. C. Nielsen, “SIMPSON: A general simulation

- program for solid-state NMR spectroscopy,” *Journal of Magnetic Resonance* **147**, 296 (2000).
- [72] A. Iserles, K. Kropielnicka, and P. Singh, “Compact schemes for laser–matter interaction in Schrödinger equation based on effective splittings of Magnus expansion,” *Computer Physics Communications* **234**, 195 (2019).
 - [73] P. Singh, “Sixth-order schemes for laser–matter interaction in the Schrödinger equation,” *The Journal of Chemical Physics* **150**, 154111 (2019).
 - [74] D. Goodacre, “Numerical methods for quantum spin dynamics,” (2022), Master’s Thesis, University of Bath.
 - [75] S. A. Smith, W. E. Palke, and J. T. Gerig, “The Hamiltonians of NMR. Part i,” *Concepts in Magnetic Resonance* **4**, 107 (1992).
 - [76] S. A. Smith, W. E. Palke, and J. T. Gerig, “The Hamiltonians of NMR. Part ii,” *Concepts in Magnetic Resonance* **4**, 181 (1992).
 - [77] S. A. Smith, W. E. Palke, and J. T. Gerig, “The Hamiltonians of NMR. Part iii,” *Concepts in Magnetic Resonance* **5**, 151 (1993).
 - [78] W. Heisenberg, *Zur Theorie des Ferromagnetismus* (Springer, 1985).
 - [79] J. Hubbard, “Electron correlations in narrow energy bands iii. An improved solution,” *Proceedings of the Royal Society of London. Series A. Mathematical and Physical Sciences* **281**, 401 (1964).
 - [80] E. Ising, “Beitrag zur theorie des ferromagnetismus,” *Zeitschrift für Physik* **31**, 253 (1925).
 - [81] S. G. Brush, “History of the Lenz–Ising model,” *Reviews of Modern Physics* **39**, 883 (1967).
 - [82] B. A. Cipra, “An introduction to the Ising model,” *The American Mathematical Monthly* **94**, 937 (1987).
 - [83] A. Kitaev, “Anyons in an exactly solved model and beyond,” *Annals of Physics* **321**, 2 (2006).
 - [84] S. Trebst and C. Hickey, “Kitaev materials,” *Physics Reports* **950**, 1 (2022).
 - [85] J. Klassen and B. M. Terhal, “Two-local qubit Hamiltonians: when are they stoquastic?” *Quantum* **3**, 139 (2019).
 - [86] G. Consani and P. A. Warburton, “Effective Hamiltonians for interacting superconducting qubits: local basis reduction and the Schrieffer–Wolff transformation,” *New Journal of Physics* **22**, 053040 (2020).
 - [87] R. S. Strichartz, “The Campbell–Baker–Hausdorff–Dynkin formula and solutions of differential equations,” *Journal of Functional Analysis* **72**, 320 (1987).
 - [88] P. C. Moan and J. Niesen, “Convergence of the Magnus series,” *Foundations of Computational Mathematics* **8**, 291 (2008).
 - [89] A. Iserles, S. P. Nørsett, and A. Rasmussen, “Time symmetry and high-order Magnus methods,” *Applied Numerical Mathematics* **39**, 379 (2001).
 - [90] G. Strang, “On the construction and comparison of difference schemes,” *SIAM Journal on Numerical Analysis* **5**, 506 (1968).
 - [91] H. Yoshida, “Construction of higher order symplectic integrators,” *Physics Letters A* **150**, 262 (1990).
 - [92] J. Oteo, “The Baker–Campbell–Hausdorff formula and nested commutator identities,” *Journal of Mathematical Physics* **32**, 419 (1991).
 - [93] B. C. Hall, *Lie Groups, Lie Algebras, and Representations* (Springer, 2013).
 - [94] A. Alvermann and H. Fehske, “High-order commutator-free exponential time-propagation of driven quantum systems,” *Journal of Computational Physics* **230**, 5930 (2011).

- [95] S. Blanes, F. Casas, and M. Thalhammer, “High-order commutator-free quasi-Magnus exponential integrators for non-autonomous linear evolution equations,” *Computer Physics Communications* **220**, 243 (2017).
- [96] S. Wiggins, *Introduction to Applied Nonlinear Dynamical Systems and Chaos*, 1st ed., Texts in Applied Mathematics (Springer New York, 1990) pp. XIV, 672.
- [97] J. Guckenheimer and P. Holmes, *Nonlinear Oscillations, Dynamical Systems, and Bifurcations of Vector Fields*, Vol. 42 (Springer Science & Business Media, 2013).
- [98] J. Sanz-Serna and A. Portillo, “Classical numerical integrators for wave-packet dynamics,” *The Journal of Chemical Physics* **104**, 2349 (1996).
- [99] E. Hairer, M. Hochbruck, A. Iserles, and C. Lubich, “Geometric numerical integration,” *Oberwolfach Reports* **3**, 805 (2006).
- [100] F. Setiawan, P. Groszkowski, and A. A. Clerk, “Fast and robust geometric two-qubit gates for superconducting qubits and beyond,” *Physical Review Appl.* **19**, 034071 (2023).
- [101] J.-M. Böhlen, I. Burghardt, M. Rey, and G. Bodenhausen, “Frequency-modulated “chirp” pulses for broadband inversion recovery in magnetic resonance,” *Journal of Magnetic Resonance* (1969) **90**, 183 (1990).
- [102] D. Goodacre and P. Singh, “**MagPy**: Magnus based time-integration for spins and qubits under a magnetic field,” (2022).

A Proof of Theorem 1

Proof. The computation of the fourth-order Magnus expansion in eq. (31) begins by establishing some fundamental properties.

Consider 2×2 matrices A , B , and their commutator $C = [A, B]$. Then

$$[A_j, B_k] = \delta_{j,k} C_k, \quad (91)$$

where $\delta_{j,k}$ is the Kronecker delta, so that

$$[\mathbf{a}^\top \mathbb{A}, \mathbf{b}^\top \mathbb{B}] = \sum_{j=1}^M a_j b_j C_j = (\mathbf{a} \odot \mathbf{b})^\top \mathbb{C}, \quad (92)$$

where $\mathbb{A} = (A_1, \dots, A_M)$, $\mathbb{B} = (B_1, \dots, B_M)$ and $\mathbb{C} = (C_1, \dots, C_M)$.

Lemma 3.

$$[\mathbf{a}^\top \mathbb{S}^X, \mathbf{b}^\top \mathbb{S}^X] = [\mathbf{a}^\top \mathbb{S}^Y, \mathbf{b}^\top \mathbb{S}^Y] = [\mathbf{a}^\top \mathbb{S}^Z, \mathbf{b}^\top \mathbb{S}^Z] = 0.$$

Property 1. The Pauli matrices $\alpha \in \{X, Y, Z\}$ satisfy

$$[X, Y] = 2iZ, \quad [Y, Z] = 2iX, \quad [Z, X] = 2iY. \quad (93)$$

Property 1 immediately leads to Lemma 4.

Lemma 4.

$$\begin{aligned} [\mathbf{a}^\top \mathbb{S}^X, \mathbf{b}^\top \mathbb{S}^Y] &= 2i (\mathbf{a} \odot \mathbf{b})^\top \mathbb{S}^Z, \\ [\mathbf{a}^\top \mathbb{S}^Y, \mathbf{b}^\top \mathbb{S}^Z] &= 2i (\mathbf{a} \odot \mathbf{b})^\top \mathbb{S}^X, \\ [\mathbf{a}^\top \mathbb{S}^Z, \mathbf{b}^\top \mathbb{S}^X] &= 2i (\mathbf{a} \odot \mathbf{b})^\top \mathbb{S}^Y. \end{aligned}$$

Our investigation now turns to the commutator $[\mathcal{A}(t_n + \xi), \mathcal{A}(t_n + \zeta)]$ in Magnus expansion, eq. (31), which can be expressed as

$$\begin{aligned} &[\mathcal{A}(t_n + \xi), \mathcal{A}(t_n + \zeta)] \\ &= -[\mathcal{H}_{\text{ss}}(t_n + \xi) + \mathcal{H}_{\text{in}}, \mathcal{H}_{\text{ss}}(t_n + \zeta) + \mathcal{H}_{\text{in}}] \\ &= -[\mathcal{H}_{\text{ss}}(t_n + \xi), \mathcal{H}_{\text{ss}}(t_n + \zeta)] - [\mathcal{H}_{\text{ss}}(t_n + \xi), \mathcal{H}_{\text{in}}] + [\mathcal{H}_{\text{ss}}(t_n + \zeta), \mathcal{H}_{\text{in}}]. \end{aligned} \quad (94)$$

The first commutator in eq. (94), $[\mathcal{H}_{\text{ss}}(t_n + \xi), \mathcal{H}_{\text{ss}}(t_n + \zeta)]$, is represented as

$$[\mathcal{H}_{\text{ss}}(t_n + \xi), \mathcal{H}_{\text{ss}}(t_n + \zeta)] = 2i ((\mathbf{e} \wedge \mathbf{e})(t_n + \xi, t_n + \zeta))^\top \mathbb{S} \quad \text{by Lemma 3 and Lemma 4,}$$

The integral of the above should lead to terms of the same form, i.e. $\mathbf{a}^\top \mathbb{S}$ for some parameters $\mathbf{a} \in \mathbb{C}^{3M}$. Structurally, this is not problematic since it fits the common structure (39).

The second commutator in eq. (94), $[\mathcal{H}_{\text{ss}}(t_n + \xi), \mathcal{H}_{\text{in}}]$, can be expressed as

$$\begin{aligned} &[\mathcal{H}_{\text{ss}}(t_n + \xi), \mathcal{H}_{\text{in}}] \\ &= \left[\mathbf{e}^X(t_n + \xi)^\top \mathbb{S}^X + \mathbf{e}^Y(t_n + \xi)^\top \mathbb{S}^Y + \mathbf{e}^Z(t_n + \xi)^\top \mathbb{S}^Z, \frac{1}{2} \mathbb{S}^\top C_{\text{in}} \mathbb{S} \right] \\ &= \frac{1}{2} \left[\mathbf{e}^X(t_n + \xi)^\top \mathbb{S}^X, \mathbb{S}^\top C_{\text{in}} \mathbb{S} \right] + \frac{1}{2} \left[\mathbf{e}^Y(t_n + \xi)^\top \mathbb{S}^Y, \mathbb{S}^\top C_{\text{in}} \mathbb{S} \right] \\ &\quad + \frac{1}{2} \left[\mathbf{e}^Z(t_n + \xi)^\top \mathbb{S}^Z, \mathbb{S}^\top C_{\text{in}} \mathbb{S} \right] \end{aligned} \quad (95)$$

The last commutator in eq. (94) has similar structure as the second commutator eq. (95), except that the time variable is replaced by ζ . Collectively, eq. (94), i.e., $[\mathcal{A}(t_n + \xi), \mathcal{A}(t_n + \zeta)]$, can be summarized as

$$\begin{aligned} &[\mathcal{A}(t_n + \xi), \mathcal{A}(t_n + \zeta)] \\ &= 2i ((\mathbf{e} \wedge \mathbf{e})(t_n + \xi, t_n + \zeta))^\top \mathbb{S} - \frac{1}{2} \left[\left(\mathbf{e}^X(t_n + \xi) - \mathbf{e}^X(t_n + \zeta) \right)^\top \mathbb{S}^X, \mathbb{S}^\top C_{\text{in}} \mathbb{S} \right] \\ &\quad + \frac{1}{2} \left[\left(\mathbf{e}^Y(t_n + \xi) - \mathbf{e}^Y(t_n + \zeta) \right)^\top \mathbb{S}^Y, \mathbb{S}^\top C_{\text{in}} \mathbb{S} \right] \\ &\quad + \frac{1}{2} \left[\left(\mathbf{e}^Z(t_n + \xi) - \mathbf{e}^Z(t_n + \zeta) \right)^\top \mathbb{S}^Z, \mathbb{S}^\top C_{\text{in}} \mathbb{S} \right]. \end{aligned}$$

Subsequently, integrating $[\mathcal{A}(t_n + \xi), \mathcal{A}(t_n + \zeta)]$ leads to the expression of the fourth-order Magnus expansion. \square

B Derivation of eq. (63)

$$\begin{aligned}
& [\mathbf{u}(t_n)^\top \mathbb{S}, \mathbf{r}(t_n)^\top \mathbb{S}] \\
&= [\mathbf{u}^X(t_n)^\top \mathbb{S}^X + \mathbf{u}^Y(t_n)^\top \mathbb{S}^Y + \mathbf{u}^Z(t_n)^\top \mathbb{S}^Z, \mathbf{r}^X(t_n)^\top \mathbb{S}^X + \mathbf{r}^Y(t_n)^\top \mathbb{S}^Y + \mathbf{r}^Z(t_n)^\top \mathbb{S}^Z] \\
&= (\mathbf{u}^Y(t_n)^\top \odot \mathbf{r}^X(t_n))^\top (-2i\mathbb{S}^Z) + (\mathbf{u}^Z(t_n)^\top \odot \mathbf{r}^X(t_n))^\top (2i\mathbb{S}^Y) \\
&\quad + (\mathbf{u}^X(t_n)^\top \odot \mathbf{r}^Y(t_n))^\top (2i\mathbb{S}^Z) + (\mathbf{u}^Z(t_n)^\top \odot \mathbf{r}^Y(t_n))^\top (-2i\mathbb{S}^X) \\
&\quad + (\mathbf{u}^X(t_n)^\top \odot \mathbf{r}^Z(t_n))^\top (-2i\mathbb{S}^Y) + (\mathbf{u}^Y(t_n)^\top \odot \mathbf{r}^Z(t_n))^\top (2i\mathbb{S}^X) \\
&= -2i (\mathbf{u}^Z(t_n)^\top \odot \mathbf{r}^Y(t_n))^\top \mathbb{S}^X + 2i (\mathbf{u}^Y(t_n)^\top \odot \mathbf{r}^Z(t_n))^\top \mathbb{S}^X \\
&\quad + 2i (\mathbf{u}^Z(t_n)^\top \odot \mathbf{r}^X(t_n))^\top \mathbb{S}^Y - 2i (\mathbf{u}^X(t_n)^\top \odot \mathbf{r}^Z(t_n))^\top \mathbb{S}^Y \\
&\quad + 2i (\mathbf{u}^X(t_n)^\top \odot \mathbf{r}^Y(t_n))^\top \mathbb{S}^Z - 2i (\mathbf{u}^Y(t_n)^\top \odot \mathbf{r}^X(t_n))^\top \mathbb{S}^Z \\
&= 2i (\mathbf{u}(t_n) \times \mathbf{r}(t_n))^\top \mathbb{S}.
\end{aligned}$$

C Proof of Theorem 3

$$\begin{aligned}
e^{iaZ} e^{ibY} e^{icX} &= ((I \cos(a) + iZ \sin(a)) (I \cos(b) + iY \sin(b))) e^{icX} (I \cos(c) + iX \sin(c)) \\
&= I \cos(a) \cos(b) \cos(c) + 2iX \sin(a) \sin(b) \cos(c) + iX \cos(a) \cos(b) \sin(c) \\
&\quad + iY \cos(a) \sin(b) \cos(c) - 2iY \sin(a) \cos(b) \sin(c) \\
&\quad + iZ \sin(a) \cos(b) \cos(c) + 2iZ \cos(a) \sin(b) \sin(c) \\
&= e^{id(k_1 X + k_2 Y + k_3 Z)}.
\end{aligned}$$

We want to express the product of the above three exponentials in the form

$$e^{id(k_1 X + k_2 Y + k_3 Z)} = I \cos(d) + i(k_1 X + k_2 Y + k_3 Z) \sin(d).$$

Matching the corresponding terms, we find

$$\begin{aligned}
d &= \arccos(\cos(a) \cos(b) \cos(c)), \\
k_1 &= p [\cos(a) \cos(b) \cos(c) - \sin(a) \sin(b) \sin(c)] (\sin(a) \sin(b) \cos(c) + \sin(c) \cos(a) \cos(b)), \\
k_2 &= p [\cos(a) \cos(b) \cos(c) - \sin(a) \sin(b) \sin(c)] (\sin(b) \cos(a) \cos(c) - \sin(a) \cos(b) \sin(c)), \\
k_3 &= p [\cos(a) \cos(b) \cos(c) - \sin(a) \sin(b) \sin(c)] (\sin(a) \cos(b) \cos(c) + \sin(b) \cos(a) \sin(c)),
\end{aligned} \tag{96}$$

where $p[x] = \frac{\arccos(x)}{\sin(\arccos(x))}$. Substituting the parameters defining E into eq. (96) gives us eq. (65).

D Proof of Lemma 2

Proof of Lemma 2.

$$\begin{aligned}
& \left[\mathbb{1}^\top \mathbb{S}^\alpha, \sum_{\beta \in \{X, Y, Z\}} (\mathbb{S}^\beta)^\top C \mathbb{S}^\beta \right] \\
&= \left[\mathbb{1}^\top \mathbb{S}^\alpha, \sum_{j=1}^M \sum_{k=j+1}^M C_{j,k} X_j X_k \right] + \left[\mathbb{1}^\top \mathbb{S}^\alpha, \sum_{j=1}^M \sum_{k=j+1}^M C_{j,k} Y_j Y_k \right] + \left[\mathbb{1}^\top \mathbb{S}^\alpha, \sum_{j=1}^M \sum_{k=j+1}^M C_{j,k} Z_j Z_k \right] \\
&= \begin{cases} \left[\mathbb{1}^\top \mathbb{S}^X, \sum_{j=1}^M \sum_{k=j+1}^M C_{j,k} Y_j Y_k \right] + \left[\mathbb{1}^\top \mathbb{S}^X, \sum_{j=1}^M \sum_{k=j+1}^M C_{j,k} Z_j Z_k \right] & \text{if } \alpha = X \\ \left[\mathbb{1}^\top \mathbb{S}^Y, \sum_{j=1}^M \sum_{k=j+1}^M C_{j,k} X_j X_k \right] + \left[\mathbb{1}^\top \mathbb{S}^Y, \sum_{j=1}^M \sum_{k=j+1}^M C_{j,k} Z_j Z_k \right] & \text{if } \alpha = Y \\ \left[\mathbb{1}^\top \mathbb{S}^Z, \sum_{j=1}^M \sum_{k=j+1}^M C_{j,k} X_j X_k \right] + \left[\mathbb{1}^\top \mathbb{S}^Z, \sum_{j=1}^M \sum_{k=j+1}^M C_{j,k} Y_j Y_k \right] & \text{if } \alpha = Z \end{cases} \\
&\hspace{15em} \text{by Lemma 1} \\
&= \begin{cases} 2i \sum_{j=1}^M \sum_{k=j+1}^M C_{j,k} (Z_j Y_k + Y_j Z_k) - 2i \sum_{j=1}^M \sum_{k=j+1}^M C_{j,k} (Y_j Z_k + Z_j Y_k) & \text{if } \alpha = X \\ -2i \sum_{j=1}^M \sum_{k=j+1}^M C_{j,k} (Z_j X_k + X_j Z_k) + 2i \sum_{j=1}^M \sum_{k=j+1}^M C_{j,k} (X_j Z_k + Z_j X_k) & \text{if } \alpha = Y \\ 2i \sum_{j=1}^M \sum_{k=j+1}^M C_{j,k} (Y_j X_k + X_j Y_k) - 2i \sum_{j=1}^M \sum_{k=j+1}^M C_{j,k} (X_j Y_k + Y_j X_k) & \text{if } \alpha = Z \end{cases} \\
&\hspace{15em} \text{by Property 1} \\
&= 0.
\end{aligned}$$

□